Acoustic Devices for the Active & Passive Control of Sound in a Payload Compartment

Ozer Sacarcelik

Thesis submitted to the Faculty of the Virginia Polytechnic Institute and State University in partial fulfillment of the requirements for the degree of

Master of Science

In

Mechanical Engineering

APPROVED:

_____

Dr. Marty E. Johnson, Chair

_____ _____

Dr. Chris R. Fuller Dr. James P. Carneal

May 20, 2004
Blacksburg, Virginia

Keywords: Helmholtz resonator, loudspeaker, active noise control

Acoustic Devices for the Active & Passive Control of Sound in a Payload Compartment

Ozer Sacarcelik
Mechanical Engineering Department
Virginia Tech

Abstract

The work presented in this thesis can be divided into two main subjects. First, lightweight designs for acoustic devices such as Helmholtz resonators and loudspeakers used for noise control in rocket payload compartments are developed. Second, active control using a hybrid control system (with structural and acoustic actuators) was tested experimentally.

Due to the weight limitations for this application, Helmholtz resonators and loudspeakers are re-designed in order to reduce the device weight as much as possible while maintaining performance. For Helmholtz resonators, this is done by modeling the resonator for different structural shapes, wall materials and wall thicknesses using a finite element analysis software. The final design is then compared to the rigid resonators and is shown to perform effectively. These designs are then successfully applied to the full-scale fairing at Boeing facilities. In order to design a lightweight loudspeaker, a comparative approach was used. A standard 12" loudspeaker is taken as the reference loudspeaker and weight reduction solutions are applied to it while maintaining performance. The loudspeaker is characterized using mechanical, electrical and acoustical theories, and an optimization process is applied in order to minimize a defined cost function, which was taken as the total sound pressure output over a targeted frequency range per mass of the actuator. The results are used to build a lightweight loudspeaker together with a lightweight box, and the new designs are tested for comparison with the reference loudspeaker and shown to increase performance by 1.7 dB over 60-200 Hz band while reducing the mass by 78%.

The second part of this thesis investigates the performance of a hybrid active control treatment featuring distributed vibration absorbers (DAVAs) and loudspeakers applied on a scale payload fairing. Several aspects such as causality, reference signals, and maximum controllable

levels of this feedforward control scheme are the subjects of analyses. The results show that this active control approach can achieve significant amount of interior noise attenuation, and the total actuator weight required to control an external level of 138 dB can be reduced to 9.2kg using lightweight loudspeakers. However, it is shown that the attenuation levels can still be improved further by actuator positioning that gives more effective coupling of the actuators with the structural and acoustic modes and by using multiple references for the control system.

Acknowledgements

I would first like to thank the Mechanical Engineering Department of Virginia Tech for giving me the opportunity to obtain a Master's degree, and the Boeing Company for funding this research.

I would also like to thank everyone associated with the Vibration and Acoustics Lab (VAL), especially my advisor, Marty, who has always been helpful and willing to teach. I am also very thankful to Jamie, Baris and Simon for their continuous help and support.

Table of Contents

List of Figures

List of Tables

Nomenclature

a	Radius of resonator neck (m)
b	Damping in loudspeaker (Ns/m)
B	Magnetic field at air gap in loudspeaker (N/Am)
$(BH)_m$	Energy product of magnet (J/m^3)
c	Speed of sound in air (m/s)
c_r	Total damping in resonator (Ns/m)
d	Vector of error sensor outputs due to primary source
$D(w)$	Vector of error sensor outputs due to primary source in frequency domain
E_o	Vector of minimized errors
E_{shell}	Young's modulus for wall material (Pa)
$E[\ ]$	Expectation operator
f_o	Natural frequency of resonator (Hz)
h	Resonator wall thickness (m)
h_c	Vector of control filter coefficients
$H(w)$	Vector of control filter coefficients in frequency domain
H_o	Vector of optimum control filter coefficients
I	Current on voice coil in frequency domain (Amperes)
J	Cost function to compute minimum error
k	Stiffness of resonator due to air suspension (N/m)
k_B	Stiffness of the loudspeaker box (N/m)
k_S	Total stiffness of the spider and the surround (N/m)
l	Length of wire on voice coil (m)
L	Length of resonator neck (m)
L_E	Inductance of the voice coil
L_r	Length of cylindrical Helmholtz resonator (m)
m	Mass of air in resonator neck including the radiation mass (kg)

m_r	Air load on resonator neck (kg)
M	Total moving mass and air load (kg)
m_o	Permeability of free space ($m_o = 4p \times 10^{-7} H/m$)
P	Incident sound pressure (Pa)
r	Radius of cylindrical resonator (m)
R	Matrix of measured transfer functions between control actuators and error microphones
R_E	Electrical resistance of voice coil (ohms)
R_o	Ratio of impedance resulting from series combination of impedances of air in resonator neck and resonator walls to impedance of air
r	Density of air (kg/m^3)
S	Diaphragm area (m^2)
S_n	Cross-sectional area of resonator neck (m^2)
U	Velocity of diaphragm in frequency domain (m/s)
n_{shell}	Poisson's ratio for wall material
V	Voltage input to loudspeaker in frequency domain (Volts)
V_b	Back electromotive force (e.m.f) (Volts)
V_g	Volume of air gap (m^3)
V_m	Volume of magnet (m^3)
V_R	Volume of resonator (m^3)
V_v	Volume velocity of air in resonator neck (m^3/s)
w_o	Natural frequency of resonator (rad/s)
X	Diaphragm displacement in frequency domain (m)
z	Vector of error sensor outputs due to secondary source
Z_o^f	Leading order impedance associated with fluid in resonator
Z_o^s	Leading order impedance associated with resonator wall
$(\,)_{elastic}$	Parameters associated with the case where resonator wall is taken to be elastic

Chapter 1: Introduction

Main purpose of this chapter is to familiarize the reader with the contents of this work and to provide a brief summary of both background and recent work on acoustic devices used for active and passive noise control applications, particularly for rocket payload compartments. The first section describes the noise problem that occurs in payload fairings due to exhaust noise and it discusses possible solutions to this problem. Then structural and acoustic devices that can be used to solve this noise problem are briefly explained. In the literature review section, a brief history of the application of these devices is given together with a description of the recent work where these devices were used to control sound in payload fairings. A subsection mentioning the general active noise control approaches is also included. The last section gives the outline of the thesis.

1.1 Motivation

High noise levels occur during rocket launch due to exhaust noise from the rocket engines and the reflection of this noise off of the ground. Fairings are exposed to this high level noise which might damage the payload inside. Although the physics of the problem is complicated, it can be simplified by assuming the external disturbance is composed of plane waves hitting the fairing from different azimuth and circumferential angles. The incident sound waves hits the surface of the cylindrical fairing and couples with the modes of the structure causing vibration. The structural vibration, which has its own frequency response characteristics depending on both the structural shape and the external excitation, then acoustically couples with the air in the cylindrical cavity. The level of this coupling is strongly dependent on both modal characteristics of the cylinder and acoustical characteristics of the cavity. Therefore, the noise field inside the cylindrical fairing has unique frequency response characteristics.

Recent introduction of lightweight composite materials for fairing construction caused an increase in the level of vibration in fairing walls, which in turn decreased the transmission loss of the cylinder. Therefore the problem of noise inside the fairing has become even more important.

There are several ways to control the interior noise. For instance, passive treatments such as acoustic blankets can successfully attenuate high frequency noise; however they perform poorly at low frequencies where damage to the payload is more likely. Therefore, controlling the internal noise in fairings at low frequencies requires a different approach. Both active and passive control strategies can be implemented for this purpose. Additionally, there are two possible paths through which the noise inside the fairings can be controlled:

i) The level of vibration on the fairing walls can be controlled using structural devices in order to reduce the consequent interior noise due to the coupling between the vibration of the walls and the acoustic modes of the cavity.

ii) The level of internal noise can be controlled directly using acoustic devices which radiate sound to cancel the internal noise or absorb acoustic energy.

Both approaches are effective in controlling the internal noise and the combination of the two approaches performs even more effectively. Devices that can be used for the active and passive control of low frequency noise in payload fairings are Helmholtz resonators, distributed vibration absorbers (DVAs), distributed active vibration absorbers (DAVAs) and loudspeakers. In terms of the path categories mentioned in the previous section, Helmholtz resonators and loudspeakers are acoustic devices, whereas DVAs and DAVAs are structural devices. As an additional classification, Helmholtz resonators and DVAs work passively, whereas loudspeakers and DAVAs work actively. Table 1.1 illustrates these devices and summarizes their classification.

Table 1-1. Acoustic and structural devices for active and passive control of sound in payload fairings.

Noise Control Devices	Passive	Active
Acoustic	Helmholtz Resonator 	Loudspeaker 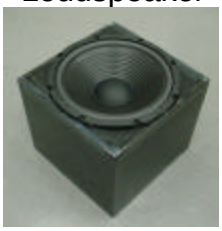
Structural	Distributed Vibration Absorber (DVA) 	Distributed Active Vibration Absorber (DAVA) 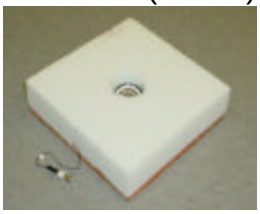

Using these devices for noise control in payload fairings causes a practical problem: All these devices, if not designed accordingly, can add a significant amount of mass to the fairing. This is an important issue especially for this application where the addition of extra weight to the system carries a large penalty. Therefore, reducing the mass of these devices while maintaining an acceptable level of performance is a top priority. Since DVAs and DAVAs are relatively light devices that have already been optimized [1,2], designing lightweight Helmholtz resonators and lightweight loudspeakers is the focus of this work.

DVAs and Helmholtz resonators have already been successfully implemented to passively control internal noise in payload fairings [3,4]. In addition, DAVAs have also been shown to perform well in attenuating structural vibrations and consequent internal noise of payload fairings [2]. However, loudspeakers have not yet been used with structural actuators in a feedforward scheme for active control of sound in payload fairings. Therefore, investigating the performance of a hybrid active noise control treatment featuring both structural and acoustic devices (DAVAs and loudspeakers) is the other main objective of this work.

1.2 Introduction to Noise Control Devices

1.2.1 Structural Devices

A DVA is modeled as a single degree of freedom system, where a plate represents the mass, and a block of foam glued to the plate represents the spring as shown in Figure 1-1(a). DVAs performs efficiently near its resonant frequency which can be adjusted by changing the foam or mass size.

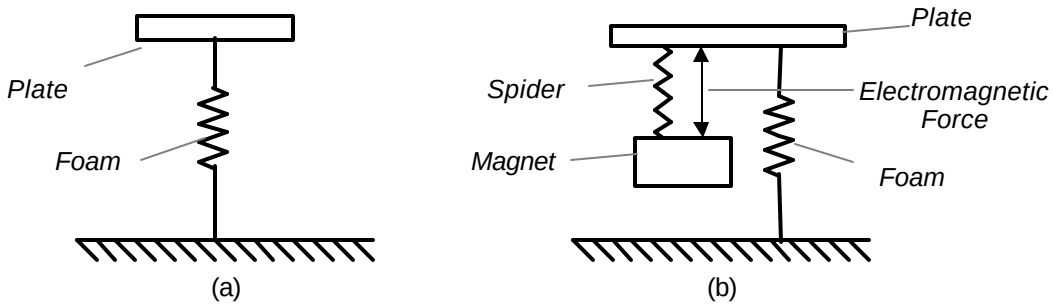

Figure 1-1. Mechanical models of (a) a Distributed Vibration Absorber (DVA) and (b) a Distributed Active Vibration Absorber (DAVA).

On the other hand, a DAVA (Figure 1-1(b)) is modeled as a two degrees of freedom system, where a honeycomb plate acts as the mass and foam provides stiffness for the passive part of the system (similar to a DVA). In addition, permanent magnet of the electro-mechanical shaker provides mass and the spider plates provide stiffness to the active part of the system. The shaker is connected to the plate which provides the source of excitation of the mass-spring-damper system with the desired frequency. DAVAs target structural vibration within a frequency bandwidth by having two resonant frequencies. Therefore the choice of the magnet and plate masses, foam size and spider stiffness can be used to change the natural frequencies of the DAVA and achieve the desired response characteristics.

1.2.2 Acoustic Devices

Helmholtz resonators are analogous to DVAs in the sense that they are single degree of freedom mass-spring systems that can be used to absorb or reflect acoustic waves instead of structural waves. Figure 1-2(a) illustrates the mechanical model of a Helmholtz resonator. The

incident waves excite the air to vibrate as a lumped mass in the neck and the air in the resonator acts like a spring due to its stiffness to pressure difference. There is also damping in the system due to viscous effects around the neck. In addition, radiation from the neck creates air load which must be added to the mass of the air in the neck. Modeling of Helmholtz resonators will be explained in detail in Chapter 2.

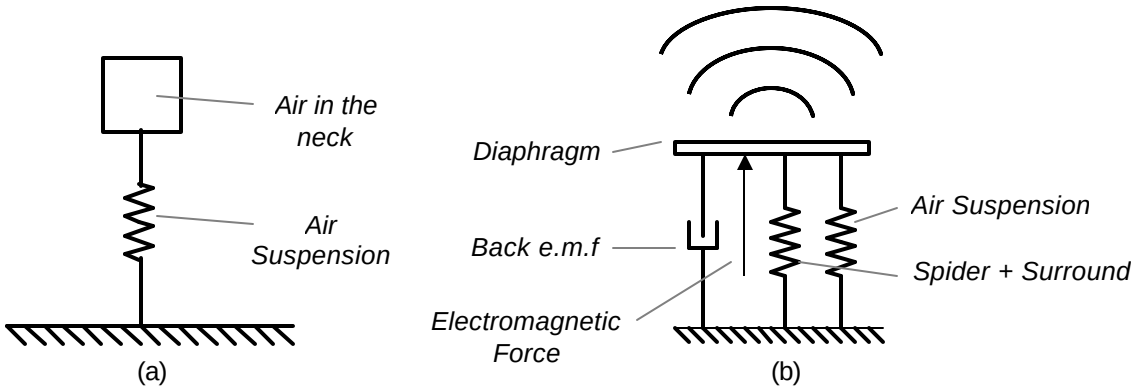

Figure 1-2. Mechanical models of (a) a Helmholtz resonator and (b) a loudspeaker.

Loudspeakers, on the other hand, are active devices that can be used to create a sound field that cancels the internal noise field. Loudspeakers can perform effectively for a broader frequency range. Figure 1-2(b) illustrates the mechanical model of a Helmholtz resonator. A stationary magnet assembly creates a magnetic field in an air gap where a charged voice coil can vibrate. A diaphragm is connected to the voice coil to initiate sound. The stiffness to the system comes from the spider and the surround. Modeling of loudspeakers will be explained in detail in Chapter 3.

1.3 Literature Review

Noise control devices have been widely used for active and passive control of sound from various types of structures. In this section, a brief review of the work that has been done on noise control devices and their applications will be given. In addition, work on active noise control approaches will also be summarized in order to be able to understand the developments and applications in this area.

1.3.1 Passive Devices

Vibration absorbers have been widely used for control of vibrations and consequent radiated noise from structures. Early work on designing vibration absorbers was done by Frahm and he patented the designs in 1909 [5]. He designed various types of devices to damp the vibration of structures. The basic vibration absorber device works on the principle of single mass-spring system having one resonant frequency which can be tuned by changing the system parameters. The resonant frequency of the absorber is adjusted close to the natural frequency of either the structure or the driving frequency. The early designs for vibration absorbers constitute the basis of the modern devices which are very convenient and effective and are widely used for passive control of sound and vibration.

Vibration absorbers were primarily designed to target structural vibration. However, they can also be used to control the noise radiation from vibrating structures. Studies on the control of noise radiating from simple structures such as plates using vibration absorbers were conducted by various authors [6,7,8]. Huang and Fuller [9,10] expanded this analysis to cylindrical structures by characterizing the vibration and interior sound fields of these structures due to different types of external loading. It was shown that a substantial reduction of vibration and internal noise around the excitation frequency could be achieved using dynamic absorbers. The effectiveness of the treatment increases as the absorbers are placed closer to the external disturbance.

Vibration absorbers are typically designed and used as lumped-masses mounted to specific points on the structures. The attenuation of structural vibrations, and therefore the consequent noise radiated, can be improved by increasing the number of vibration absorbers used. Distributing the mass of the absorber over the structure can further improve the amount of attenuation and this idea was used at VAL to design and test active and passive distributed vibration absorbers (DVAs and DAVAs) and this created a broad area of research. The DVAs were used in the form of a distributed elastic layer connected to a plate, i.e. distributed mass. This form was analytically modeled [1] and experimentally tested [11] to control the interior noise field on a composite cylinder which is baffled and simply supported. The cylinder is excited with external disturbance which is assumed to be composed of planar waves. The application was successful in damping the structure resonances especially when DVAs were placed at mode maxima. It was shown that the positioning of the DAVAs could be optimized using a modal model of the cylinder in order to maximize performance.

Helmholtz resonators have been widely used for various types of applications. They are effective in passive control of sound of single resonant peaks by acting directly on the noise field. There has been much work on the theory of Helmholtz resonators, calculating resonant frequencies and effects of resonator shape on its characteristics [12,13,14]. The interaction of Helmholtz resonators with modes of an acoustic enclosure was examined [15] and the optimal damping equation for broadband excitation control was derived. Cummings [16] used a multi-mode theoretical analysis to validate the performance of a resonator array in reducing the response of an acoustic cavity to an arbitrary source distribution. Doria [17] used a multiple resonator that interacts with lower modes of an enclosure, which resulted in breaking each resonant peak into two peaks of lower amplitude.

Typically Helmholtz resonators were assumed rigid. This is a reasonable assumption, since the walls of the resonator are generally thick, and the forces on the walls due to the fluid inside (air most of the time) is too small to cause siginificant deformation of the walls. However, in order to build lightweight resonators, lighter materials and thinner walls have to be used and therefore the walls can not be assumed rigid. Photiadis [18] examined the effects of wall elasticity on the properties of Helmholtz resonators by using an approach that incorporates an effective stiffness which resulted from series addition of the wall elasticity to the resonator stiffness. This caused a decrease in resonant frequency of the resonator. This work was further extended [19] and an approach introducing a spherical cavity with a thin shell was used to derive the theory regarding the effects of wall elasticity. The equations comparing the velocities of the shell and the air in the neck were derived. These equations are of great importance in order to compute the total volume velocity provided by a Helmholtz resonator. Equations for cylindrical resonators were also given in addition to the spherical ones.

As an application related to this thesis, local and global strategies for performance of adaptive Helmholtz resonators in controlling the noise inside a cylinder was compared [20]. By using Helmholtz resonators together with DVAs, the noise transmitted to a cylinder was passively controlled and this combination was proven to be effective [3,4,21]. An analytical model of optimally damped Helmholtz resonators and DVAs were applied on the vibro-acoustic model of the cylinder and it has been shown that [3] this combination can lead to 7.7dB attenuation over 50-160 Hz bandwidth. The reason for targeting low frequency is that the lower orders of low frequency modes are shown to be dominant in this particular system. The effectiveness of this

combination is verified [4] by the experiments conducted on a composite cylinder at airport lab of VAL. DVAs are also combined with adaptive Helmholtz resonator where a local adaptive strategy is introduced [21].

1.3.2 Active Devices

By adding an active excitation component to the DVA, a distributed vibration absorber (DAVA) was built at VAL. The active component can take a form of a curved polymer piezoelectric PVDF sheet mounted in the elastic layer [22,23] as well as an electrodynamic shaker connected to the plate mass of the absorber [24,2]. The PVDF based DAVAs cannot offer authority at low frequencies where large displacements are required. Electrodynamic shaker based DAVAs were proven to be more effective at frequencies as low as 50 Hz by providing a higher force per voltage response compared to the PVDF-based DAVAs.

Loudspeakers are very widely used both for scientific and entertainment purposes, and there has been enormous amount of work on working principles, modifications and improvements of the characteristics of loudspeakers. This is a very broad area and readers should refer to books such as the one by Dickason [25] which provides a very detailed approach on loudspeaker design. Being more specific and related to the discussion of this thesis, only the work on loudspeakers for active noise control applications will briefly be discussed.

Loudspeakers are the most commonly used actuators for active noise control. Elliott [26] has a fundamental work on the active control of sound in enclosures by using loudspeakers. He discusses the practical aspects of using a control system consisting of microphones and loudspeakers for reduction of automobile interior noise. A work [27] on attenuating aircraft engine noise for environmental considerations also features the use of wall-mounted loudspeakers attenuating the sound at its source. Improving the loudspeaker characteristics in order to increase its effectiveness for active noise control of acoustic enclosures has drawn much attention. For this purpose, Lane and Clark [28] worked on improving the loudspeaker performance by designing a velocity estimator to compensate the loudspeaker reliably. An approach [29] introducing an evacuated enclosure and a nonlinear suspension to conventional loudspeakers can reduce the natural frequency of the device, thus increasing the low frequency output which is significant in active noise control applications.

Loudspeakers are heavy and bulky and they are not as suitable for aerospace applications for this reason. Therefore, different types of lightweight acoustic actuators have also been designed and developed for active noise control. For example, electrostrictive polymer films [30,31] as well as piezoelectrically driven speakers [32] can offer good performance at low frequencies. However, despite of their compact and light weight, these actuators are not as efficient as electrodynamic loudspeakers in converting the input energy to acoustic energy and they are still in development phase.

1.3.3 Active Noise Control

There is more emphasis on active control in this thesis; therefore a brief history of active noise will be given in this section. Although active noise control is a relatively recent area due to the late developments in computational hardware and software, there has been much work especially on theoretical aspects and feasibility of active control on different type of systems. More detail on general active control techniques can be found in the books by Nelson and Elliott [33], and Fuller et al [34]. A very good two-part paper by Tu and Fuller [35,36] about multiple reference feedforward active noise control provides both frequency and time domain approaches to obtain an optimum solution. Various types of control architectures together with the potential applications are given as an overview to the active control of sound and vibration area [37].

An active control description was first patented by Lueg [38]. In this patent, sound waves are traveling down a duct, and a microphone upstream picks up the noise signal which is sent to the loudspeaker downstream. The loudspeaker then creates a sound field which is out of phase with the noise field. This feed-forward scheme forms the basis of many active noise control systems today. A feedback approach for active noise control of sound requires an error microphone close to the loudspeaker, and this approach provides local noise attenuation and can actually increase the far-field sound levels [39]. Elliott [26] not only compares the feedback and feedforward strategies, but also sets acoustic limitations for global and local strategies for the active control of sound in enclosures by using loudspeakers.

For active control of sound in payload fairings, there are several factors that should be taken into account in order to be able to achieve maximum attenuation of the complicated internal noise field. Other than the physics of the phenomena, the response characteristics of the devices should also be well-known. Information from reference signals (e.g. external

microphones) is required in order to drive the active actuators with the appropriate frequency and amplitude. The transfer function between the devices and the internal sound pressure must be known a priori in order to achieve attenuation. Active noise control techniques to reduce the internal noise level of lightweight aerospace structures have been the subject of some recent research [40,41,42,43]. This work showed that attenuation is possible when applied to scale models. For large aerospace structures actuators contributes too much to weight and volume and do not have enough authority to reduce interior noise. Therefore, more powerful and lighter actuators should be designed.

There are a few factors affecting the performance of an active noise control system other than the factors related to the level of control authority provided by actuators. The spatial and spectral extents of the system are both crucial in the sense that they increase the load on the controller and potentially reduce performance. However, recent developments in digital electronic technology with faster computation have reduced the effect of these two factors. The most important factor in this sense is the availability of good quality reference signals. A recent work [44] discusses the number and location of reference signals required to provide high coherence levels in controlling the sound transmission into a payload fairing. Having perfect secondary sources and perfect controller, quality of reference signals determines the upper limit to how well the controller can perform. It was shown that ten times as many reference sensors will be required circumferentially as axially and the coherence drops below 0.5 for a spatial separation of only $1/6^{th}$ of a wavelength around the circumference of the cylinder.

1.4 Outline of the Thesis

This thesis discusses the use of acoustic devices for the active and passive control of sound in payload compartments. Weight restrictions in aerospace applications were taken into account throughout the actuator designs. Therefore, detailed weight reduction solutions for the two treatments, Helmholtz resonators and loudspeakers, are given in separate chapters.

Chapter 2 discusses the weight reduction limits in the design of Helmholtz resonators using lightweight thin-walled structures. As the thickness is reduced, the loss of rigidity of the structure results in performance loss. Using finite element analysis the effects of wall elasticity on resonator performance is analyzed. The results are validated by experiments and the design is

finalized to produce the Helmholtz resonators used successfully on a full-scale fairing together with the DVAs at the Boeing facilities in December 2003.

Chapter 3 presents a comparative approach to loudspeaker design. The idea is to select a standard commercial loudspeaker and apply weight saving solutions without loosing performance. With the weight saving goal in mind, components of the loudspeaker were designed using a detailed loudspeaker characterization. The performance of the resulting lightweight loudspeaker is then compared both numerically and experimentally to that of the reference loudspeaker.

For active control tests, loudspeakers and previously designed DAVAs were used on a scale model of fairing at Virginia Tech. Different combinations (i.e. position and number) of the devices were tested and the results were analyzed. Individual effects of DAVAs and loudspeakers on the attenuation levels were investigated in order to be able to understand the behaviors of these devices for this particular active noise control application. The subjects such as optimum control, maximum controllable external level and causality are analyzed in detail and the weight of the total noise control application is calculated. The results are presented in detail in Chapter 4.

Chapter 5 provides the conclusions together with the possible future work that would be complementary to the work done for this thesis. In the appendix, models for 2 degrees of freedom acoustic devices are presented.

Chapter 2: Lightweight Helmholtz Resonators

A Helmholtz resonator (HR) is one of the most common devices for passive control of sound. It is very efficient in controlling the noise over a narrow frequency band and it has been applied successfully to many acoustic enclosures. There has been a lot of work on modifying the design of resonators in order to optimize its performance for specific applications. Almost all of the work on Helmholtz resonators assumes that the resonator walls are rigid. This is an acceptable assumption if resonator walls are thick and the fluid of interest is air. However, thick-walled Helmholtz resonators are heavy, especially for noise control treatments in aerospace applications, where weight is of great importance. The solution to this weight issue is to build lightweight Helmholtz resonators by using thinner walls and lighter wall materials. However this might lead to a reduction in the stiffness of the resonator walls and they can no longer be modeled as being rigid. This results in significant reductions in both the natural frequency and the maximum output of the resonator. In view of this, the subject of this chapter is the design of Helmholtz resonators as light as possible, while maintaining rigidity high enough to ensure good performance. The first part of the analysis is to mathematically model a Helmholtz resonator, and then define a performance criterion for the resonator. The next step is to introduce the wall elasticity into computations and calculate the change in performance. Once the theoretical expressions are derived, the Helmholtz resonator is modeled using finite element analysis, where various possible solutions for compensating for the negative effect of wall elasticity on performance are proposed. Finally, experimental results comparing a rigid cardboard resonator with a thin-walled lightweight resonator is given at the end of the chapter.

2.1 Theory

A Helmholtz resonator is principally composed of a volume of fluid (air for this application) and a neck that connects the fluid to the surrounding. The air in the neck can be considered as a lumped mass moving in the neck. This motion of air in the neck causes slight fluctuations in the internal pressure, thus the volume of air inside the resonator can be considered to act like a spring. These two together form a single degree of freedom system having one

resonant frequency. When the Helmholtz resonator is exposed to an external sound pressure, harmonic motion of the air in the neck is initiated. The frequency response of this motion depends on the resonator characteristics, such as dimensions of the neck and volume of the resonator. There is also significant damping in the system especially due to the air moving in the neck and the vortices that occur around neck edges. At the resonant frequency of a resonator, theoretically, the air in the neck creates a sound pressure that cancels the incident sound pressure (i.e. low acoustic impedance), therefore the response of the Helmholtz resonator at and close to the its natural frequency is the primary criterion for its performance. This single degree of freedom characteristic of Helmholtz resonators makes them useful for targeting peaks in the noise spectrum of the system to be controlled. Therefore, different resonators can be assigned to different acoustic modes in the system in order to be able to achieve the maximum control performance [3].

2.1.1 Mechanical Model

Figure 2.1 illustrates the mechanical model of a Helmholtz resonator modeled as a mass-spring-damper system. The harmonic forcing applied on the mass is in reality the incident pressure on the air in the neck. The transfer function between the incident sound pressure and the volume velocity of the air in the neck is calculated to be

$$\frac{V_v(w)}{P(w)} = \frac{S_n{}^2 jw}{\left(-w^2 m + k\right) + jwc_r} \tag{2.1}$$

where S_n is the cross sectional area of the neck, m, k, and c_r are the mass of the air in the neck (including the radiation mass), stiffness due to the volume of air in the resonator, and damping due to viscous effects, respectively.

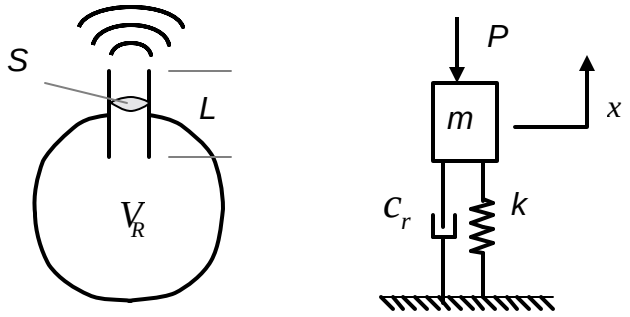

Figure 2-1. Mechanical Model of a Helmholtz Resonator.

The natural frequency of the resonator is therefore given as

$$w_o = \sqrt{\frac{k}{m}} \tag{2.2}$$

The natural frequency of a resonator depends on the volume of air in both the neck and in the resonator. For damped systems the maximum value of the response occurs slightly below the natural frequency of the resonator. However, if the damping is low (which is the case for Helhmoltz resonators), frequency of the peak response is very close to the natural frequency, and therefore the peak response can be assumed to occur at the natural frequency of the system. The peak value of the response is then

$$\left(\frac{V_v}{P}\right)_{\max} = \frac{S_n{}^2}{c_r} \tag{2.3}$$

The peak response depends on the area of the neck and the damping in the system. The expressions for mass and stiffness of the system are given by [45]

$$k = rc^2 S_n{}^2 / V_R \tag{2.4}$$

$$m = rS_n\left(L + 1.4a\right) \tag{2.5}$$

The $1.4a$ term in the above expression compensates for the radiation mass of the neck assuming that both ends of the neck are unflanged which is typical considering the neck shape of a Helmholtz resonator. Therefore, the natural frequency of a Helmholtz resonator having a volume V_R, and a neck with dimensions S_n, L, and a (cross sectional area, length and radius) is given in Hertz as

$$f_o = \frac{c}{2p}\sqrt{\frac{S_n}{(L+1.4a)V_R}} \tag{2.6}$$

A cylindrical Helmholtz resonator with a body radius of r, and a body length of L_r, has a natural frequency of

$$f_o = \frac{ca}{2pr}\sqrt{\frac{1}{(L+1.4a)L_r}} \tag{2.7}$$

2.1.2 Effects of Wall Elasticity

Performance of a Helmholtz resonator in its ability to absorb incident sound pressure can significantly reduce if the resonator walls are not stiff enough. This is a problem that can be encountered when using very thin walls. Quantitative work was done on the effects of wall elasticity on the resonator parameters [18,19]. The net volume velocity of air out of the resonator due to an external sound pressure on the neck is a measure of how well the resonator works. The elastic walls move out of phase with the air in the neck reducing the total volume velocity of the resonator. The following equation for the ratio of the inward flux of the shell to the outward flux of the air in the neck is significant in this sense.

$$\frac{inward\ \ flux\, of\ \ shell}{outward\ \ flux\ from\, neck} = 1 - R_o \tag{2.8}$$[19]

where R_o is the ratio of the impedance resulting from the series combination of the impedances of air in the neck and of the resonator walls (shell) to the impedance of air and is given by

$$R_o = \frac{Z_o^s}{Z_o^f + Z_o^s} \tag{2.9}$$

Z_o^s and Z_o^f are the impedances associated with the wall and the fluid (air), respectively. The following expression for the net volume velocity of air out of the resonator can be written by using Equation 2.8 as

$$\left(\Delta V_v\right)_{out} = R_o V_v \tag{2.10}$$

The resultant stiffness of the series connection is always less than the smaller of the individual stiffness values, which makes R_o always between 0 and 1. Therefore, Equation 2.10 demostrates that the elasticity of the walls leads to a reduction in total resonator volume velocity output. The stiffness k in Equation 2.1 for the rigid-walled resonator case was solely due to air suspension, however for elastic walls, the stiffness of the system is now the resultant of air suspension and wall stiffness, connected in series. This stiffness of the system is given by

$$\left(k\right)_{elastic} = R_o k \tag{2.11}$$

Using the Equations 2.10 and 2.11, the transfer function between the incident sound pressure and the net volume velocity of air out of the resonator in Equation 2.1 can be modified for Helmholtz resonators with elastic walls to give

$$\left(\frac{V_v(w)}{P(w)}\right)_{elastic} = \frac{R_o {S_n}^2 jw}{\left(-w^2 m + R_o k\right) + jwc_r} \tag{2.12}$$

Therefore, the natural frequency and the peak response of a resonator with elastic walls are now given by

$$(w_o)_{elastic} = \sqrt{R_o} w_o \tag{2.13}$$

$$\left(\left(\frac{V_v}{P}\right)_{\max}\right)_{elastic} = \frac{R_o S_n^{\,2}}{c} \tag{2.14}$$

Equations 2.13 and 2.14 show how the characteristics of a resonator changes, by both reducing the total output by R_o and decreasing the natural frequency by square root of R_o. The R_o value is therefore an important factor in changing the performance of a resonator. The expressions for R_o depends on the shape of the resonator, and for a cylindrical Helmholtz resonator having a radius r, and wall thickness h, it can be computed by using the shell and air impedances [19]. Ignoring the higher order terms leads to

$$R_o = \left(1 + \frac{2 r \rho c^2 \left(1 - \nu_{shell}^{\,2}\right)}{E_{shell} h}\right)^{-1} \tag{2.15}$$

The R_o value is highly dependent on the modulus of elasticity E_{shell} of the wall material. It is important to note at this stage that when calculating the impedances it is assumed that the resonator is baffled infinitely at the ends, in other words it has perfectly rigid end caps. This assumes that all of the deformation occurs at the cylindrical side. Figure 2.2 shows the R_o values for cylindrical Helmholtz resonators made of three different materials; aluminum, Polyethylene Terephthalate Glycol (PETG), and acrylic. The radius of the resonator is taken to be 5 cm. It can be seen that R_o value is almost one for the aluminum resonator for even very thin walls. For a wall thickness of 0.5 mm, R_o values are about 0.99 for both PETG and acrylic resonators. This result means that the cylindrical resonators hardly deform on the cylindrical surface. The theory derived here will be validated by the finite element analyses results of the next section.

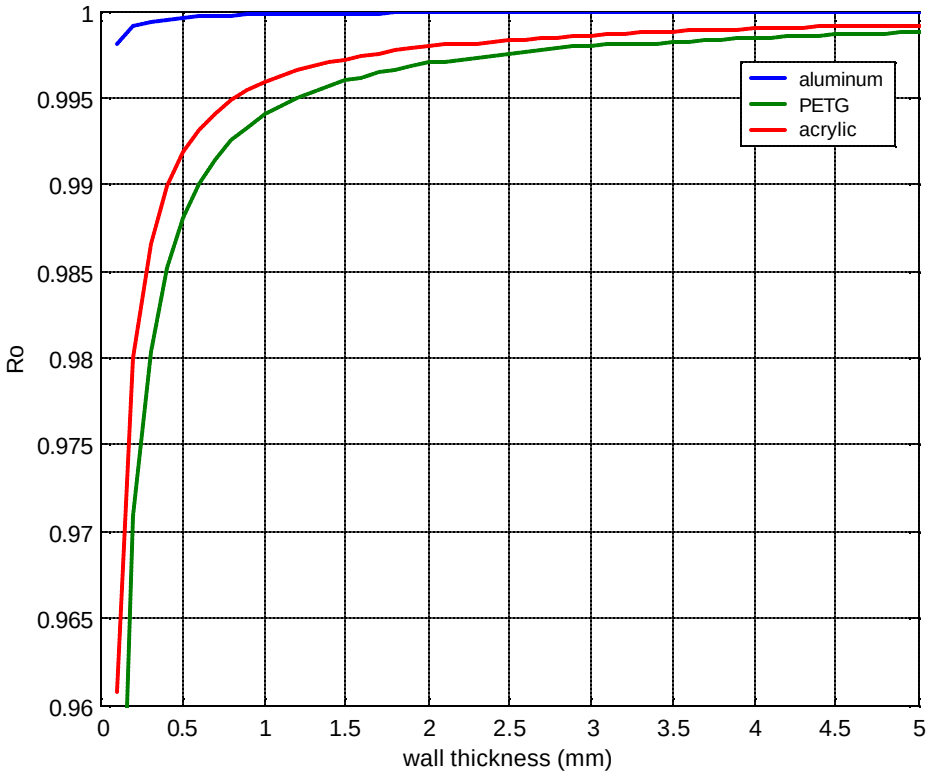

Figure 2-2. Theoretical R_o values for Helmholtz resonators of different materials. The end caps are assumed to be rigid.

2.2 Finite Element Analysis

In an attempt to investigate the effects of wall stiffness on the performance of a cylindrical Helmholtz resonator, the finite element analysis (FEA) software ANSYS was used to model a resonator. The theory derived in the previous section to express the effects of wall elasticity assumed the end caps being rigid, which gave a limited understanding of the overall structural stiffness of the cylindrical resonator. FEA provides a deeper insight for structural behavior. However, even FEA is still an approximation to the reality, because it does not incorporate damping in the model. This approximation is acceptable since the target of using FEA for this work is essentially extracting resonant frequency values and deformation shapes of the resonator. The results are not greatly affected by the damping in the system, especially when the damping ratios measured for typical Helmholtz resonators are as small as 0.05. In practice

damping is controlled in the system via a wire mesh on the neck in order to achieve desired performance.

2.2.1 Modeling

In modeling the geometry, the cylindrical neck of the resonator was located on the end cap, which resulted in symmetry in the structure and allowed the use of axisymmetric elements. This greatly reduced the computation effort, which in turn gave the opportunity to use more elements and therefore increasing the accuracy of the results. Figure 2.3 shows two samples of meshed model of the resonator with flat and hemispherical end caps. Air in the resonator was modeled by using acoustic elements and the resonator walls were modeled as solid elements. In FEA, acoustic elements have pressure as the nodal degree of freedom (DOF), whereas solid elements have translational DOFs. In order to be able to model the coupling between the air inside and the resonator walls, fluid-structure interaction (FSI) elements were used which are shown in red color in Figure 2.3. FSI elements have both pressure and translational DOFs to achieve this coupling.

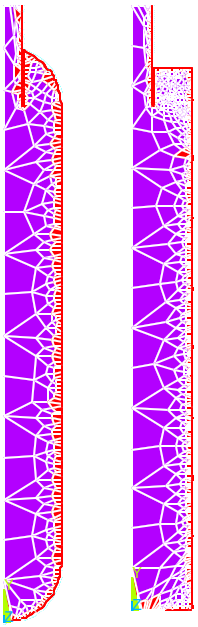

Figure 2-3. Meshed samples of axisymmetric finite element model for cylindrical Helmholtz resonators. Hemispherical and flat end caps are modeled.

In the preliminary analyses using this model, it was shown that the pressure inside the resonator does not have significant spatial variation which allowed the use of coarser meshes for acoustic elements. On the other hand, the mesh size was kept finer for solid elements, since the deformation of the resonator walls are the key in this analysis. Another reason for this is to maintain the aspect ratio close to 1 for solid elements which increases the accuracy of the computations and therefore the quality of simulation of the real structure. This refinement of the mesh size over the whole structure led to a great reduction in model size.

Air surrounding the resonator was not modeled for this case, because in ANSYS, the pressure degree of freedom of acoustic element nodes is expressed as absolute pressure relative to the atmospheric pressure. Therefore there is no pressure difference between the air in and out of the resonator in the model when the resonator is not excited. However, omitting the modeling of surrounding air discards the fact that the radiation out of the neck has an effect on the walls through the surrounding air. The radiation loading on the neck was also not included in the model. These effects were assumed to be negligible. The system was physically modeled as if a piston moving in the neck was creating a pressure in the resonator volume and wall elasticity contributing to the resonator response. The resulting pressure inside the resonator was taken as the output of the model and the frequency spectrum characteristics of the resonator were investigated using this output. The way to create the model of a piston motion in the software was to apply pressure inputs on the nodes at the mouth, and read the pressure results of an acoustic element node inside the resonator over a frequency range. Since the damping due to viscous effects around the neck is difficult to model, the system was modeled as undamped. Therefore, the peak response analysis was excluded and the scope of the investigation was limited to observe only the change in the natural frequency of the resonator. In fact, this was enough to compare the FEA results to the theory, because the R_o value, which is the measure of the change of performance of the resonator, was calculated using Equation 2.13 and is related the natural frequency.

2.2.2 Effects of different end cap shapes

Figure 2.4 shows the deformation shape of the flat-end shape resonator at resonance. It should be noted that the displayed displacements are exaggerated. This result clearly shows that

the majority of the compliance comes from the end cap. Therefore stiffening the end caps can reduce the total wall elasticity, which in turn decreases the loss of performance. For this purpose, it is possible to use stronger materials for the end caps or adding supporting bars to reduce the amount of deformation. However, these possible solutions would add significant amount of mass to the resonator keeping in mind that the resonator itself is very light. In this section, a solution to this problem is sought by investigating the cases where different end shapes having the same material as resonator walls are used. In these cases there is no additional mass, however the performance of this application compared to the rigid wall case should be analyzed to obtain the best solution.

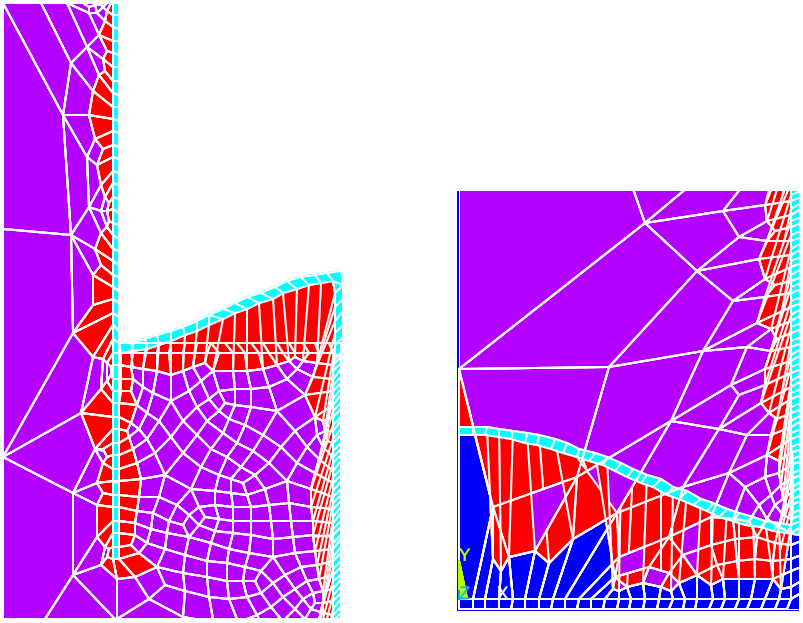

Figure 2-4. The deformation at the top end cap (left) and bottom end cap (right) of a cylindrical Helmholtz resonator. The deformation is exaggerated for easier visualization.

For this purpose, two additional end cap shapes – in addition to the flat end caps - for the resonator were selected for comparison, namely, hemispherical and thick-flat end caps. Figure 2.5 shows the inner dimensions of the resonator with each configuration. The resonator has the same volume, neck radius and length for all end cap shapes, to ensure that the natural frequencies are equal, which makes it more convenient to compare their performances relative to each other. The thickness of the thick-flat end cap was taken to be 3 times of the thickness of the wall.

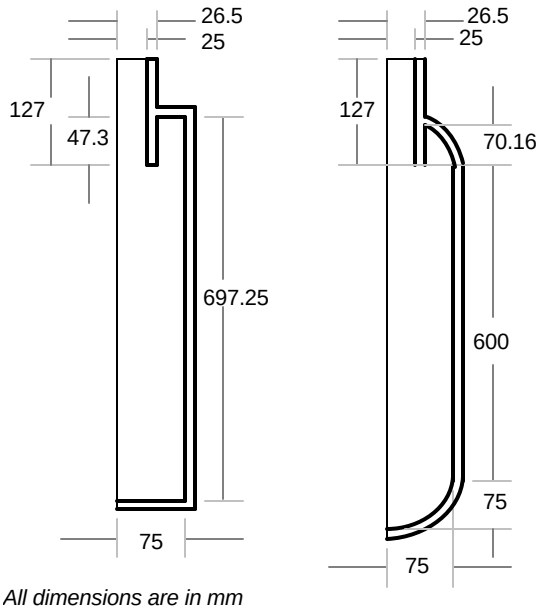

Figure 2-5. Inner dimensions of the two Helmholtz resonators modeled for FEA.

In order to compare the different end cap shapes, the model was solved by using aluminum as the wall material and the thickness of the walls were changed in the range of 0.1-5 mm. The theoretical value of the natural frequency for these resonators is calculated to be 54.37 Hz by using Equation 2.7, and the FE model gives the natural frequency as 55.07 Hz for hemispherical ended resonator and 55.00 Hz for flat ended resonators for rigid wall case. The R_o value was computed using Equation 2.13 for each case, and the results are plotted in Figure 2.6 together with the R_o value calculated theoretically from Equation 2.15.

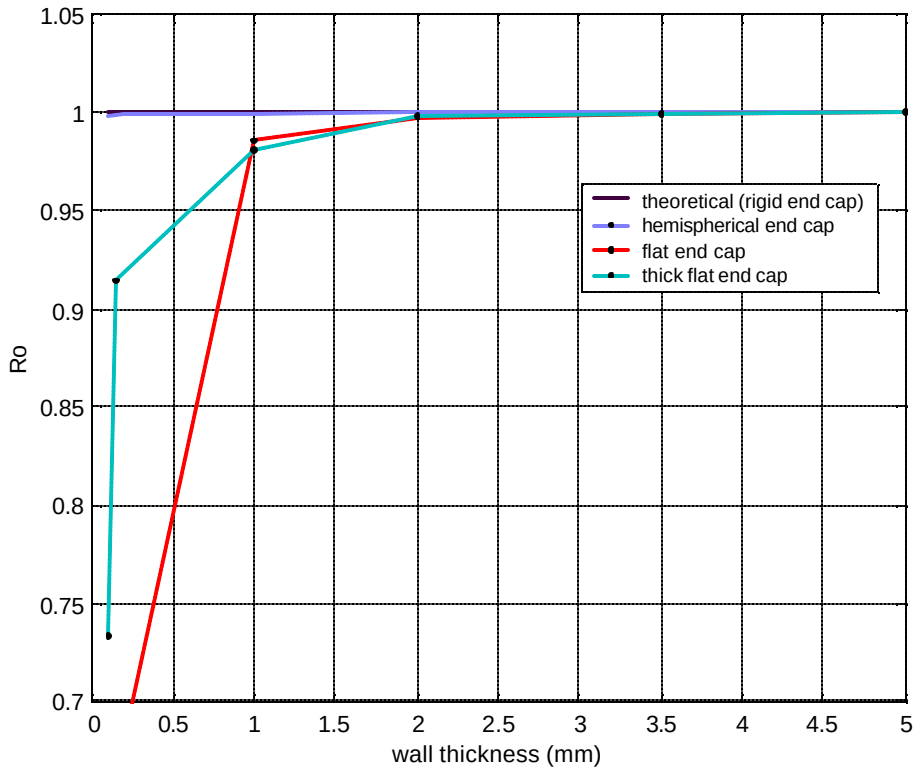

Figure 2-6. FEA results comparing R_o values for aluminum Helmholtz resonators of different end cap shapes.

It should be noted that R_o being equal to 1 means that the structure behaves as a perfectly rigid Helmholtz resonator with no loss in performance. The theory was derived assuming rigid end caps, and therefore, with this assumption, structural deformation can only occur at the cylindrical surface. However, both Figure 2.2 and Figure 2.6 show that, for wall thickness even as small as 0.1 mm, the R_o value is still 1, which means that the cylindrical side of the resonator is still rigid for small wall thickness values. Therefore all possible deformation occurs at the end caps for a cylindrical Helmholtz resonator.

Figure 2.6 also shows that hemispherical end caps perform almost as well as rigid end caps, which makes them very efficient for this application. Thick flat end caps performs better than the thin flat end cap, as expected, however there is significant difference between the performance of these two and the hemispherical end cap case. As a comparison, for a wall thickness of 0.5 mm, the peak values of the output of the resonator relative to the rigid wall case are 75%, 94% and 100% for flat, thick-flat and hemispherical end caps, respectively.

Hemispherical end caps perform successfully even for a thickness of 0.1mm, therefore, at this stage by using hemispherical end caps, only limitation to building lighter Helmholtz resonators is the manufacturability of such thin plates and maintaining their shape undeformed while handling. In terms of wall rigidity, the ideal shape for a Helmholtz resonator is a sphere, however, assuming a sphere is perfectly rigid, it is shown in the previous discussion, cylindrical resonators with hemispherical end caps can provide stiffness as good as spherical resonators. In addition, the advantage of cylindrical resonator on spherical resonator is its practicality of implementation because of its shape. For instance, for this application one dimension of the resonator should be less than 15 inches and cylindrical resonators are well suitable for this case.

2.2.3 Effects of different wall materials

Using lighter materials in additional to using thinner walls is the other way to reduce the total weight of a resonator. For this purpose, comparison of the performances of different wall materials is made in this section by using three different wall materials: aluminum, acrylic and Polyethylene Terephthalate Glycol (PETG). The properties of these materials can be found in Table 2.1.

Table 2-1. Material properties of aluminum, acrylic and PETG used in the FE model

	Aluminum	***Acrylic***	***PETG***
Density (kg/m^3)	2700	1180	1270
Young's Modulus (Pa)	7.1x10^{10}	2.93x10^9	2.067 x10^9
Poisson's Ratio	0.33	0.4	0.36

Performance comparison of these materials is made by solving the flat ended resonator model separately for different wall materials, and the resulting R_o values for each resonator of different material are plotted in Figure 2.7. Flat end caps are used in order to be able to show the difference more clearly, because they provide less structural stiffness compared to hemispherical end caps. It can be seen that the stiffness of the resonator mainly depends on the modulus of elasticity of the material as predicted before in Equation 2.15.

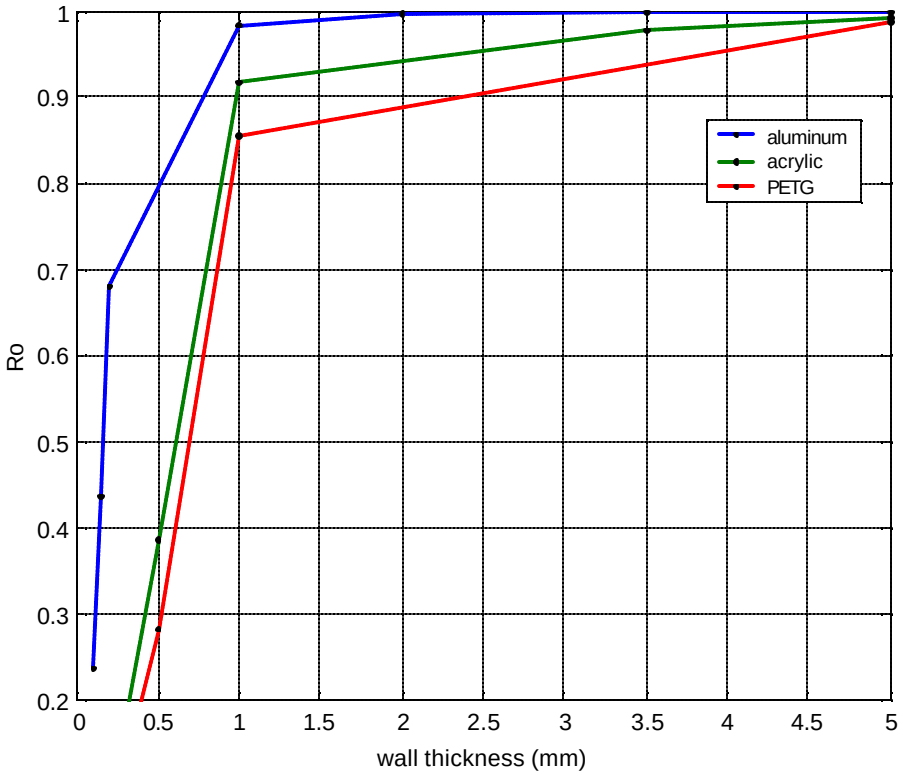

Figure 2-7. FEA results comparing R_o values for flat-end cap Helmholtz resonators of different wall materials.

Figure 2.8 summarizes the results of using different materials and end shapes. For aluminum, hemispherical end cap provides almost no performance loss; meanwhile, thick flat end cap and flat end cap have performance of 94% and 80%, respectively, for a wall thickness of 0.5 mm. As the wall thickness decreases, the difference in the performance between different end cap cases increases. Another significant result of this analysis is that, for hemispherical end cap case, the performance of resonators with the three different wall materials are within 2%. This shows that even used with different materials, hemispherical end caps still provide good performance. The theoretical results of Figure 2.2 (which assumes rigid end caps) are the same as the FE results of Figure 2.7 (which has hemispherical end caps), which is another indication of the very good performance of hemispherical end caps.

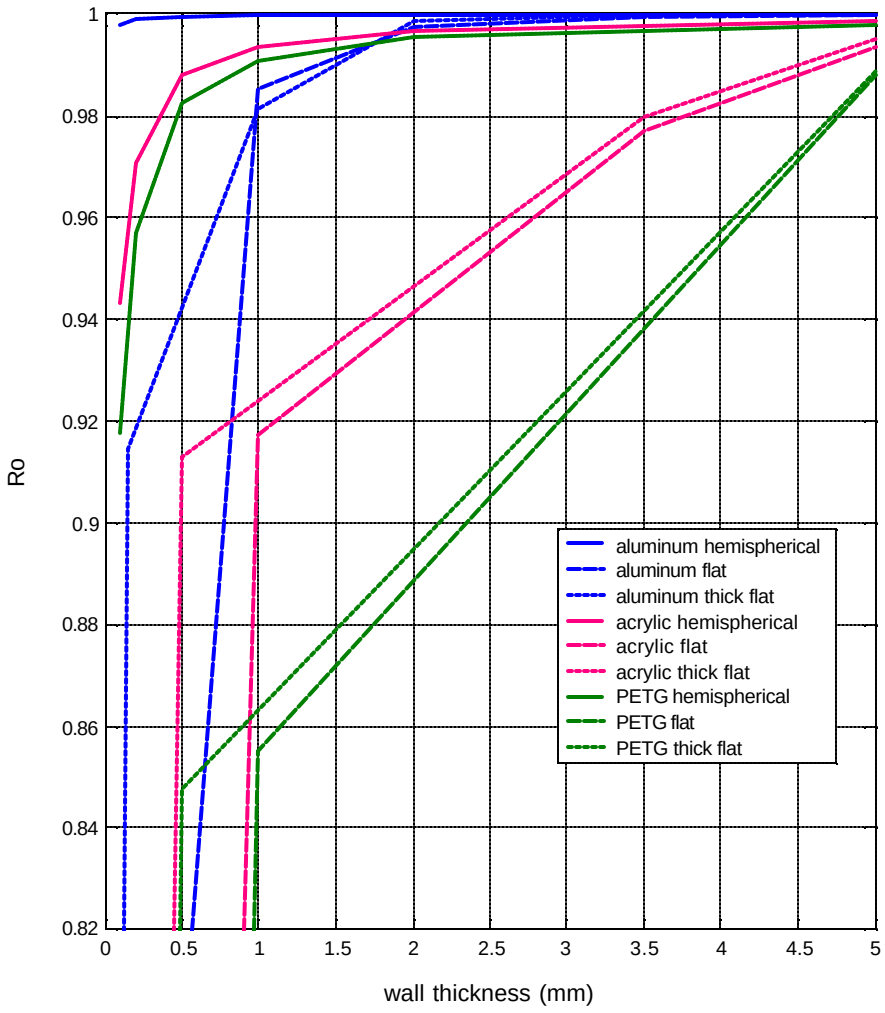

Figure 2-8. Summary of FEA results comparing R_o values for Helmholtz resonators of different wall materials and end caps shapes.

2.2.4 Weight Considerations

After the investigation of the performance of a cylindrical Helmholtz resonator for different wall materials and end cap shapes, these results should be combined with the weight considerations, in order to be able to examine the possibility of designing the resonator as light as possible and yet having adequate performance. For this purpose, the mass of a single resonator with the dimensions given in Figure 2.5 is calculated for different thickness values using the densities of the three different materials. Figure 2.9 shows these results together with R_o values

for the hemispherical end cap case, since this case provides the highest structural stiffness, and hence the best performance.

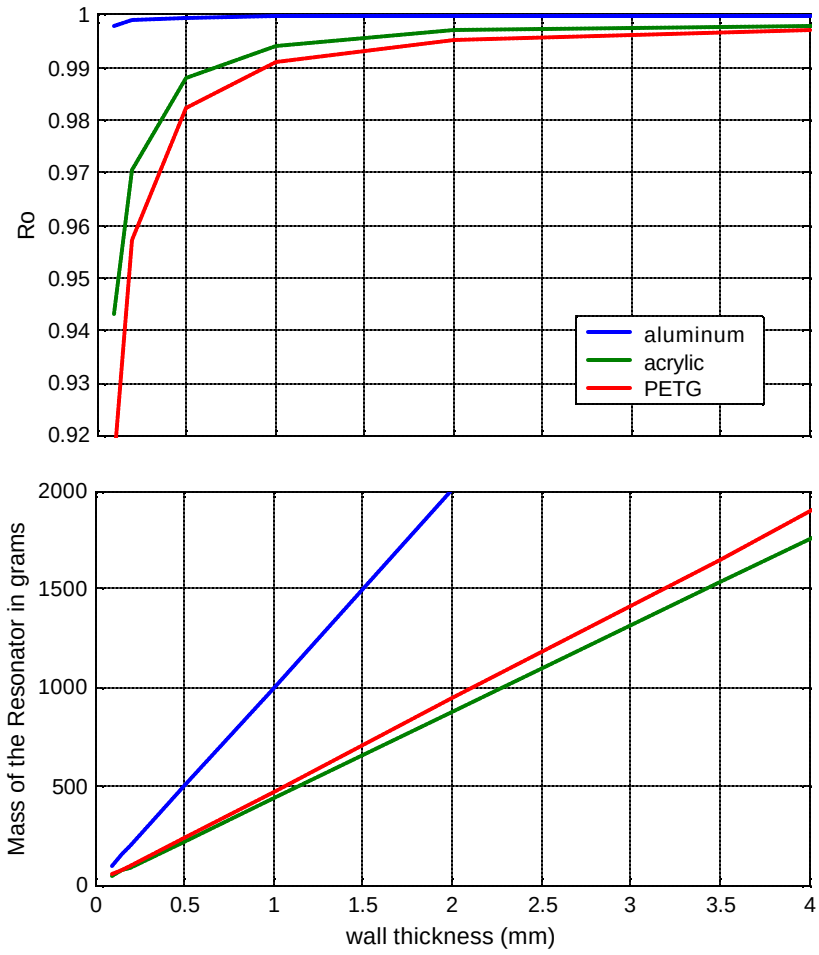

Figure 2-9. FEA results giving R_o values and individual masses for hemispherical-end cap cylindrical Helmholtz resonators of different wall materials.

Using aluminum as wall material gives almost perfect stiffness, however it adds relatively high mass to the resonator. On the other hand, by using acrylic or PETG walls the total weight of the resonator can be kept significantly low, but the output of the resonator also reduces. At wall thickness of 0.5 mm, the loss of performance for using PETG or acrylic is within 2% relative to using aluminum, which is reasonable, and the weight reduction is almost 50%. Therefore, it can be concluded that this is a trade-off between choosing the criterion that is

more important for the type of application. For this case, the savings in resonator mass is much more valuable than the small loss in performance.

2.3 Testing Helmholtz Resonators

Helmholtz resonators were tested in the Vibration and Acoustics Labs of Virginia Tech before finalizing the design that will be implemented in the full scale fairing at the Boeing facilities in Huntington Beach California. Two different wall materials, cardboard and PETG, were used in order to be able to compare the stiffness of the structures and its effect on performances.

2.3.1 Test Setup

Figure 2.10 illustrates the test setup. The resonators are covered with melamine foam, because this is the configuration that will be used in the final installation. Three speakers were used to excite the resonator with white noise in the 63 Hz and 80 Hz third octave bands. The transfer function between the two microphones, one placed inside the resonator and the other placed on a stand right above of the mouth of the neck, was measured to evaluate the resonator performance.

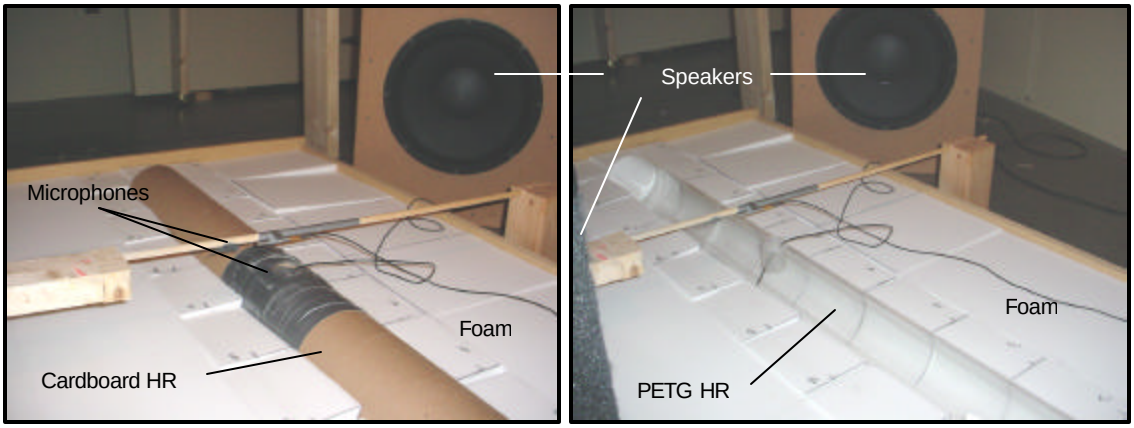

Figure 2-10. Test setup for performance measurement of Helmholtz resonators.

Two different sizes of resonators were used and dimensions of these two configurations are illustrated in Figure 2.11. The thickness of the PETG walls is 0.025".

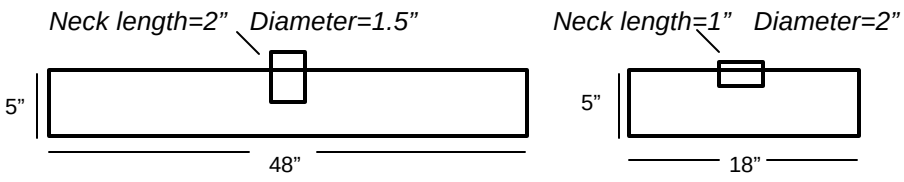

Figure 2-11. Configuration#1 (left) and configuration#2 (right) of Helmholtz resonators tested.

2.3.2 Test Results

Figure 2.12 shows the measured transfer functions for the cardboard and PETG resonators of the first configuration. The blue curve represents the measured data and the fitted curve is in green. The measured natural frequencies of the cardboard and PETG resonators are 50.8 Hz and 49.3 Hz, respectively. In comparison, the theoretical value of the natural frequency (calculated by using Equation 2.7) for this case is 51 Hz. The measured damping ratios are 0.057 and 0.081, respectively. The peak values for the two cases are slightly different which is due to the difference in the damping of the two resonators. This can be compensated by adjusting the damping of the resonators by applying a wire mesh in the throat opening. The cardboard resonator weighs 1.6 kg, whereas, the PETG resonator weighs 0.47 kg. The cardboard resonator can be assumed to be close to perfectly rigid, and the performance of the PETG resonator is almost the same as the cardboard resonator and it is more than 3 times lighter.

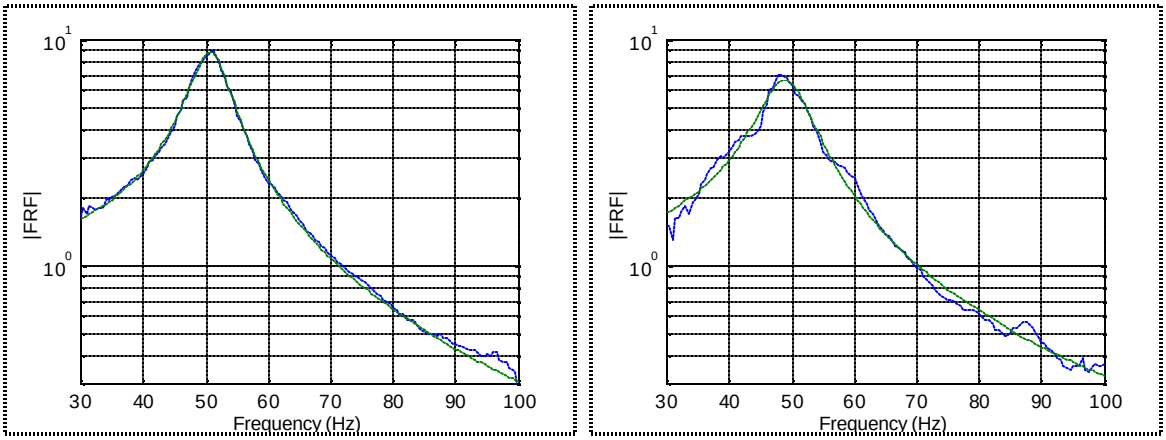

Figure 2-12. Measured transfer functions (blue curves) between the internal and external microphones for cardboard (left) and PETG (right) Helmholtz resonators of configuration#1, and the fitted curves (green curves).

Figure 2.13 shows the measured frequency responses for the second set of resonator dimensions shown in Figure 2.11. The measured natural frequencies are closer to each other in this case: 137.5 Hz for the cardboard resonator and 137.4 Hz for the PETG resonator. The measured damping ratios are 0.039 and 0.022, respectively. In this case, PETG resonator is lightly damped, causing the peak to be relatively sharper, which again can be adjusted by using wire mesh at the throat opening. The cardboard resonator is 0.6 kg, and PETG resonator is 0.2 kg. For this configuration, the performances of the two resonators are very similar to each other, and the difference in weights of the resonators is again large.

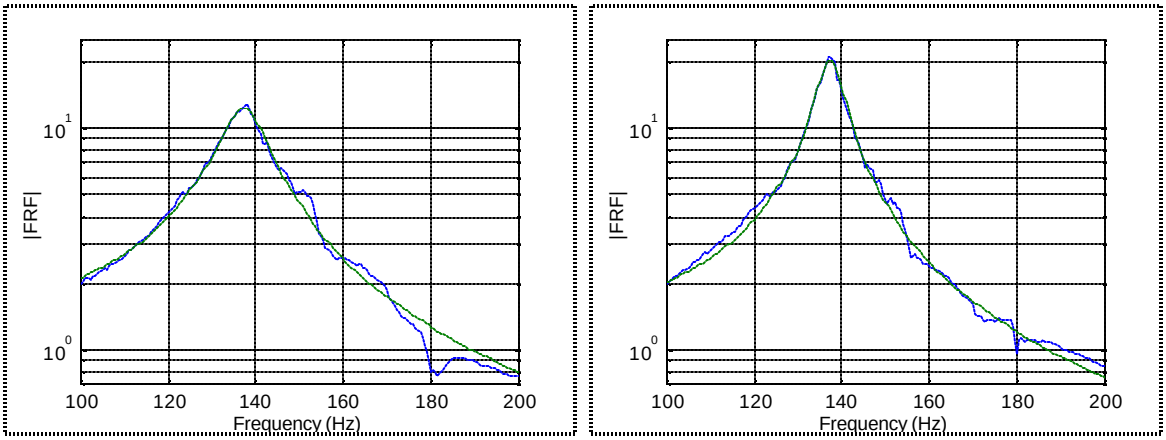

Figure 2-13. Measured transfer functions (blue curves) between the internal and external microphones for cardboard (left) and PETG (right) Helmholtz resonators of configuration#2, and the fitted curves (green curves).

White thick plastic flat end caps were used for the PETG resonators and the first configuration of resonator weighs 470 grams. However by using hemispherical end caps with the same thickness as cylindrical walls, the resonator would weigh 410 grams, which is 13% lighter than the one tested. On the other hand the performance of the hemispherical end cap resonator would be even better which was shown in finite element analysis where hemispherical end caps were stiffer than the thick flat end caps. As a conclusion, the tests agreed with the finite element analysis results in the sense that great weight reductions are possible by using thin and light walls for Helmholtz resonators without loosing performance which is directly related to the stiffness of the resonator structure. Even lighter Helmholtz resonators can be built by using thinner composite materials, and the only limitation for those designs would be the manufacturability of the parts.

2.4 Passive Control Tests

The passive control tests that were conducted on a full scale fairing model at Boeing facilities in Huntington Beach California utilized DVAs and lightweight Helmholtz resonators. Lightweight HRs used in these tests were designed at VAL by using the results of the analyses discussed previously in this chapter. Due to the time and cost restrictions at the Boeing facilities, individual effects of the acoustic devices were not tested, instead, an overall performance of the hybrid system using one set of test configuration was evaluated. Therefore it was difficult to validate the results of previous wall elasticity discussions for lightweight HRs using these tests on the full-scale model. However, this final lightweight design performed well together with the DVAs.

2.4.1 Test Setup

Passive control tests using Distributed Vibration Absorbers (DVAs) and Helmholtz resonators were conducted on the full-scale fairing which is shown in Figure 2-14. The fairing measures 14.3m in height and 5m in diameter, and it has a volume of 212m^3, surface area of 200m^2 and mass of 1600Kg. The lightweight Helmholtz resonators designed in VAL at Virginia Tech were used in these tests. However, the test setup also included the DVAs and acoustic blankets, thus, the individual performance of Helmholtz resonators are difficult to evaluate. The acoustic blankets are effective above 110 Hz, therefore they do not interfere with the performance of DVA and HR combination.

Figure 2-14. Picture of the test fairing together with the speakers providing external disturbance.

For these tests two different sizes of Helmholtz resonators were used: 149 resonators of 40 inches long, weighing 440 grams each; and 63 resonators of 22 inches long, weighing 260 grams each. Both of these sets had various neck diameter and length values, yielding different natural frequencies in order to be able to target different acoustic modes inside the cylinder. Figure 2-15 shows the final design of the Helmholtz resonators. The stiffeners were added to the structure in order to prevent breathing deformation of the cylindrical part and maintain structural stiffness, thus performance.

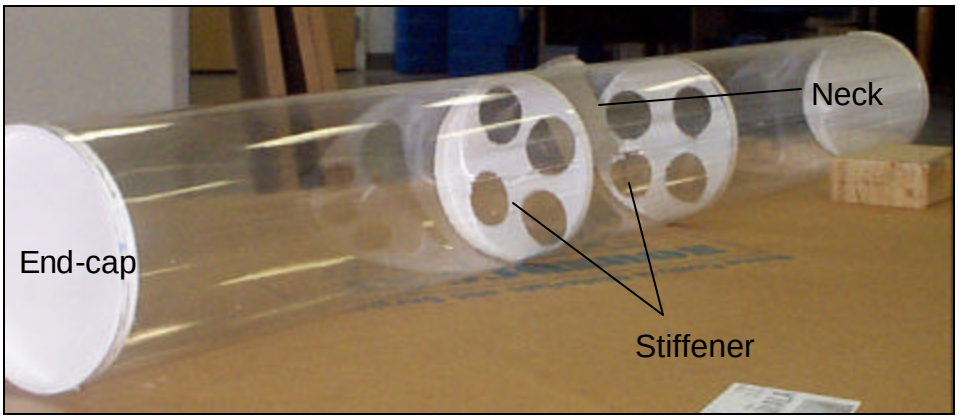

Figure 2-15. Final design of Helmholtz resonators.

The resonators weigh 82Kg in total and they contribute 4.5% to the mass and 1.1% to the volume of the fairing. The internal sound level was measured by 30 microphones, positions of which were changed three times during the measurements to give SPL readings at 90 different locations inside the cylinder.

2.4.2 Test Results

The resonators damped the noise peaks, reducing two peaks by 5dB and 10dB. The overall attenuation from 30-90Hz is 3.2dB. A maximum of 5.2dB is obtained in 31.5Hz third octave band. Attenuation of 1.1dB, 3.6dB, 4.2dB and 2dB were obtained in the 40Hz, 50Hz, 63Hz, and 80Hz third octave band, respectively. For proprietary reason the acoustic performance of the treatment cannot be shown in this thesis.

The Helmholtz resonators used in these tests have thick flat plastic end caps. However, the analyses given previously in this chapter yields a 13% decrease in mass of a single resonator when hemispherical end caps are used. Therefore, in this application of HRs on the full-scale fairing, the contribution of HRs with hemispherical end caps to the total mass of the fairing would be 3.9%. The performance of these HRs were proved to be similar to the perfectly rigid HRs previously in this chapter using both finite element analysis and experimental comparisons.

Chapter 3: Lightweight Loudspeakers

There are several types of acoustic actuators working on electrostatic, electromagnetic, piezoelectric and magnetostrictive principles. However, conventional moving-coil loudspeakers are the most common acoustic actuators used in engineering applications because of their low-price and relatively high efficiency. For noise control applications, high frequency noise problems can be solved by using passive devices such as acoustic blankets, however this solution is not effective at low frequencies, for which active noise control (ANC) can be applied. In ANC, there are two paths for controlling noise: attenuating the vibrations of the structure that creates the noise, and driving the acoustic field directly in order to attenuate the noise. For the second path, moving-coil loudspeakers play an important role since they are even more efficient at low frequencies relative to the newly-developed lightweight acoustic actuators such as electrostrictive polymer films and piezoelectrically driven speakers. However, the drawback of using moving-coil loudspeakers is that they are heavy and bulky, which makes them unsuitable for the applications where weight is an important consideration such as in aerospace applications. On the other hand, significant reductions in the weight of a loudspeaker and its enclosure are possible and this will be the subject of this chapter. For this purpose, a standard 12" Pioneer loudspeaker was taken as the reference, and weight reduction solutions were sought by re-designing it using the results of loudspeaker characterization.

3.1 Loudspeaker Characterization

Loudspeakers, as devices converting electrical energy into acoustic energy, have simple working principles. Figure 3.1 illustrates the components of a typical loudspeaker. A diaphragm and a voice coil are connected to each other forming the moving parts of a loudspeaker. This moving assembly is attached to a stationary frame by a spider and a surround, which provide stiffness and damping to the system. Loudspeakers are also attached to a box from behind to baffle the loudspeaker (increasing their output) and the box also provides extra stiffness to the system. The driving force that excites the voice-coil and the diaphragm to move is created by the magnetic interaction between a magnet assembly and the voice coil. The magnet assembly is

composed of a permanent magnet and surrounding permeable material (yoke) to complete the magnetic loop. An air gap in the magnetic loop, through which the voice coil can move, is arranged to have maximum magnetic flux. An input voltage applied to the terminals of the voice coil initiates a current flowing through the coil. This current in the magnetic field of the magnet assembly creates a force between the voice coil and the magnet assembly. The magnetic force is on the plane that is perpendicular to the plane spanned by the current and magnetic field vectors. Since the magnet assembly is stationary, the voice-coil moves together with the diaphragm in the direction of the resultant magnetic force. The motion of the diaphragm excites the mass of air in contact with the diaphragm surface and as a result sound is created. Therefore, the motion of the diaphragm can be controlled by alternating the input voltage to the voice coil in order to obtain the desired sound pressure output. This is basically how moving coil loudspeakers work.

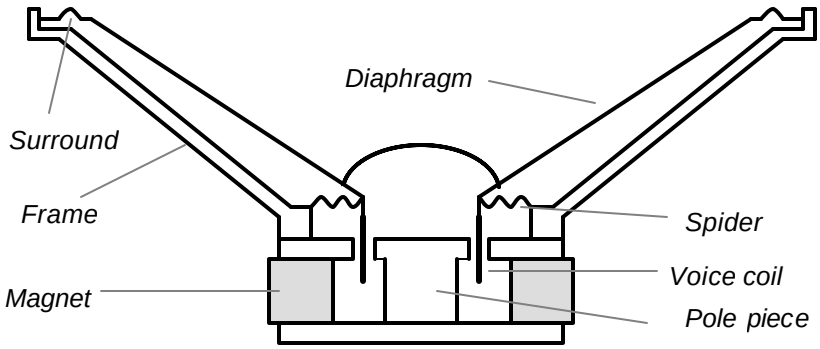

Figure 3-1. Components of a typical permanent-magnet moving voice-coil loudspeaker.

In order to derive the equations that relate the electrical input of the loudspeaker to the mechanical output, the loudspeaker system can be characterized in mechanical, electrical and acoustic terms separately. The force on the voice coil due to the current applied relates the electrical part of the characterization to the mechanical part, whereas the interaction between the diaphragm surface and the air in front of it connects the acoustical part of the characterization to the mechanical part.

3.1.1 Mechanical Characterization

The dynamics of a loudspeaker together with its enclosure can be modeled as a single degree of freedom mass-spring-damper system. The diaphragm, the voice coil and the air load

(or the acoustic radiation component) on the diaphragm all together represent the mass M. The total stiffness of the surround and the spider k_s, and the suspension due to the air in the enclosure k_b together represent the total stiffness. The total damping b is due to the surround and the spider. Figure 3.2 illustrates the mechanical model of a loudspeaker. The force on the voice coil F is the product of the magnetic field B, the voice coil length l and the voice coil current i.

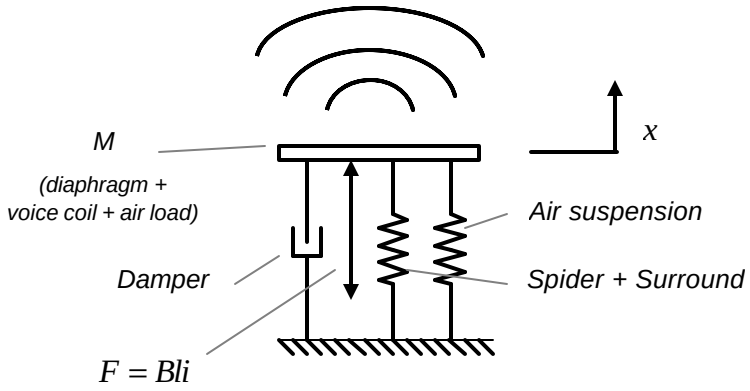

Figure 3-2. Mechanical model of a loudspeaker.

Therefore the transfer function between the voice coil current and the diaphragm displacement can be found through an equation of motion for the mass M as

$$\frac{X(w)}{I(w)} = \frac{Bl}{\left(-w^2 M + jwb + k_S + k_B\right)} \tag{3.1}$$

At low frequencies, the equation for the total air load on both surfaces of the diaphragm of radius a and area S is given by [45]

$$m_r = 2\rho_o S(8a/3\pi) \tag{3.2}$$

where ρ_0 is the density of air.

3.1.2 Electrical Characterization

Figure 3.3 illustrates the electric circuit that represents the electrical characterization of a loudspeaker. When the voice coil starts moving in the magnetic field with a velocity v, a current flow in the opposite direction is also induced, which creates a back electromotive force (e.m.f) Blv. The effect of the e.m.f. is to add damping to the system, which is included in the electric circuit equation.

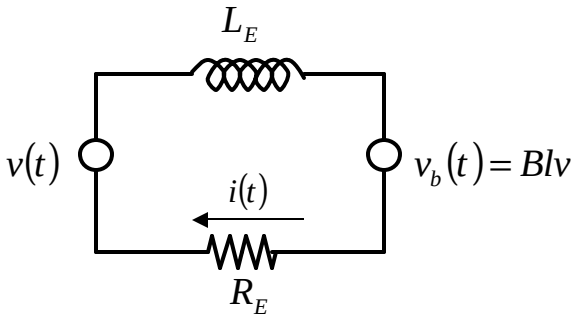

Figure 3-3. Electrical model of a loudspeaker.

The ratio of the resistance R_E to the inductance L_E of a loudspeaker is generally high enough such that the loudspeaker can be considered to be resistive at low frequencies. Therefore the inductance of the loudspeaker, together with the effects of eddy currents, is ignored, which leads to the following equation for this electric circuit:

$$V(w) = I(w)R_E + BlU(w) = I(w)R_E + jwBlX(w) \tag{3.3}$$

Combining Equations 3.1 & 3.3 gives the following transfer function between the input voltage to the voice coil and the displacement of the diaphragm:

$$\frac{X(w)}{V(w)} = \frac{\left(\frac{Bl}{R_E}\right)}{-w^2M + jw\left(b + \frac{B^2l^2}{R_E}\right) + (k_S + k_B)} \tag{3.4}$$

3.1.3 Acoustic Modeling

To compute the acoustic output of a loudspeaker for a given voltage input to the voice coil, an acoustics relation for the sound pressure due to the diaphragm motion should be derived. The loudspeaker having a diaphragm of radius a can be considered as a monopole with source strength

$$Q = pa^2U \tag{3.5}$$

where U is the magnitude of diaphragm displacement. The expression for the amplitude of sound pressure at a distance r due to a simple source is given by the following equation [45] as

$$P(r) = \frac{1}{4r} w r a^2 U \tag{3.6}$$

Modifying the equation in order to express it in terms of the diaphragm displacement gives

$$P(r,w) = \frac{r w^2 a^2}{4r} X(w) \tag{3.7}$$

Combining Equations 3.4 & 3.7 yields the transfer function between the voltage applied to a loudspeaker and the sound pressure at a distance r :

$$\frac{P(w)}{V(w)} = \frac{-w^2 r \left(\frac{a^2}{4r}\right)\left(\frac{Bl}{R_E}\right)}{-w^2 M + jw\left(b + \frac{B^2 l^2}{R_E}\right) + (k_S + k_B)} \tag{3.8}$$

3.1.4 Magnetic Field B in the Air Gap

As will be discussed later in this chapter, magnet assembly contributes significantly to the total mass of a loudspeaker. Therefore, the effects of the properties and dimensions of the magnet assembly on loudspeaker dynamics should be well-understood especially when weight saving solutions without loss of loudspeaker performance need to be found. The magnetic field B at the air gap created by the permanent magnet is a significant factor in this sense, because its magnitude directly influences motor strength (Bl) of the loudspeaker. Therefore, expressions for the magnetic field B were derived using elementary electromagnetism theory.

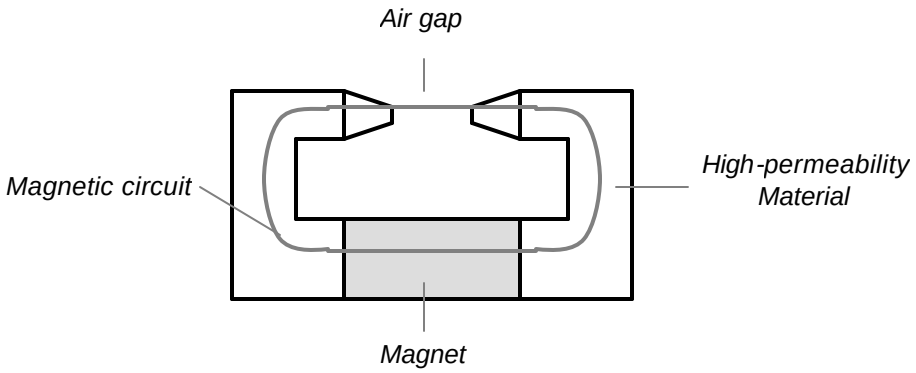

Figure 3-4. Sample magnetic loop for computing the magnetic field in an air gap.

Figure 3.4 shows a simple magnetic loop where the magnetic field created by the magnet passes through the yoke (composed of the pole piece, back & front plates) and through the air gap completing the loop. The permeability of the yoke material is much greater than that of the air gap, which also means that it has negligible reluctance; thus the influence of the yoke material on the magnetic circuit equations is neglected. Therefore the expression for the magnetic field at the air gap is given by:

$$B = \sqrt{-\frac{\mu_o (BH)_m V_m}{V_g}} \tag{3.9}$$

where μ_o is the permeability of free space ($\mu_o = 4\pi \times 10^{-7} H/m$), $(BH)_m$ is the energy product of the magnet in J/m^3, V_m is the volume of the magnet, and V_g is the volume of the air gap.

Therefore, keeping the air gap volume constant, using a small volume of a powerful magnet would reduce the weight of the magnet assembly, while maintaining the motor strength.

3.1.5 Simulation of Loudspeaker Performance

Knowing the transfer functions and the value of the magnetic field in the gap, performance of a standard 12" Pioneer loudspeaker was numerically simulated over a frequency range. Some practical limitations, such as maximum voltage and current on the voice coil and maximum diaphragm displacement, were included in the computer code in order to be able to obtain more accurate and realistic results. Figure 3.5 illustrates the simulation results as sound pressure level output (SPL, referenced to 20×10^{-6} Pa) 1 m away from the diaphragm with 1 Volt-rms voltage input to the loudspeaker at every frequency together with the corresponding transfer function.

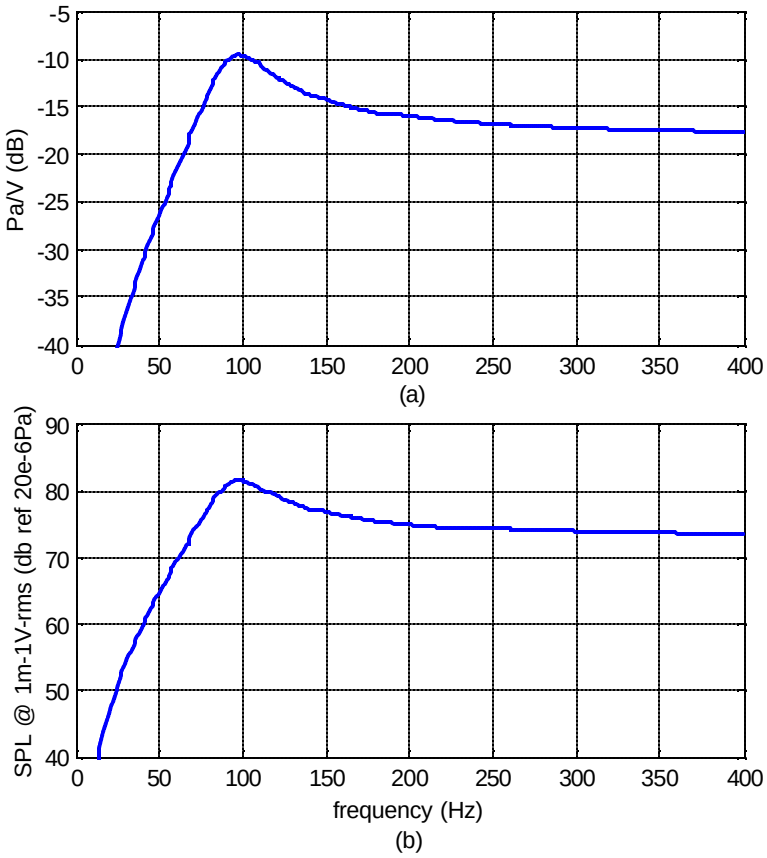

Figure 3-5. Performance of the standard 12" Pioneer loudspeaker. (a) Transfer function between the input voltage and output pressure at 1m. (b) SPL output at 1m with 1V-rms input.

3.1.6 Effects of the Motor Strength

The product of the magnetic flux density B, and the voice coil wire length l, gives what is called 'motor strength' (Bl, units: Newtons/Amper). This value is a characteristic of magnet assemblies and greatly affects the dynamics of a loudspeaker. As can be seen from Equation 3.4, changing the motor strength would change both the gain of the transfer function between the input voltage to the loudspeaker and the displacement of the diaphragm, and the damping in the system. As a comparison, the numerical simulation mentioned in the previous section was used to compute the output of the standard 12" Pioneer loudspeaker varying motor strength values, and the results are shown in Figure 3.6.

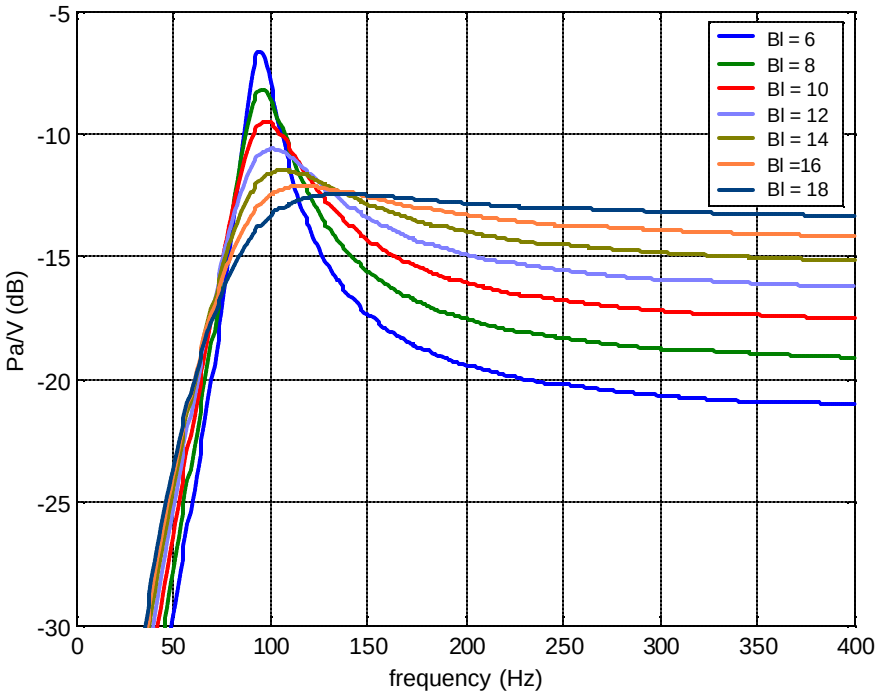

Figure 3-6. Variation of performance with motor strength for the standard 12" Pioneer loudspeaker.

Increasing the motor strength means increasing the force applied on the diaphragm which provides more acoustic output. However the drawback is an increase in damping which tends to lower the output curve at frequencies close to the natural frequency. Small values of motor strength tend to yield higher acoustic output around the resonance peak and lower acoustic

output at higher frequencies. Resonant behavior should be avoided in loudspeaker design. Therefore, a reasonably damped loudspeaker with sufficient acoustic output should be designed. In this sense, a flat response over the frequency of interest is favorable. For example, for a bandwidth of 60-200 Hz, motor strength values of 14 to 18 N/A give appropriate curves as can be seen in the figure.

3.2 Weight Reductions

In order to able to create an approach to the problem of how to reduce the weight of a standard loudspeaker, weight contributions of each component of the loudspeaker should be known first. As can be seen in Table 3.1, the magnet assembly contributes the most to the weight of a loudspeaker. Since the loudspeaker is used together with the enclosure, weight reduction solutions for the loudspeaker box should also be sought.

Table 3-1. The weight contributions of each component of the 12" Pioneer loudspeaker (Model: A30GU30-55D).

Component	Weight (g)
Magnet	852
Magnet assembly (magnet + yoke)	2380
Moving parts (voice coil + diaphragm)	61
Frame (including moving parts)	685
Total	3065
1 ft^3 box (using ½" plywood)	2753

In conventional loudspeakers, ferrite magnets, which are not magnetically too powerful, are used because of their low price. Therefore, a larger volume of magnet is needed in order to achieve strong magnetic field in the air gap (from Equation 3.9). This also requires the use of a larger yoke, which also contributes to the weight significantly. The most reasonable solution to this problem is using rare-earth magnets (NdFeB), which can be more than 10 times more powerful than a ferrite magnet. (Maximum energy product of a ferrite magnet is around 2-4 MGOe, whereas NdFeB magnets can reach up to 50 MGOe). Therefore, much less volume of a

rare-earth magnet would create the same magnetic field as a standard ferrite magnet does. Another component that has a considerable amount of weight is the frame. For this loudspeaker, the frame is composed of steel plates which can be replaced by a lighter metal for weight reduction, such as aluminum. The loudspeaker box is another heavy component, and using a lighter material can lead to great weight reductions.

The approach that was used in obtaining a lightweight loudspeaker was using the 12" Pioneer loudspeaker as the reference, and then designing a new loudspeaker of almost equal performance and with maximum weight reduction. This would be accomplished by maintaining the motor strength Bl of the new design as close as to that of the reference loudspeaker. In addition, the same diaphragm is used to ensure that the dynamics of the loudspeakers are as close as possible to each other. As a summary, the approach to reducing the weight of this loudspeaker can be divided into three steps:

i. Using a rare-earth magnet, which would reduce the volume of the whole magnet assembly (both the magnet and the yoke) without changing the magnetic field in the gap
ii. Using a lighter material for the frame (e.g. aluminum)
iii. Using a lighter material for the speaker box (the overall stiffness of the box must be maintained so that performance is not lost)

3.2.1 Magnet Assembly

The conventional magnet assembly for a loudspeaker was shown in Figure 3.1. Introducing the powerful NdFeB magnet and mounting it at the center of the magnet assembly further reduces the weight. Figure 3.7 shows the new configuration for the magnet assembly.

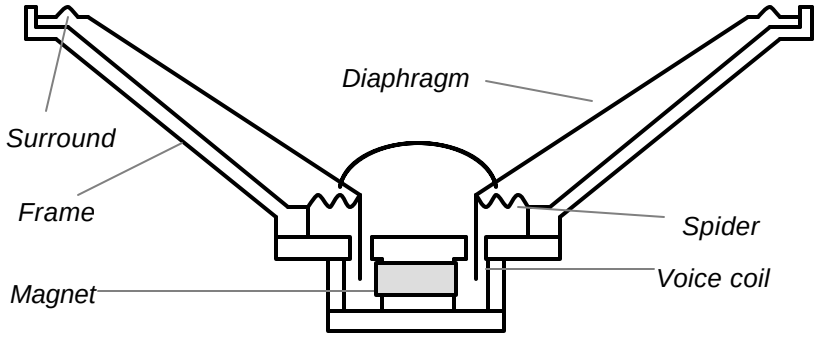

Figure 3-7. Components of the lightweight loudspeaker. The design is based on the standard 12" Pioneer loudspeaker.

At this point the aforementioned computer code for computing the performance of a loudspeaker can be modified and used to find the optimum size for the disc magnet. There are several factors affecting the output of a loudspeaker and therefore following assumptions were made in order to reduce the variables in the analysis:

i. Size and weight of the diaphragm are kept constant
ii. Thickness of the yoke material is equal to that of the air gap, and only its radius changes with the radius of the magnet changing
iii. The voice coil has constant height and number of layers, therefore its length only changes with the radius of the magnet changing

With these assumptions, the dimension of the disc magnet is the only factor that can change the output of the loudspeaker and weight of the magnet assembly. Therefore, the only two independent variables are the radius and the height of the disc magnet. A computer code was written for various values of these two variables in order to evaluate their effects on both the output of the loudspeaker and the weight of the magnet assembly.

Figure 3.8 shows the mass of the magnet assembly for various magnet dimensions. The code was written so that values larger than 1 were cut off in order to be able to emphasize the small values on the graph. Compared to the magnet assembly mass of the reference Pioneer loudspeaker (2.254 kg), great reductions in mass can be achieved by just using the magnet as small as possible. However, this is not practical, because the ratio of the air gap size to the magnet assembly size should be kept small to ensure that the assumptions made using the electromagnetic theory still hold.

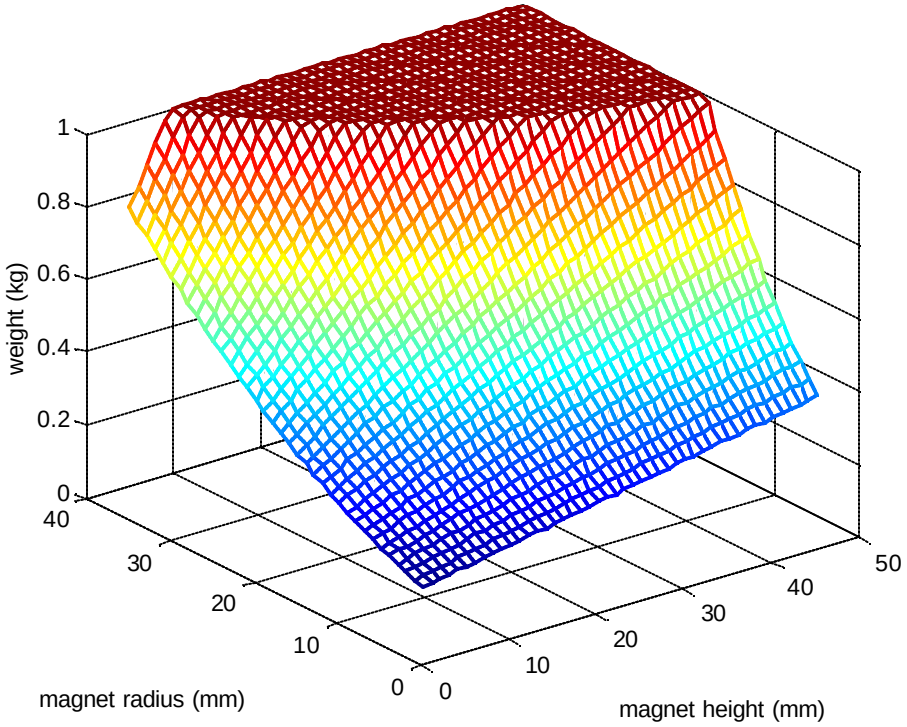

Figure 3-8. Total mass of the magnet assembly for different disc magnet sizes.

For the analysis on loudspeaker performance over a certain frequency range for various magnet sizes, a performance criterion is needed. For this purpose, power output of the loudspeaker can be averaged over the frequency range of interest. This can be done using the following formula giving an equivalent sound pressure level L_{eq}:

$$L_{eq} = 10\log\left(\frac{\sum_{i=1}^{n} 10^{\frac{SPL_i}{10}}}{n}\right) \tag{3.10}$$

This equation basically sums the squares of the sound pressure output (SPL_i) of the loudspeaker over n frequency points and averages them. Figure 3.9 shows the equivalent SPL output (1V-rms input at 1m) of the loudspeaker over the low frequency range 60-200 Hz for different values of magnet dimensions.

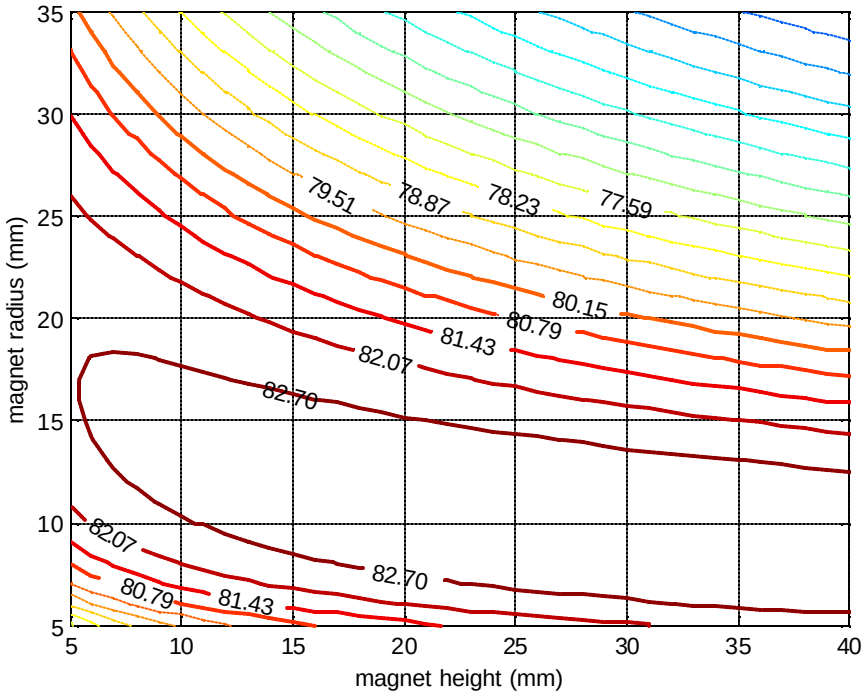

Figure 3-9. Equivalent SPL over 60-200 Hz (@ 1m-1V-rms) of the loudspeaker for various magnet sizes.

The peak value for the equivalent SPL occurs at $r = 9mm$ and $h = 40mm$ and equals to 83.3 dB. Figure 3.10 shows the SPL output and the transfer function for the loudspeaker with these dimensions. In comparison, this value for the reference Pioneer loudspeaker was computed to be 80.8 dB.

The magnet assembly with the maximum equivalent SPL value will weigh more relative to the smaller dimensions according to Figure 3.8. The comparison of acoustic output with the total loudspeaker weight will be made later in this chapter after including the weight contributions of frame and box.

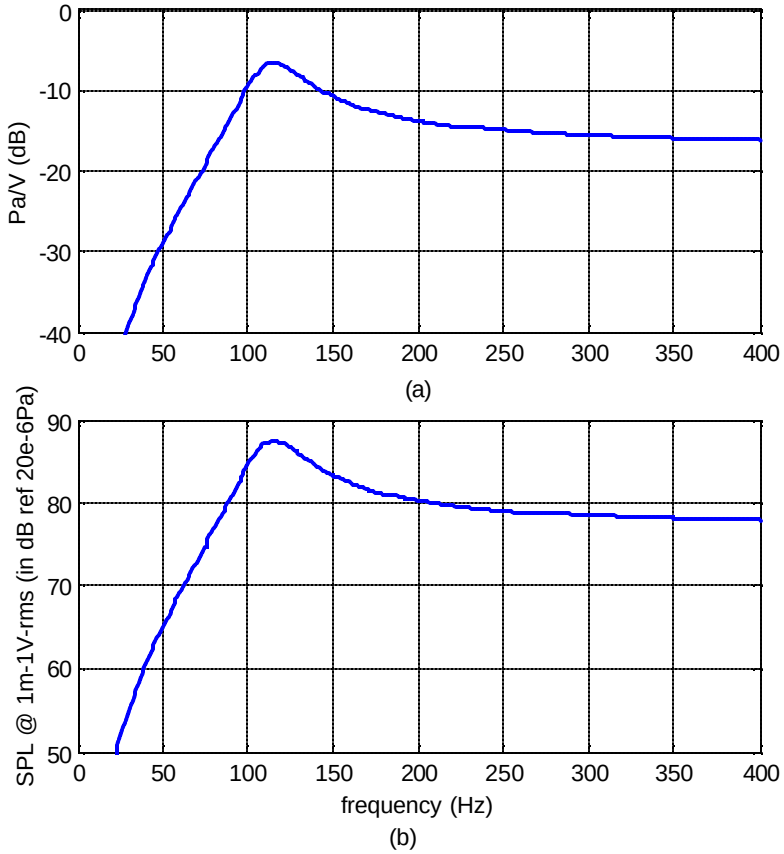

Figure 3-10. The performance of the loudspeaker with the optimum magnet size. (a) The transfer function between input voltage and output pressure at 1m. (b) 1V-rms-1m SPL output.

The loudspeaker can be designed to maximize the performance over the desired frequency range. For example, for the previous analysis the frequency range was taken to be 60-200Hz which is the target range for the active control tests for the payload fairing discussed in Chapter 4. Therefore, for such an application the output curve of the loudspeaker should rise close to its maximum value before 50 Hz.

3.2.2 Frame

The frame (support) of a loudspeaker essentially holds the components of the loudspeaker together. The main purpose of the frame is to provide a rigid support for the surround and the spider, and to carry the magnet assembly. For commercial loudspeakers, in addition to this, the frame has to be able to withstand external forces, such as impacts that might occur under working conditions. Therefore, they are designed with an additional strength by using heavier

materials, which also increases the weight of the frame. For a lightweight loudspeaker the strength of the frame is not of great importance as for commercial loudspeakers, since the mass that the frame holds is much less. However, the frame should still provide some rigidity to ensure that it does not move relative to the diaphragm. Therefore the weight of the frame can be reduced by selection of a lighter material, such as aluminum or even carbon fiber, instead of steel. Using less volume of material would further reduce the weight of the frame.

3.2.3 Box

Loudspeaker boxes are essential in the sense that they effectively increase the acoustic output of loudspeakers by converting them from a dipole to a monopole. In addition, they add stiffness to the dynamics of a loudspeaker, value of which can be set in order to change the output performance of the loudspeaker. The level of rigidity of the box is significant, because it can reduce the effectiveness of the box by reducing its stiffness contribution to the system. This might lead to both changing the natural frequency of the loudspeaker and reducing the acoustic output of the loudspeaker. This is very similar to the problem discussed in Chapter 2 for Helmholtz resonators loosing performance due to the elasticity of the resonator walls. Assuming a perfectly rigid box, the size of the box changes the performance of the loudspeaker by shifting the natural frequency. Figure 3.11 illustrates the effect of box size on speaker performance for a standard 12” Pioneer loudspeaker.

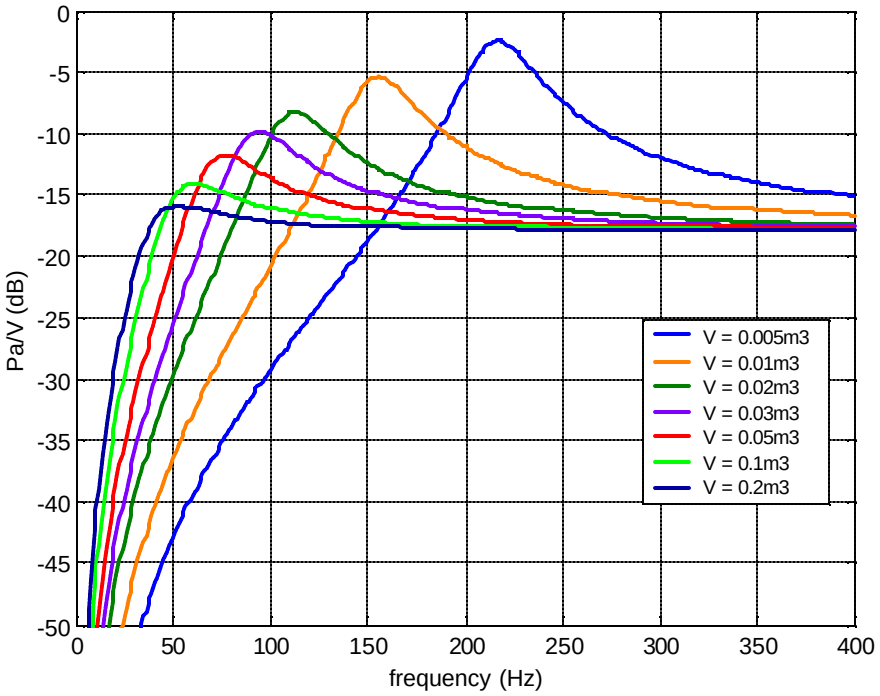

Figure 3-11. Effect of box volume on loudspeaker acoustic output. Increasing the box volume decreases the natural frequency of the loudspeaker.

A flatter response is favorable, and for a targeted frequency range of 60-200 Hz, a box of $1ft^3$ ($0.028m^3$) is selected. Smaller boxes would be lighter; however they perform poorly at low frequencies. The reason for that is an increase in stiffness due to smaller box volume, and this reduces the ease with which the diaphragm can move large amounts of air (i.e. large pressure increases inside a small box).

For commercial loudspeakers, relatively heavier boxes are used to ensure rigidity and preventing external damages. However, the weight can be reduced by using lighter materials. For this purpose, Glass/Nomex plates with honeycomb structure were selected due to their high stiffness to weight ratio. The woven fiberglass is bonded to both sides of the Nomex honeycomb core and the resulting panel is very lightweight and stiff. Figure 3.12 shows the picture of a 1 ft^3 loudspeaker box that was built in VAL. Triangular pieces were also used to support the connecting edges, which contributed to the rigidity of the box. The panel used was ¼" thick and the box weighs just 850 grams. The box was tested and compared to a rigid box and the results are given in the section 3.3.

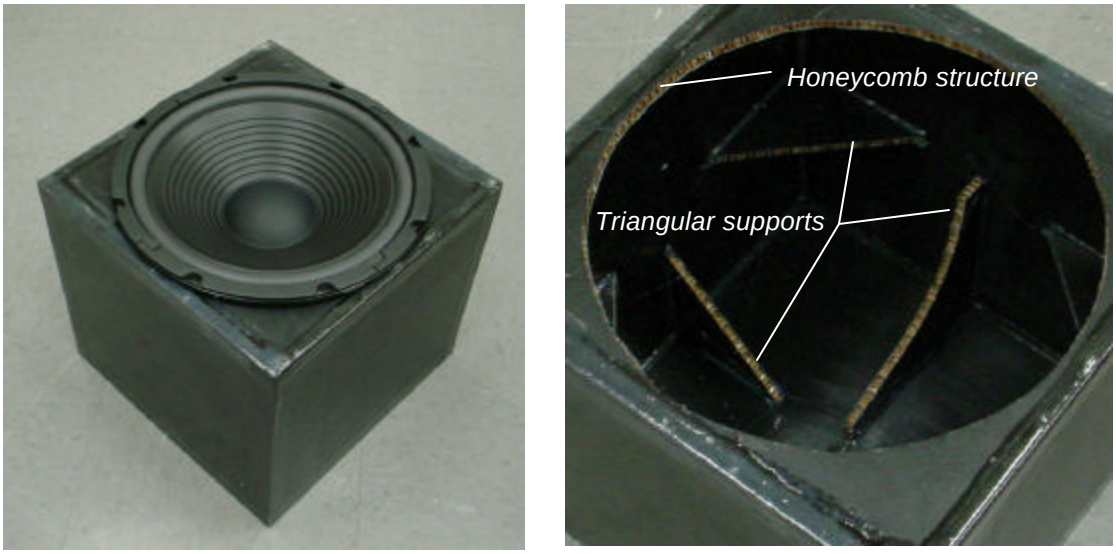

Figure 3-12. Lightweight speaker box built in VAL. The wall material is glass/nomex panel with honeycomb structure providing very high stiffness to mass ratio.

3.2.4 Total Weight of the Loudspeaker

After analyzing all possible weight reductions in the magnet assembly, frame and the box, the computer code can be modified in order to numerically compute the total weight of the loudspeaker for different values of previously mentioned variables: radius and height of the disc magnet. This can be used to compute the sound pressure created by unit mass of the loudspeaker, which is the main criterion required in order to be able judge the effectiveness of the weight reduction. From this analysis, the optimum size of the magnet can be found which gives maximum output per mass ratio for a single loudspeaker. Figure 3.13 shows the squares of the pressure output averaged over 60-200 Hz per unit mass of a single loudspeaker for different values of the two design variables.

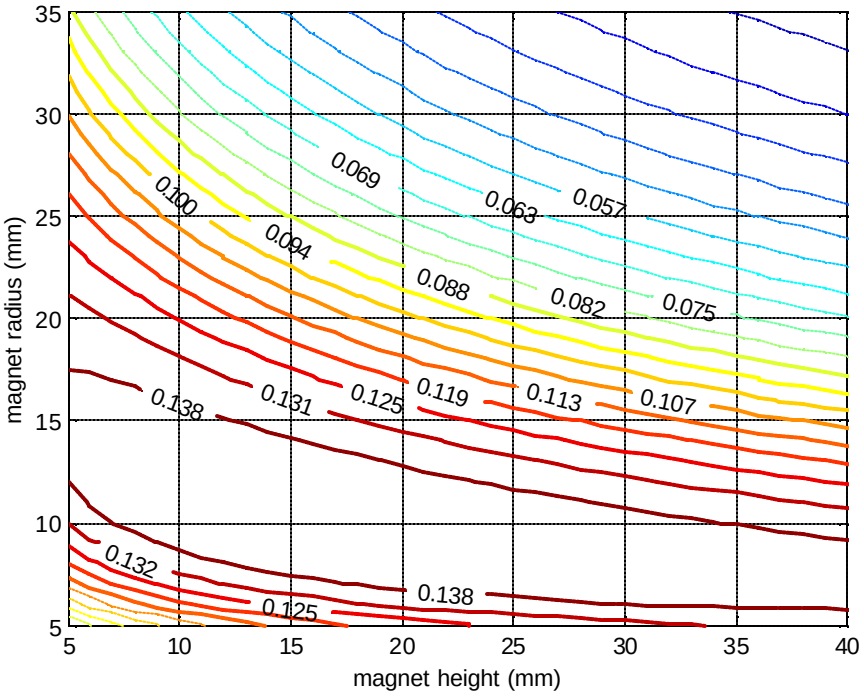

Figure 3-13. Average SPL (over 60-200 Hz, @ 1m-1V-rms) per mass (magnet assembly + 1.7kg of frame & box) of a single loudspeaker for different magnet dimensions.

The optimum magnet size is represented by the area surrounded by the contour line having the value 0.138 Pa/kg. Any radius-magnet combination in this area would have the same cost function; however it should be avoided to choose the extremes of this area where the ratio of radius to height of the magnet is either too high or too low. This is both because the lack of ease in manufacturability of the magnet assembly and possibility of lack of accuracy in electromagnetic theory used.

3.3 Testing Loudspeakers

With the design criteria based on the weight considerations of the previous sections, a new lightweight loudspeaker is built. In this section, the design procedure to build the lightweight loudspeaker is given and the results of the loudspeaker and box tests are discussed. The lightweight loudspeaker is tested in an anechoic chamber in order to evaluate its performance relative to the reference loudspeaker. In addition, the lightweight box built is also

tested to compare its performance to a rigid box. The overall weight reduction and performance change relative to the reference loudspeaker are presented.

3.3.1 Building a Lightweight Loudspeaker

The approach to design a lightweight loudspeaker is to take a standard 12" Pioneer loudspeaker as reference and apply weight reduction solutions while maintaining the acoustic performance of the new loudspeaker at least equal to the reference loudspeaker. Diaphragm, spider, surround and frame of the reference loudspeaker are used with no change for the new design to ensure that the dynamics of the new loudspeaker is as close as to the reference. The magnet assembly is replaced by a smaller assembly introducing a powerful NdFeB magnet. The shape of the new assembly is as given in Figure 3-7. The pieces surrounded the disc magnet are made out of steel and they are machined on lathe to obtain desired dimensions. The voice coil was also replaced by a new one in order to match the size of the new assembly. Figure 3-14 shows the pictures of the reference loudspeaker and the new design for comparison.

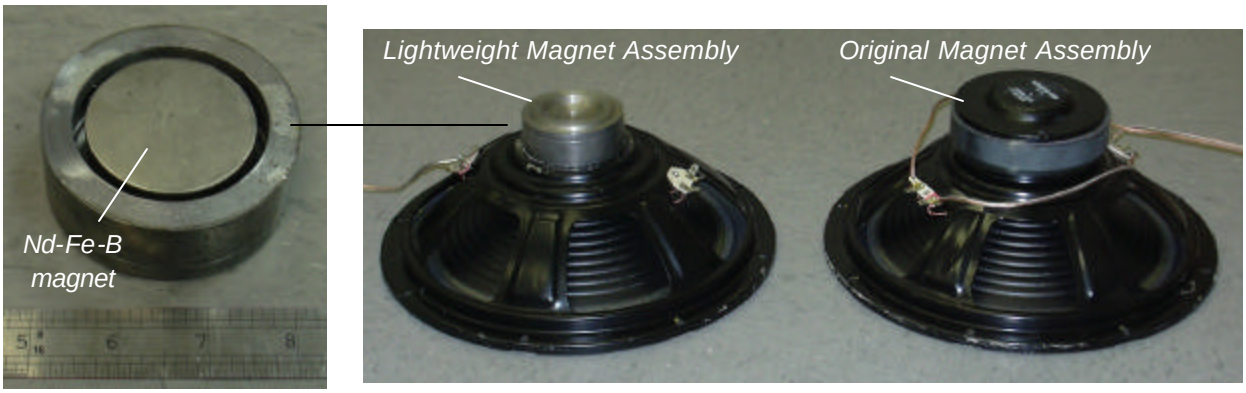

Figure 3-14. (a) The new magnet assembly, the disc magnet is at the center. (b) The lightweight loudspeaker (left) and the reference loudspeaker (right).

The new magnet assembly weighs only 755 grams whereas the old one weighs 2380 grams. This yields a total loudspeaker weight of 1440 grams in comparison to the 3065 grams of the reference loudspeaker. The weight reduction of the loudspeaker is 53%. By including the weights of the boxes, the reference loudspeaker weighs 5818 grams with its ½" plywood box and 10,465 grams with its ¾" plywood box, whereas the new loudspeaker with its lightweight box

weighs only 2290. The total weight reductions compared to the reference loudspeaker with ½" and ¾" thick boxes are 61% and 78%, respectively. It should be noted that the magnet assembly is heavier than the optimum sized magnet assembly given in weight reduction analyses. This is because the NdFeB magnets come in standard sizes and the selected size is greater than the optimum size which yielded a larger magnet assembly. For this design the original frame was used to make the process of building the new loudspeaker more convenient. However, a lighter material could be used to build a new frame which would weigh much less than the original structure. A 50% weight reduction of frame would result in 11% more reduction in loudspeaker weight and 5% more reduction in total weight which includes the box.

3.3.2 Test Setup

New designs of lightweight loudspeaker and lightweight box were tested in the anechoic chamber of VAL. A hemispherical array of microphones was created by connecting 13 microphones on a hemispherical frame hung by the ceiling. The loudspeaker to be tested was hung using a stand and the center of the loudspeaker cone was placed at the center of the hemispherical array of microphones in order to be able to simulate the free field radiation of a monopole source. Figure 3.15 shows the test setup.

Figure 3-15. The loudspeaker to be tested is located at the center of a hemispherical array of microphones in an anechoic chamber.

The measurements were taken once when the loudspeaker faces the array of microphones and once when it faces the opposite direction. This gives the radiation from the loudspeaker measured on a complete sphere with 26 microphones. The loudspeaker was excited by white noise band-filtered at 40-1250 Hz and signals from the microphones were recorded. For transfer function measurements, the input voltage to the loudspeaker was also recorded. The distance of each microphone to the center of the hemisphere was not constant due to the frame being not perfectly hemispherical; therefore the signals from each microphone were corrected by distance coefficients to give the acoustic output on a 37" radius sphere.

3.3.3 Box Performance

The performance of the lightweight glass/nomex composite box was evaluated by comparing it to a ¾" plywood box which weighs 7.4 kg and was assumed to be rigid. The boxes were of equal volume and the same reference loudspeaker was placed in both of the boxes to

ensure that all other parameters in this comparison are the same for both cases. Output of the loudspeaker over the spherical array of microphones was measured. The squares of the transfer functions between the input voltage to the loudspeaker and sound pressure output from the microphones were spatially averaged over the complete sphere. Therefore, the resulting single transfer function represents the amount of average sound pressure achieved by the loudspeaker on a 37"-radius sphere for a given input voltage. Figure 3-16 illustrates the comparison of these two boxes over the low-frequency range of 50-250 Hz.

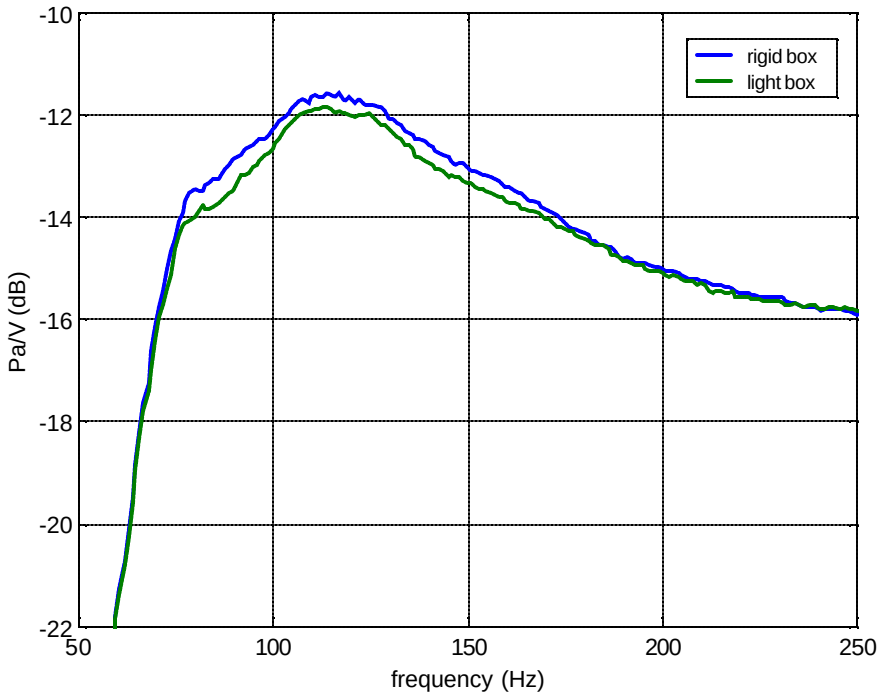

Figure 3-16. Spatial average of the transfer functions between the voltage input to the loudspeaker and pressure (@ 1m) output from the microphones.

It can be seen that the lightweight box performs almost equal to the rigid box. In 60-200 Hz bandwidth, the total loss in the output of the loudspeaker is 0.24 dB which corresponds to a loss of 2.8%. It should be noted that the lightweight box weighs only 850 grams compared to the 7.4 kg of the rigid box. Therefore, the amount of loss in performance is acceptable considering the amount of weight saved for the box.

3.3.4 Loudspeaker Performance

Several tests were conducted to determine the different aspects of the performance of the newly designed lightweight loudspeaker. This was done by comparing the performances of the new loudspeaker together with its lightweight box and the reference loudspeaker together with its rigid ¾" plywood box. Transfer functions, efficiencies and -most significantly- maximum outputs of the two loudspeakers were compared. The sound pressure was again measured over a spherical array of microphones in the anechoic chamber to simulate the free-field condition. Figure 3-17 shows the spatial average of the transfer functions between the input voltage to the loudspeaker and the sound pressure at microphone locations.

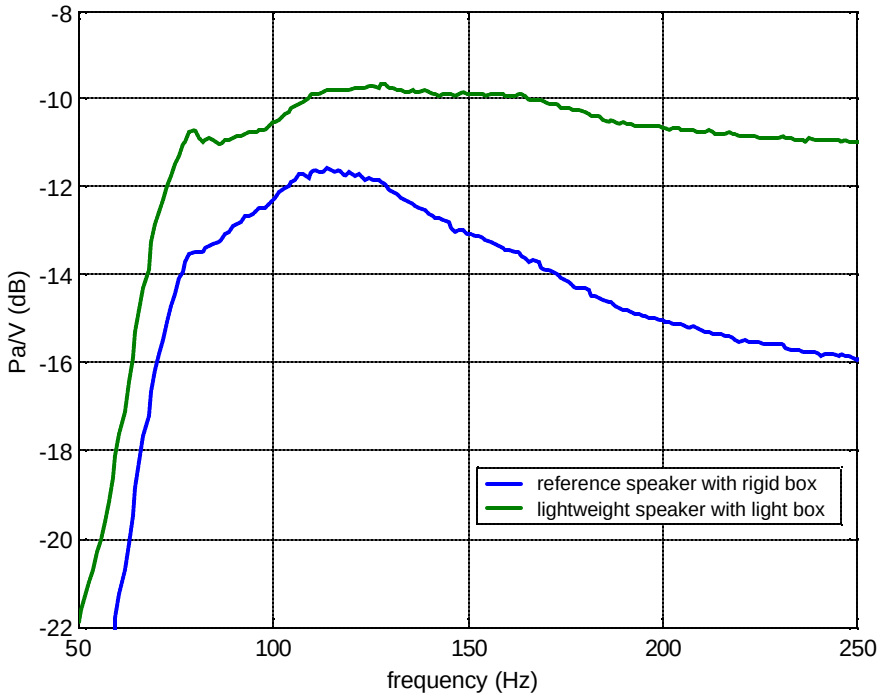

Figure 3-17. The spatial average of the transfer functions between the input voltage to the loudspeaker and the sound pressure from the spherical array of microphones. The lightweight loudspeaker provides more output and more damping.

There is an increase in both the magnitude of the transfer function and the damping in the system compared to the reference loudspeaker which seems to contradict the design approach that aimed to maintain the output of the reference loudspeaker constant. This is because the magnet used was larger than the optimum size and therefore the magnet assembly is magnetically more powerful than that of the reference loudspeaker. The increased force on the

diaphragm caused an increase in the output and the damping of the loudspeaker also increased due to a larger back e.m.f. The output of the new loudspeaker is 2.8 dB more than the reference loudspeaker over 60-200 Hz frequency band. This corresponds to a linear efficiency increase of 38%. In addition, increased damping in the system flattened out the response over 100-250 Hz range, which is favorable for active noise control applications.

The more important criterion for the performance of a loudspeaker for this application is its maximum output. In order to compare the maximum outputs of the new lightweight loudspeaker and the reference loudspeaker, they were operated at the maximum voltage level of their linear working range, which is about 30 V-rms over 40-1000Hz band for both. The reference loudspeaker could operate with input voltages above 30 V-rms, however the response is not linear which was deduced from the significant drop in the coherence of the measurements. The resulting sound pressure levels on the front hemisphere of the loudspeaker were spatially averaged and Figure 3-18 illustrates the comparison between the reference and lightweight loudspeakers.

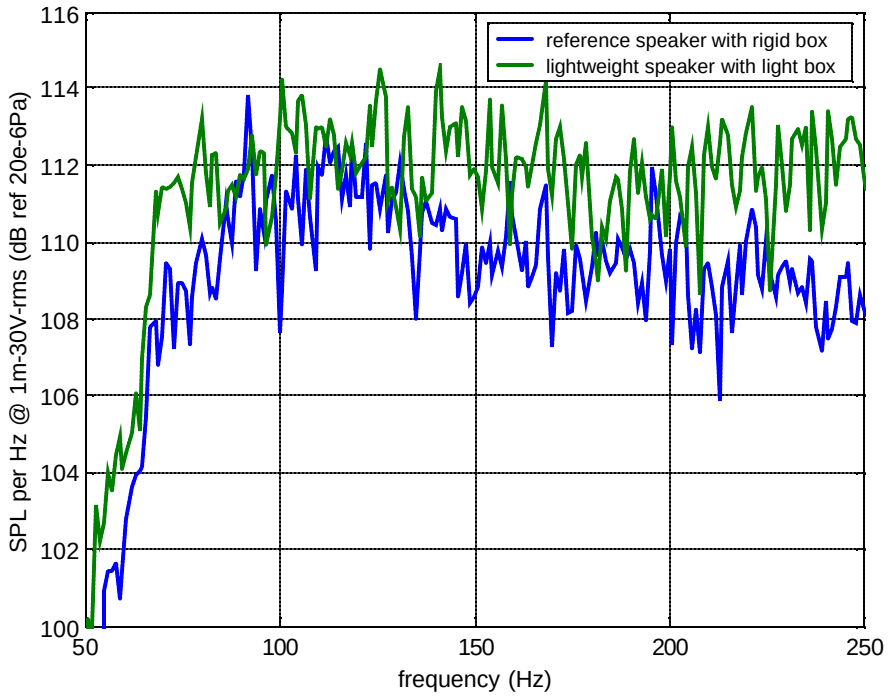

Figure 3-18. Spatial average of the sound pressure levels on the front hemisphere of microphone array while maximum voltage input is applied.

The total sound pressure output of the lightweight loudspeaker over 60-200 Hz bandwidth is 1.7 dB larger than that of the reference loudspeaker.

The linearity of the new loudspeaker is worthwhile to check by measuring the transfer functions for various values of input voltage to the loudspeaker and plotting them on the same graph. Figure 3-19 illustrates the results.

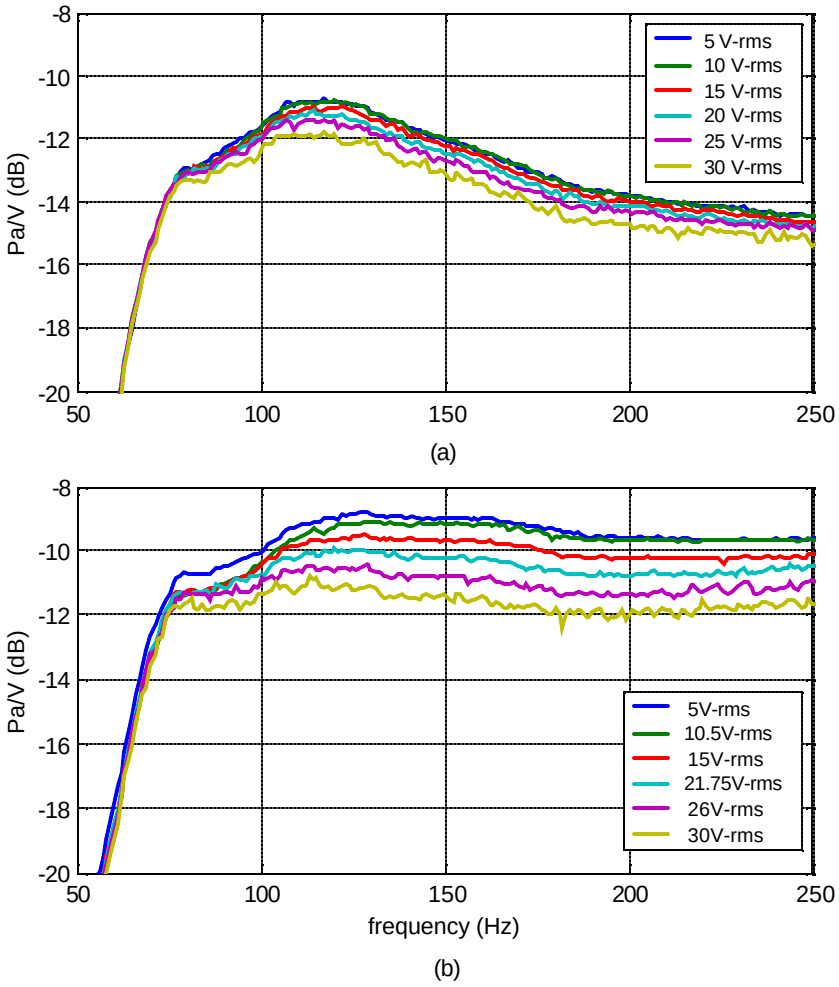

Figure 3-19. The spatial average of the transfer functions between the input voltage to the loudspeaker and the sound pressure from the front hemisphere array of microphones for various input voltage values for (a) the reference loudspeaker and (b) the lightweight loudspeaker.

The transfer function curve for the reference loudspeaker shifts down by about 1 dB from 5 V-rms to 30 V-rms input, whereas this value for the lightweight loudspeaker is about 2 dB. Therefore, Figure 3-18 gives a better comparison of these two loudspeakers than Figure 3-17, because the latter was taken at 5 V-rms input. As a comparison, the differences in total

outputs of the two loudspeakers in 60-200 Hz bandwidth are 2.7 dB and 1.6 dB for 5 V-rms and 30 V-rms voltage inputs, respectively.

3.3.5 Conclusions

In this section, the performance change and weight reduction for the new lightweight loudspeaker compared to the reference loudspeaker will be combined to analyze the desired cost function determined for loudspeakers in active noise control applications. This cost function is the maximum total sound pressure over 60-200 Hz bandwidth per unit mass of the loudspeaker. It should be noted that the sound pressure values were measured on a 37" radius sphere. Table 3.2 summarizes the results.

Table 3-2. Maximum output, weight and cost function comparisons of the new lightweight loudspeaker to the reference loudspeaker (12" Pioneer A30GU30-55D).

Configuration	Increase in SPL Output rel. to the Reference (60-200 Hz)	Total Weight (grams)	Pa/kg Cost function rel. to the Reference
Reference loudspeaker with ¾" plywood box	0	10,465	1
Lightweight loudspeaker with composite box and original frame	1.7 dB	2290	5.61
Lightweight loudspeaker with composite box and 50% lighter frame	1.7 dB (assumed)	1950	6.60

Chapter 4: Active Control Tests

In this chapter, the results of the active control tests on a payload fairing using the previously mentioned active acoustic devices will be discussed. In addition to the loudspeakers, distributed active vibration absorbers (DAVAs) were also used in these tests. Brief explanations on the working principles of DAVAs will be given further in this chapter. The tests resulted in significant amount of attenuation in the interior noise of the test cylinder.

DAVAs were previously tested on the test cylinder and were shown to be effective [2]. For this set of active control tests, DAVAs were again used, now together with loudspeakers in order to investigate the performance of a "hybrid" system. Individual applications of these devices (i.e. just DAVAs or just loudspeakers) was shown to achieve good performance; however they often struggled to attenuate particular modes. The use of a hybrid system allowed one set of these devices to compensate for the inefficiency of the other set yielding better attenuation over the entire frequency range of interest. For active control tests, which were conducted at the airport lab of Virginia Tech in December 2003, different combinations of the devices and various options provided by the controller were tested to investigate their effects on performance.

The issue of 'causality', which is of importance in active noise control with random disturbances, was analyzed in order to determine its effects on control performance. Causality analysis was done through the 'delay' function of the controller, where the information about the disturbance signal is used by the controller before it is received by the reference. A discussion on the performance of an optimum controller is also included in order to determine the performance limits due to actuator numbers and locations. The tests were not conducted using the maximum output of the actuators; however for one set of tests the loudspeakers were operated at maximum capacity in order to find the maximum controllable external noise level. This gives a measure to how much actuator mass is needed for a certain level of external noise. All of these analyses are discussed in further detail in this chapter following a brief section describing the working principles of DAVAs.

4.1 Distributed Active Vibration Absorber (DAVA)

Distributed active vibration absorbers were designed at VAL by Steve Booth and Tony Harris [2] in order to be able to create a more sophisticated vibration absorber than a single DOF vibration absorber. The idea behind the design was to create a 2 DOF system with two resonant peaks providing performance over a range of frequencies. The design target was to maximize the attenuation for low frequency vibration over 50-200 Hz. A DAVA (pictured in Figure 4.1(a)) is basically composed of two single DOF systems coupled to each other. A honeycomb plate is glued to a melamine foam of density 8.5mg/cm^3 to form a mass-spring system where the plate represents the mass and the foam represents the spring. The desired natural frequency of this system can be adjusted by changing the ratio of the stiffness of the foam to the mass of the plate. On the other hand, a shaker composed of a rare-earth permanent magnet (Nd-Fe-B), spider plates, an electrical coil and a casing, is the active element and provides the other single DOF system. Spider plates provide stiffness (similar to the spider in loudspeaker configuration) and the magnet provides the mass. An input voltage to the coil creates a current, which in turn results in a magnetic force due to the magnetic field of the magnet. This force is applied both on the magnet and the coil, but since the coil is connected to the casing and is stationary, the magnet is excited in motion. The mechanical properties of this system can be altered by changing the stiffness with different spider materials or changing the mass of the magnet. The characterization of this single DOF electro-mechanical shaker is very similar to that of a loudspeaker discussed in Chapter 3, the only difference is that in this case the magnet is the moving part instead of the voice coil of a loudspeaker. These two single DOF systems are then coupled together by gluing the shaker to the plate and the free-body diagram of the new configuration is also given in Figure 4.1(c).

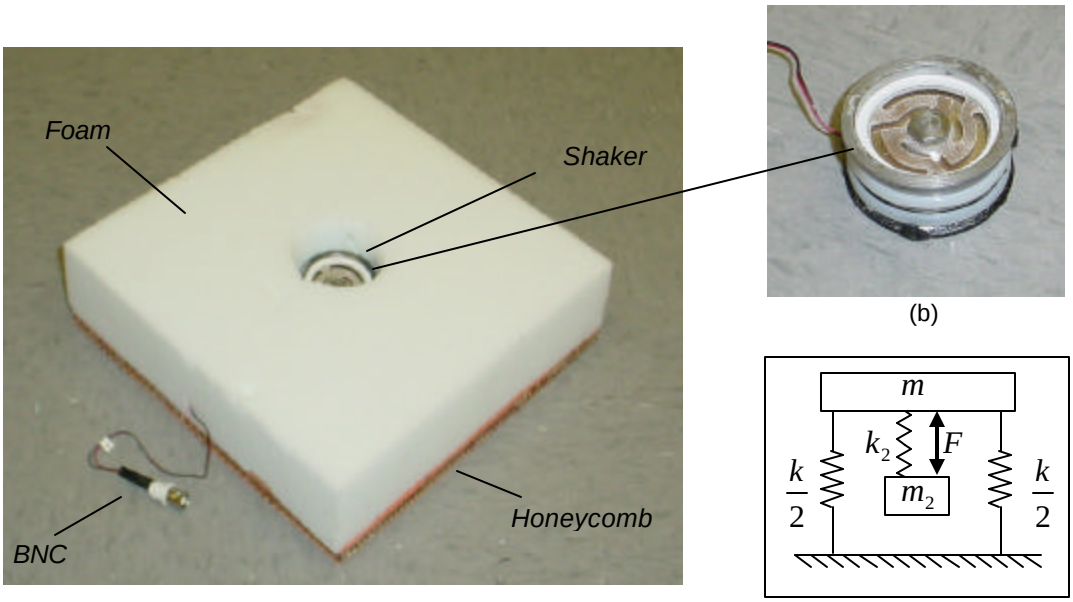

Figure 4-1. Pictures of (a) the DAVA and (b) the shaker used for DAVAs. (c) Mechanical model of a DAVA.

The DAVAs that were used in the active control tests were specifically designed in order to give the maximum performance over 50-200Hz frequency range. For this purpose different sizes of foam and plates were previously tested by Harris [2] and Figure 4.2 illustrates the performance of these configurations in terms of the output force of the absorber per input voltage to the shaker. The magnitude of the output transfer function increases as the mass of the DAVA increases. Therefore, the total force output summed over the frequency bandwidth of interest divided by the total mass of the DAVA, was used as the efficiency of the actuator. The foam having the dimensions 9.5”x9.5”x2” was selected for the active control tests because of its highest effectiveness among other available sizes. The effectiveness of the selected DAVA compared to the point actuators was calculated to be 32% higher [2], which shows the superiority of DAVA over the point actuators.

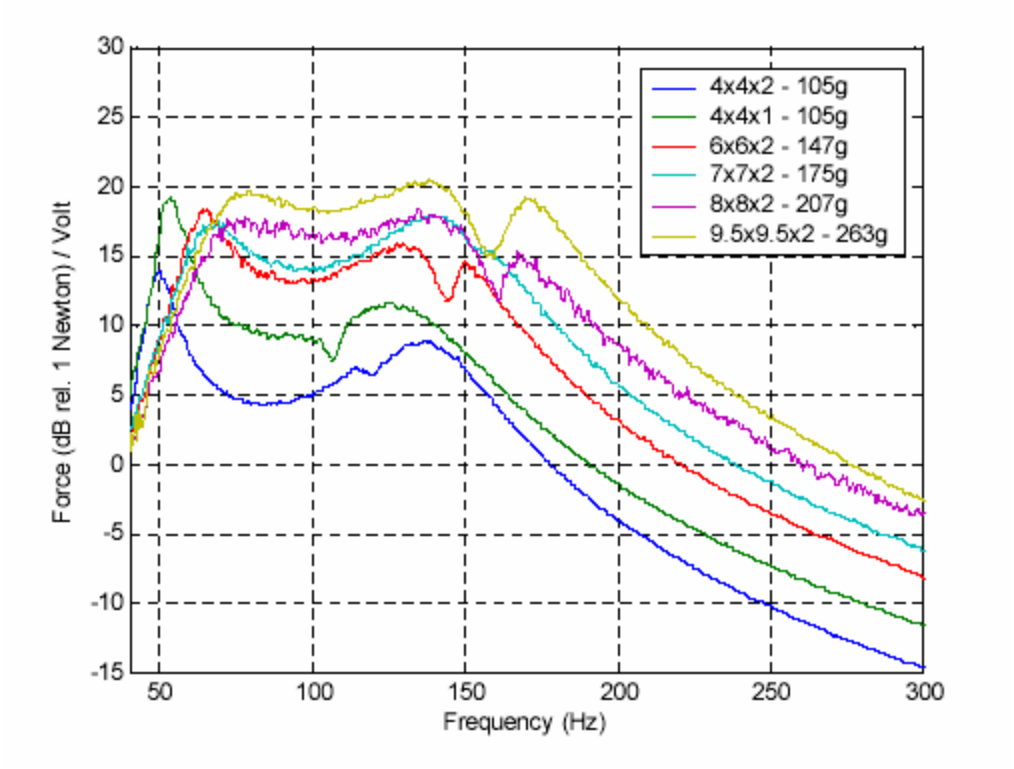

Figure 4-2. Force output per voltage input of a DAVA for different foam and plate dimensions[2].

The same weight considerations are applied to DAVAs as to HRs and loudspeakers analyzed in Chapters 2 and 3. The honeycomb plates of the selected design are 9.5”x9.5”x3/8” and weighs 183 grams. The 9.5”x9.5”x2” foam and the magnetic shaker weigh 25 grams and 154 grams, respectively, and the resulting weight of a single DAVA is therefore 362 grams.

4.2 Test Setup

The test cylinder, shown in Figure 4.3, is provided by Boeing and is made of honeycomb core with a graphite epoxy skin. The cylinder has a height of 2.8m and diameter of 2.46m. The end caps of the cylinder are composed of 5.72 cm thick-layered plywood, which is stiffened by I-beams in order to be able to model the cylinder as if in an infinite baffle.

Figure 4-3. Picture of the composite test cylinder in the airport lab of VAL.

The cylinder was excited by an external speaker positioned about the same level as the bottom cap of the cylinder. The position of this speaker is taken as the reference (as 0 degrees) for angular positioning of the 4 loudspeakers, 4 DAVAs and 15 microphones mounted in the cylinder. The positions and numbering of the test components are shown in detail in Figure 4.4.

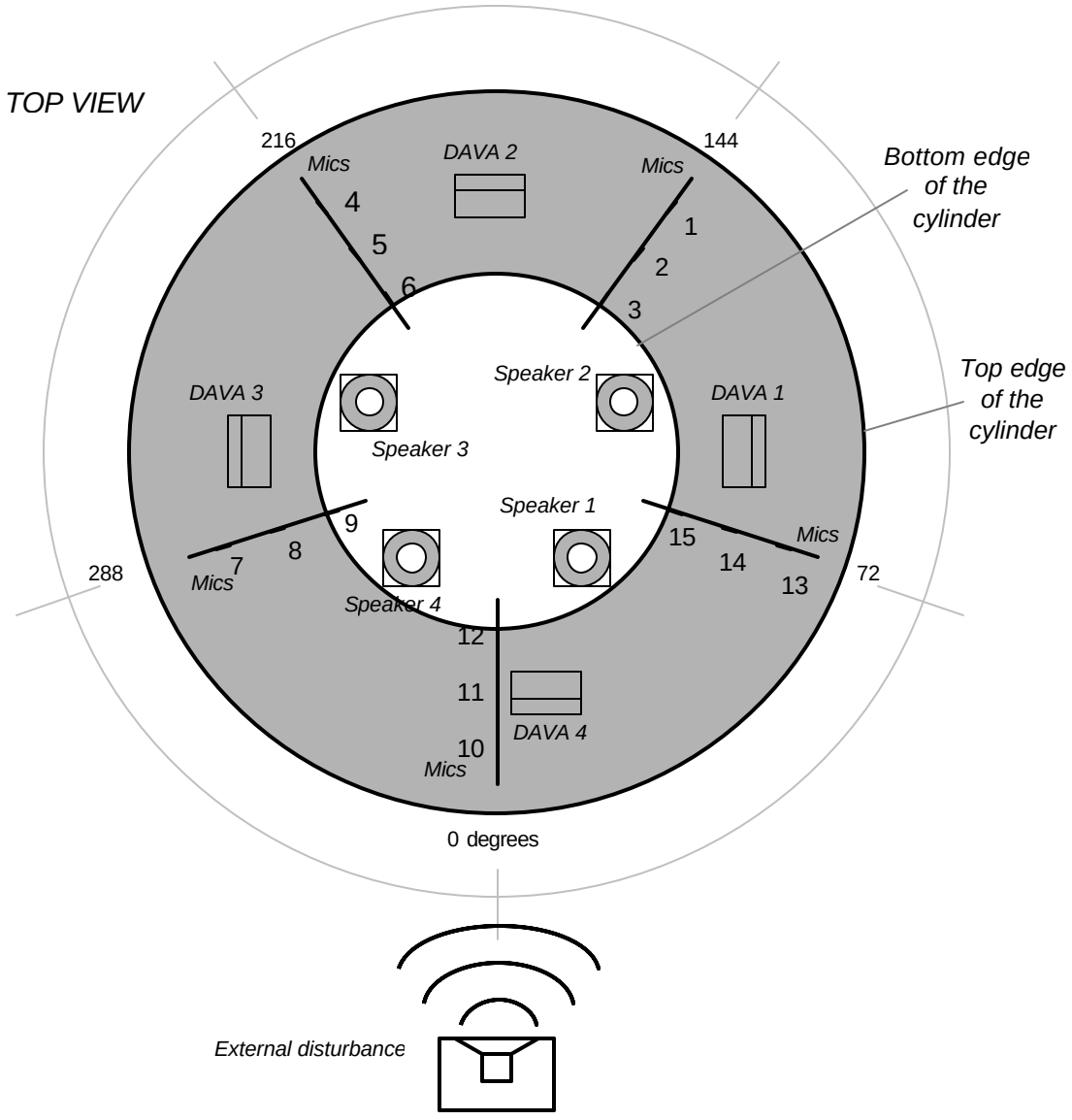

Figure 4-4. Positioning and numbering of the active control test components on and around the test cylinder (top perspective view).

The DAVA's are taped on the inner wall of the test cylinder as a horizontal ring, about one-third of the height from the bottom cap. This implementation increases the effectiveness of the DAVAs by means of better coupling with the first and second order axial modes of the cylinder, which were shown to dominate low frequency response [3]. The edges of the foam were tapered in order to fit to the curved surface of the cylinder. The 4 loudspeakers, on the other hand, are placed on the cylinder floor as close as possible to the diameter and facing upwards. They are mounted symmetrically with respect to the reference angle. Close positioning of the

loudspeakers with any of the error microphones is avoided in order to prevent near field effect of loudspeaker response. This also prevented the possibility of relatively higher signals from the close error microphone. The 15 microphones are tied on 5 vertical strings having equally divided circumferential angles and first 12 were used as error sensors. Figure 4.5 shows the photo of the placement of each of these components.

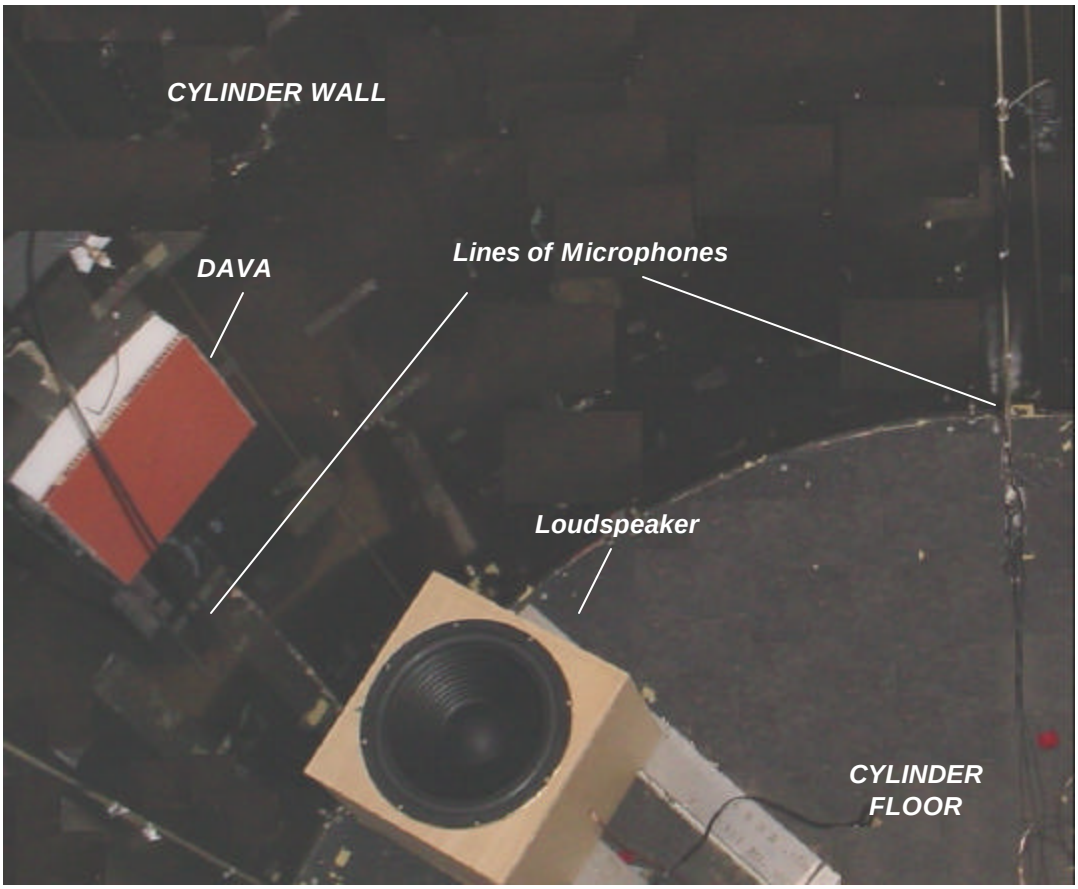

Figure 4-5. Pictures of a DAVA, a loudspeaker and lines of microphones mounted on the cylinder for active noise control tests.

The controller used for the tests was developed by Virginia Tech and provides adaptive feed-forward active structural acoustic control (ASAC). It features multiple-input multiple-output (MIMO) filtered X-LMS systems based on a Texas Instrument's C40 DSP platform. Figure 4.6 illustrates the control diagram for a filtered X-LMS control system. This controller is a time domain based system that drives the actuators by filtering the reference signal *x* through a set of finite impulse response filters *H*. The system converges to the optimal set of causal filters needed to minimize the errors.

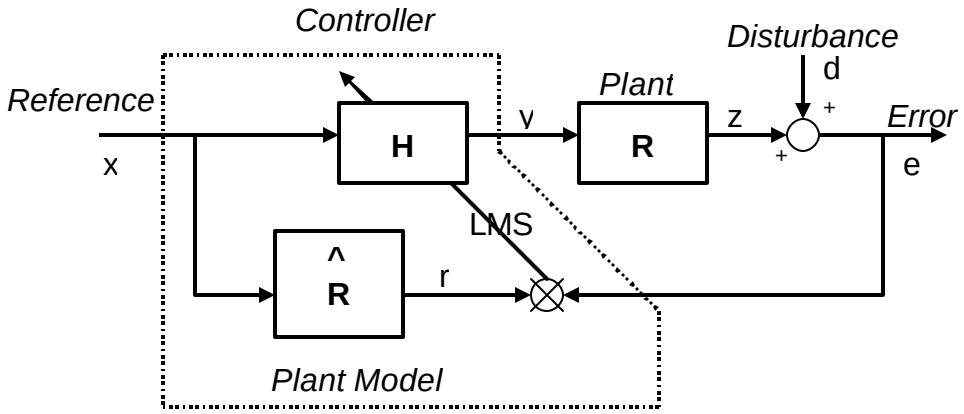

Figure 4-6. Filtered X-LMS control scheme.

For these experiments, the controller was used with 1 reference, 8 outputs and 12 inputs. The following is a brief description of how the controller is operated. The first step is the input range check where it is ensured that all the signals from the system components are within the pre-determined range value (i.e. no clipping). The next step is the system identification stage which is very important in setting up the controller, because the LMS controller requires a good estimate $\hat{R}$ of the plant R in order to work. The filter lengths and convergence coefficient for the controller can also be adjusted during the system identification process. If the system is resonant (i.e. not damped enough), then longer filters are needed in order to obtain better system identification; however this leads to increased computation. The convergence coefficient determines how fast the filter coefficients converge, however high convergence coefficient values might cause the controller go unstable and damage the actuators. Once the filter coefficients are converged, then the controller is ready to be activated. The filter coefficients (i.e. in H) are updated continuously while the controller is on. This compensates for any slight change in the system that may occur during the controlling process.

The general block diagram of the test setup is given in Figure 4.7. The controller creates a random noise, which is band-pass filtered and amplified before reaching the external loudspeaker and in turn excites the cylinder and internal acoustic field. This constitutes the primary source path of the control system (disturbance). The reference microphone x is an external microphone that is used to drive the actuators through a filter H. The error microphones inside the cylinder create error signals which are the combination of the disturbance signals and the output from the

actuators. They are then passed through a signal conditioner and band-passed before being received by the input ports of the controller. The controller then uses these signals to adjust the filters H that create signals at the output ports, which are band-pass filtered and amplified before reception by the actuators (loudspeakers and DAVAs). The data acquisition (DAQ) system receives the band-pass filtered error signals together with the accelerometer signals for analysis purposes. The DAQ system used was based on the LabView software and was specifically developed by Jamie Carneal and Rick Wright of Virginia Tech. The DAQ system records the auto-spectra of each channel, and the real and imaginary components of the cross-spectra between each channel and the reference channel (voltage to the external disturbance in these tests).

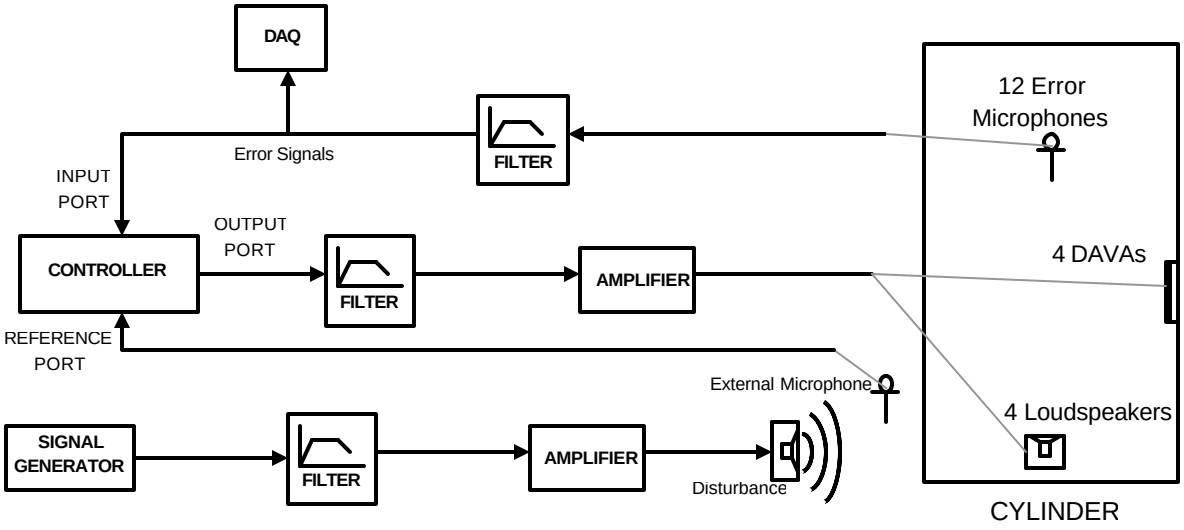

Figure 4-7. Block diagram of the active control test scheme.

4.3 Cylinder Response

The test cylinder has its own response characteristics when it is exposed to external acoustic excitation. Considerable amount of work was done on analyzing the structural and acoustic modes of the cylinder and the coupling between the two [3]. For the purposes of this work, the comparison of external and internal sound levels is sufficient to understand the nature of the system. In other words, for a random external disturbance the acoustic modes occur in the cylinder at various frequency values. The two transfer functions; between the voltage input to the

primary source (disturbance) and the external microphone signals, and between the voltage input to the primary source (disturbance) and the average of error microphones signals are given in Figure 4.8. The external microphone exhibits fluctuations in its frequency response due to reverberant effects influenced by the location of the external microphone, since the tests were conducted in a closed environment (i.e. resulted in reflection from the walls of both the room and the cylinder). On the other hand, the internal microphones exhibit the effect of the cylinder structure on the response due to the structural-acoustic coupling.

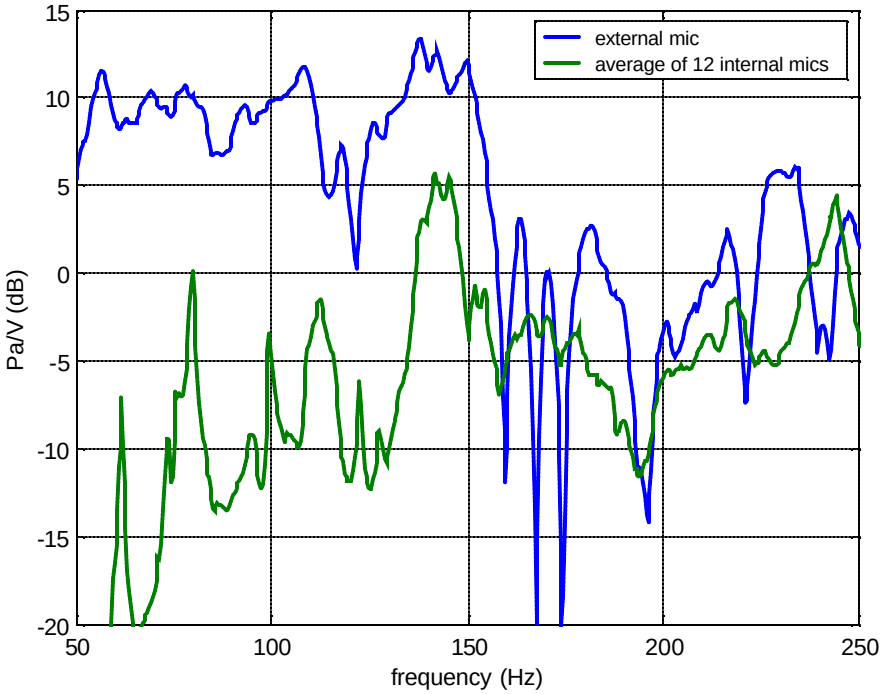

Figure 4-8. Transfer functions for external microphones and for internal microphones referenced to the voltage input to the primary disturbance.

Figure 4.9 shows the corresponding sound pressure levels inside and outside the cylinder. The SPL inside the cylinder is averaged over 12 error microphones. It should be noted that the external sound level is about the same throughout all control measurements in the tests. The external sound level that occurs at the external microphone location (i.e. between the primary source and the cylinder) in 60-200 Hz bandwidth is 92.6 dB, and the sound level inside the cylinder is 80.5 dB over the same bandwidth. The cylinder itself attenuates about 12.1 dB of the external noise level.

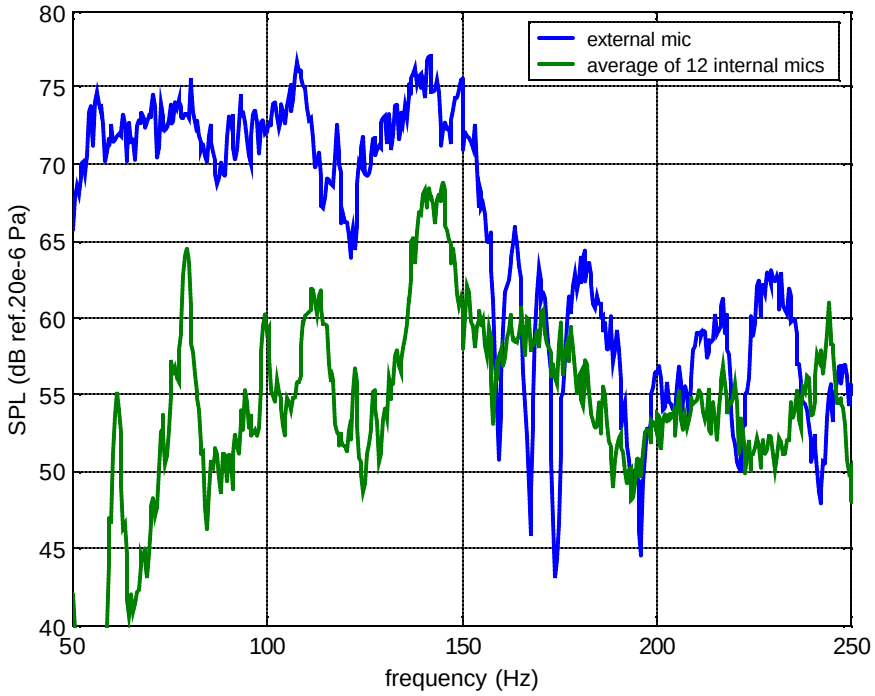

Figure 4-9. Sound pressure levels inside and outside the cylinder. Internal SPL is averaged over 12 microphones.

4.4 Optimum Control Analysis

The controller uses the error signals to create the best possible control filter coefficients in order to minimize the error signals. For practical reasons, it is impossible for a controller to achieve the maximum possible control. However, knowing the maximum control (therefore maximum attenuation) provides important information about the control limitations and helps to determine whether the controller performance can be improved. Therefore, the transfer functions between the actuators – i.e. reference disturbance, DAVAs and loudspeakers – and the error microphones were measured in order to be able compute the optimum control filter coefficients for the system.

The method used to compute the optimum control coefficients is discussed by Nelson and Elliott [33]. Assuming linearity, the vector of error signals **e** from the microphones are the sum of the vector of error sensor outputs **d** due to primary source (disturbance) and the vector of error sensor outputs **z** due to the secondary sources (control actuators):

$$\mathbf{e} = \mathbf{d} + \mathbf{z} \tag{4.1}$$

The length of these vectors is equal to the number of error microphones, 12 in this case. The signals that are sent to the actuators are passed through a vector of control coefficients $\mathbf{h_c}$, in order to give the vector of error sensor outputs $\mathbf{z}$:

$$\mathbf{z} = \mathbf{R}\mathbf{h_c} \tag{4.2}$$

where R is the matrix of measured transfer functions between the control actuators and the error microphones and is 12x8 in this case (number of error microphones times the number of control actuators). The analysis is made frequency by frequency; therefore Equation 4.1 can be rewritten as

$$E(w) = D(w) + R(w)H(w) \tag{4.3}$$

The optimum control coefficient vector $H(w)$, that gives the minimum value for the total error signals, can be determined by defining a cost function

$$J(w) = E\left[\mathbf{e}^H \mathbf{e}\right] \tag{4.4}$$

where the expectation operator E refers to an ensemble average of records of infinite duration. However, it can be assumed that the function of this operator is negligible since the measurements were taken over finite number of averages which gives a reasonable approximation. From the substitution of Equation 4.3 in Equation 4.4, the vector of optimum control coefficients can be found as

$$H_o(w) = -E\left[R^H R\right]^{-1} E\left[R^H d\right] \tag{4.5}$$

Introducing a signal conditioning coefficient a, the corresponding vector of minimized error signals can be found as

$$E_o(w) = D(w) - R(w)E\left[R^H R + aI\right]^{-1} E\left[R^H d\right] \tag{4.6}$$

Using these equations, optimum filter coefficients are computed from the system transfer functions and the resulting sound level using the optimum coefficients is shown in Figure 4.10. Optimum control provides a 13.6 dB attenuation in the 60-200 Hz bandwidth. This is the maximum achievable attenuation for the given system having an ideal controller which has perfectly converged coefficients and a sufficiently causal reference signal (with perfect coherence). In other words, this calculation was conducted in the frequency domain without any consideration to the causality of the filters in the time domain where the real control system must operate.

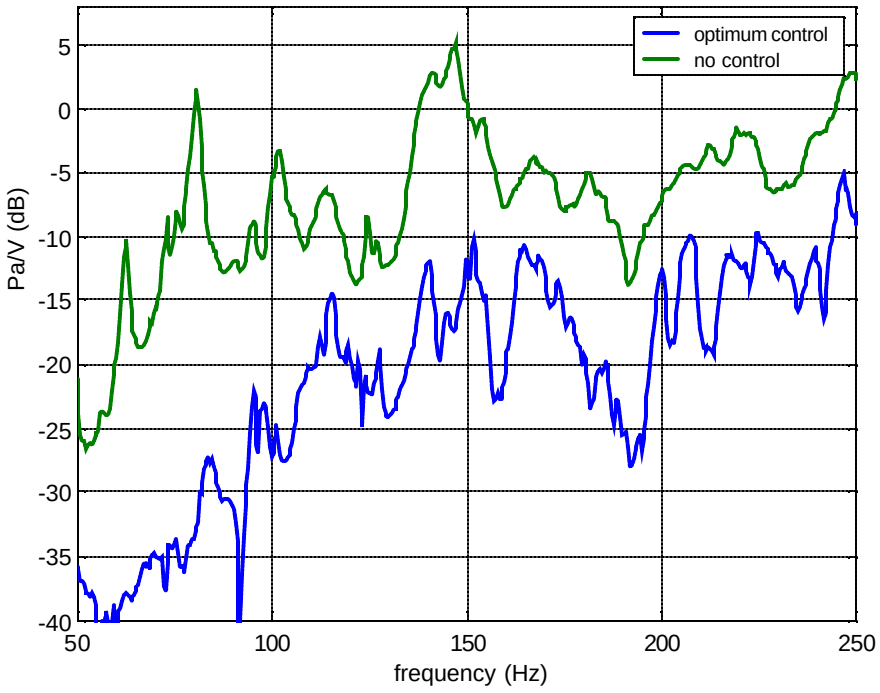

Figure 4-10. Transfer functions between the error microphones and the voltage input to the primary source using perfectly converged control coefficients (maximum control).

The performance shown represents the upper control limit due to the physical setup and to achieve better performance than this implies that the number of actuators needs to be increased or the actuator locations changed.

4.5 DAVA and Loudspeaker Performances

Three sets of measurements were conducted in order to compare the individual and combined actuator performances using: (i) 4 DAVAs, (ii) 4 loudspeakers and (iii) the hybrid system with all 8 actuators. The reference signal is chosen to be the external microphone signal which is generally the case for active noise control applications and represents a realistic reference signal. The control filters are 500 taps in length and the sample rate is 700Hz which corresponds to a filter length of 0.71 seconds.

The resulting averaged transfer functions between the primary source and the error microphones for all three sets, with and without control, are plotted in Figure 4.11. Since these sets of measurements were taken at different times, the curves representing the cases without control are not exactly equal, thus the transfer function curve for no control case is obtained from averaging the corresponding curves from all three sets. In 60-200 Hz bandwidth, attenuations of 1.5 dB, 2.2 dB and 3.2 dB in internal sound level are achieved by DAVAs, loudspeakers, and the combination of the two, respectively.

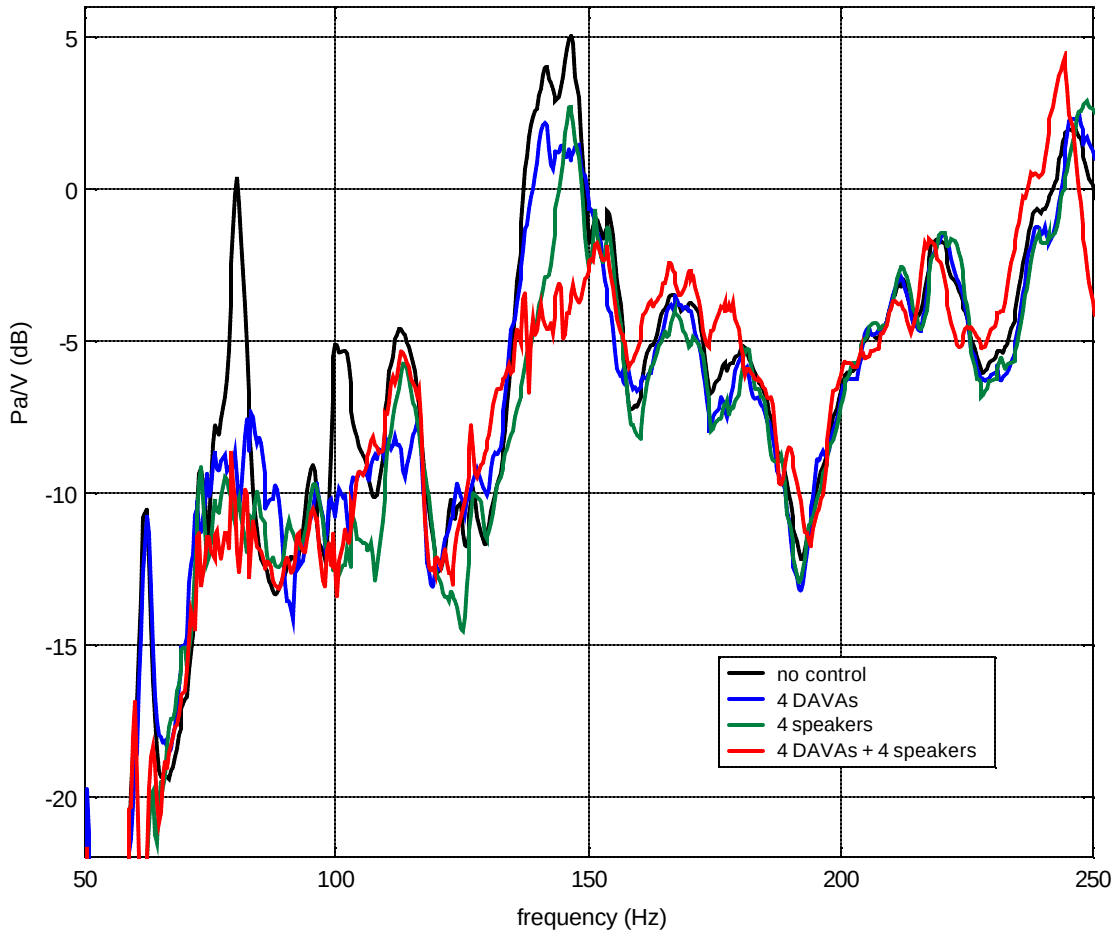

Figure 4-11. Transfer functions between the error microphones and the voltage input to the primary disturbance for three sets of control actuator sets. The reference for the controller is the external microphone signal.

The comparison of the behaviors of the different sets at single frequencies shows that the DAVAs and the loudspeakers achieve similar attenuations at all the peaks (typically 10dB attenuation) except the one at about 120 Hz where the DAVAs perform better and the one at 60Hz where the loudspeakers perform better. The hybrid system provides better attenuation at almost all of the peaks. However none of the configurations can achieve attenuation above 160 Hz which is more likely due to the absence of distinct peaks at this region. At the highest peak, which occurs within a frequency range of 140-150 Hz due to coupling of the modes, the attenuations are about 4 dB, 3 dB, and 7 dB by DAVAs, loudspeakers, and the combination of the two, respectively. The DAVAs perform slightly more effective than the loudspeakers, because, they attenuate the structural vibration which, in terms of control path, is one step before the loudspeakers.

Figure 4.12 shows the resulting averaged sound pressure levels for the three sets of measurements. The observed effect of the hybrid system is to flatten out the pressure level curve over the bandwidth which is typical in active control of noise applications.

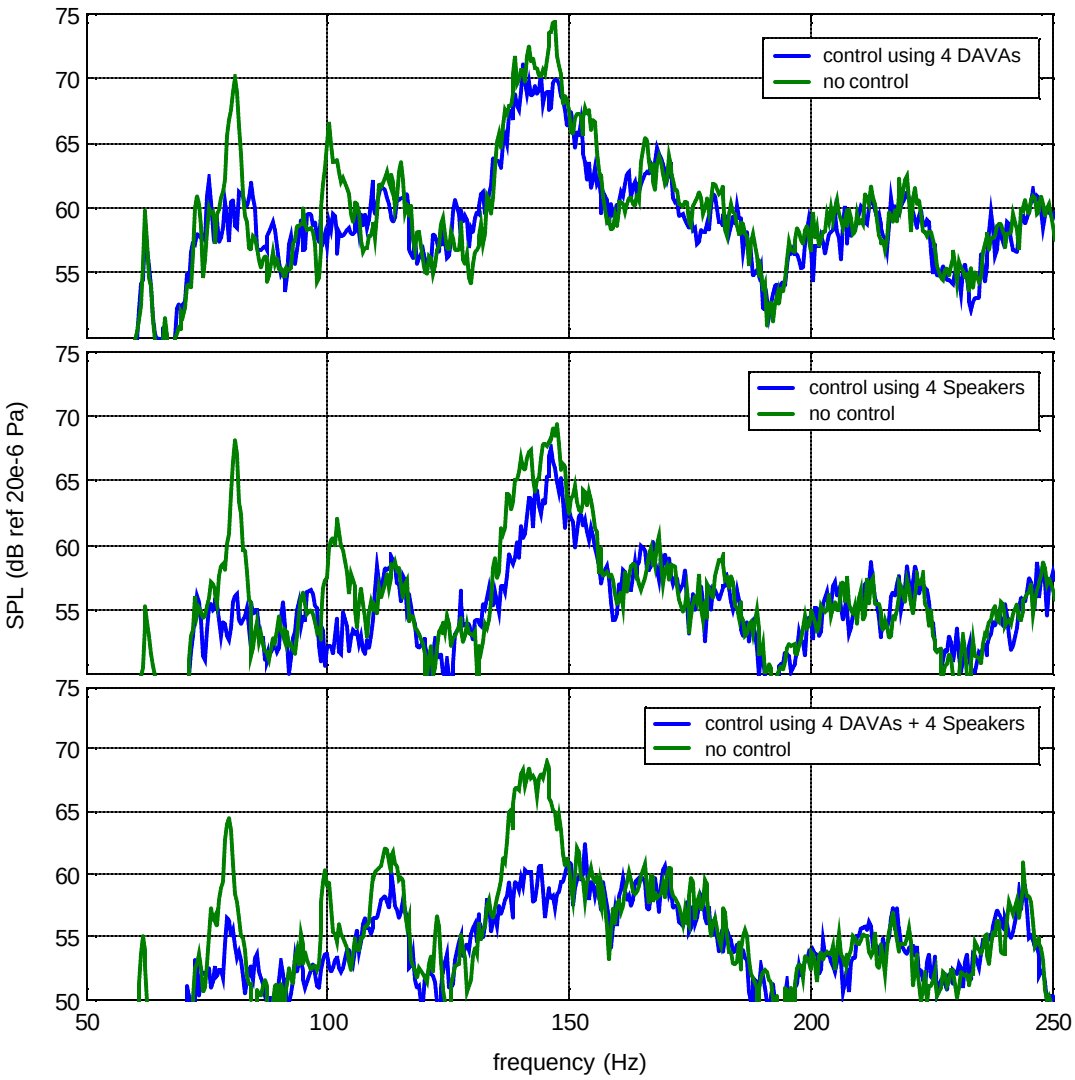

Figure 4-12. Average internal SPL levels for three sets of control actuator sets. The reference for the controller is the external microphone signal.

4.6 Reference Signal Analysis

The quality of the reference signals in active noise control systems is significant. The coherence level between the reference signal and the interior noise field (error sensors)

determines the quality of the reference signal. In addition, the more time advance that the reference signals provide to the control system the better control can be achieved. In an effort to show the significance of time advance, the voltage input to the primary source is used as a reference instead of the external microphone signal. The results of the comparison are shown in Figure 4.13.

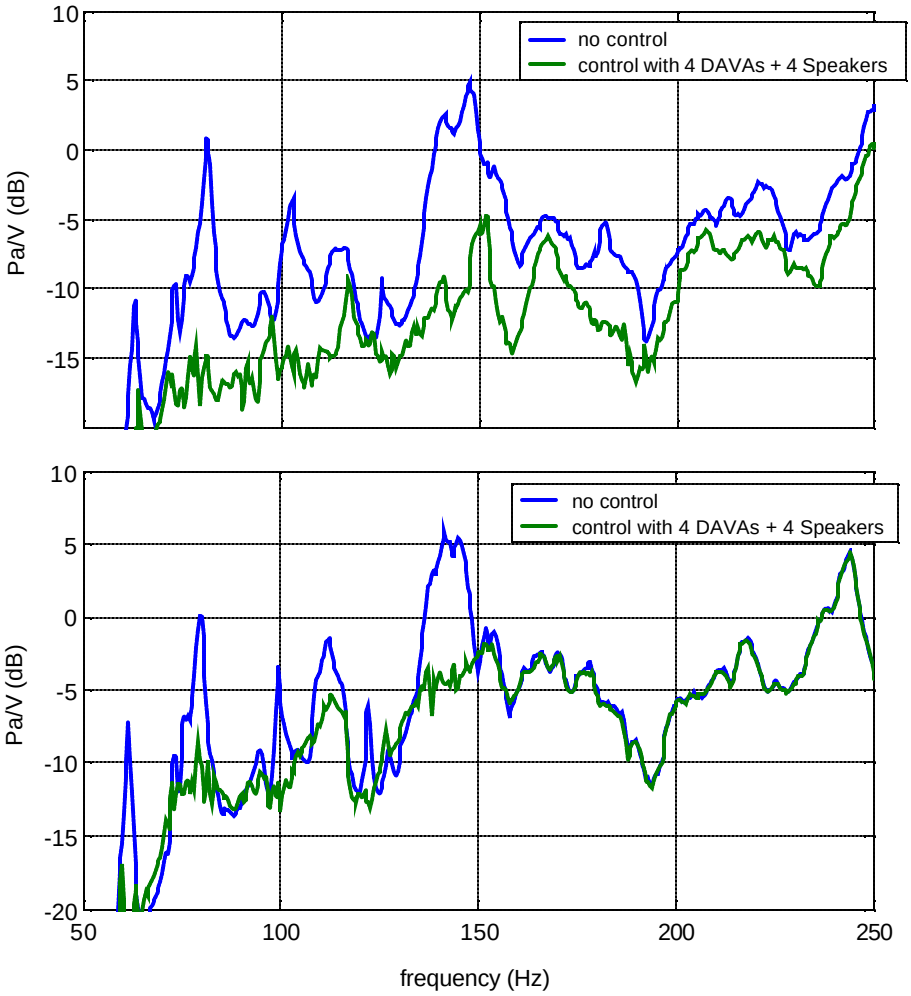

Figure 4-13. Transfer functions between the error microphones and the voltage input to the primary source. The voltage input to the primary disturbance is the controller reference (top). The external microphone signal is the controller reference (bottom).

The voltage input to the primary source is a more "upstream" than the external microphone and also excludes the noise that might be measured by the external microphone signal. Therefore, as a result, an improved attenuation level of 7.4 dB over 60-200 Hz bandwidth is achieved in this case compared to the 3.2 dB of the latter case. As a comparison, the outside

tests conducted previously on the cylinder using 8 DAVAs resulted in 7dB attenuation over 80-200Hz [2].

Causality is the reason for this difference in attenuation level, because by changing the reference from external microphone, which is close to the error microphones, to the voltage input to the primary source makes the primary sound field more predictable. The details of the effects of causality are given the following section.

4.7 Causality Analysis

For a system to be "causal" its impulse response must have 0 values for the time $t<0$. In other words, the disturbance from the primary source cannot reach the error sensors before the signals from the control actuators. When controlling single frequency noise, the noise field is predictable into the future and "causality" is not an issue. However it plays an important role especially for the systems where primary sources have random time history output. Therefore the location of the reference signal is a crucial factor in control performance, because, the secondary source output should have sufficient time to reach the error microphones before the primary source output travels from the reference location to the error microphones. One way to prove the importance of causality is to move the reference signals more upstream or even incorporate a 'delay' in creating the primary source signals at the controller. In this case, a delay of 63 sampling points is set which corresponds to 90 milliseconds at the sampling frequency of 700Hz. The comparison of the transfer functions for the cases of with and without delay, while controller reference is taken to be the voltage input to the primary source, is given in Figure 4.14. The attenuation in 60-200 Hz bandwidth is 9.1 dB compared to the 7.4 dB of the case without delay.

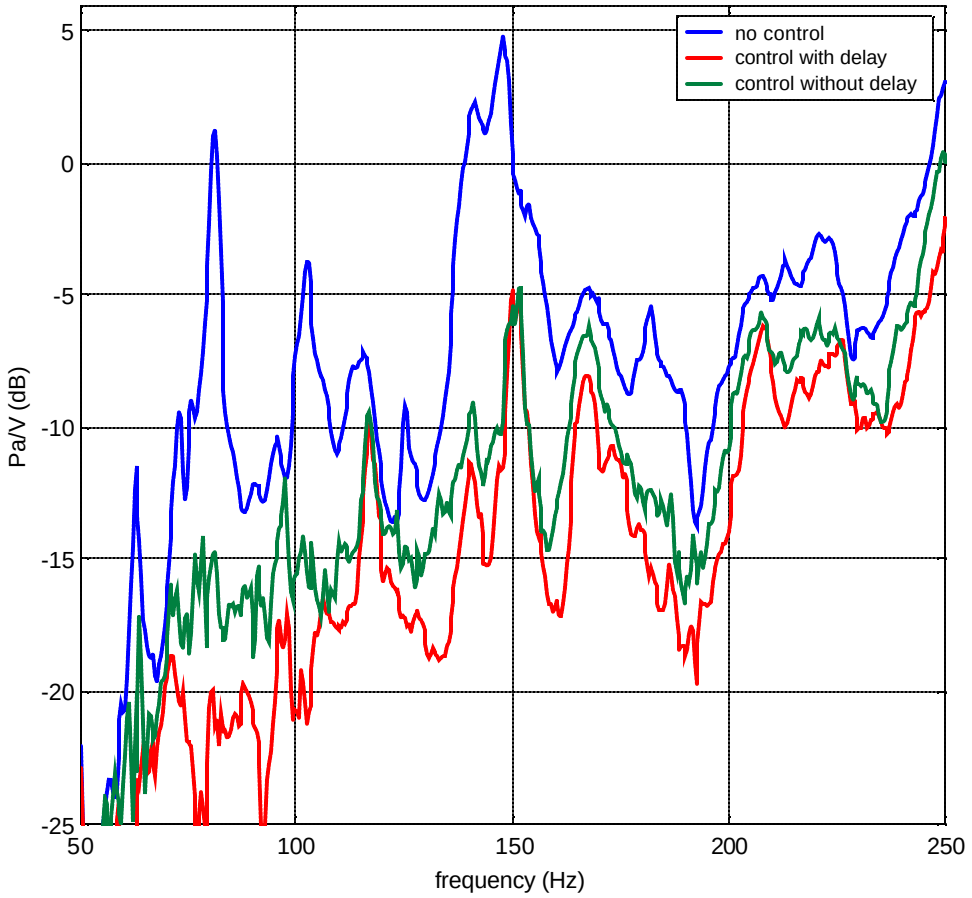

Figure 4-14. Transfer functions between the error mic rophones and the voltage input to the primary source. The voltage input to the primary disturbance is delayed by 90 milliseconds (top). The voltage input to the primary disturbance is not delayed (bottom).

The effect of causality in this case can also be demonstrated by plotting the time domain version of the optimum control filter coefficients that were computed before (section 4.4). This can be done using inverse Fast Fourier Transform (inverse FFT) and Figure 4.15 shows the filter for loudspeaker#1 in optimum control case. The optimum filter coefficients were band-pass filtered in the 40-400 Hz range by a 4^{th} order Butterworth filter in order to be able to concentrate on the targeted frequency content. It can be seen that a significant part of the filter coefficients lie in the negative time, which means that some information should be known beforehand, i.e. acausal.

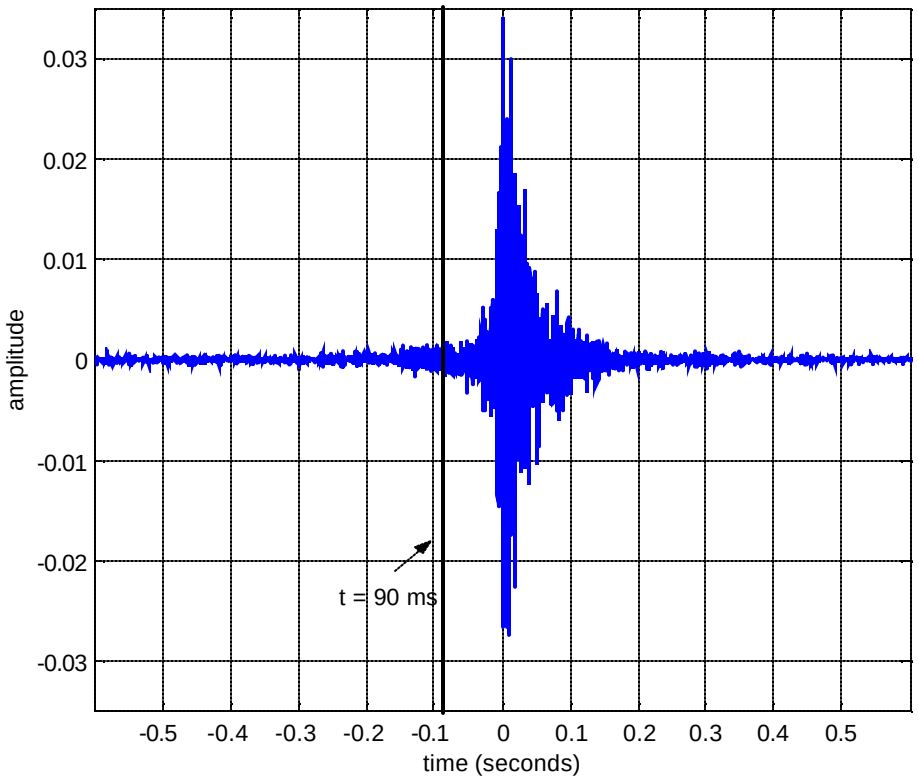

Figure 4-15. Time history of the optimum filter coefficients for loudspeaker#1.

The previous analysis introducing a "delay" of 90 milliseconds showed close to optimal results (Figure 4.14), the reason of which can be seen here. The -90ms line shows how much extra information can be used by the controller when delay is added. It should be noted that this interval includes almost all of the signals in the negative time domain which have amplitudes greater than 0.002. Figure 4.16 shows the corresponding time domain signal of the optimum filter for the DAVA#3.

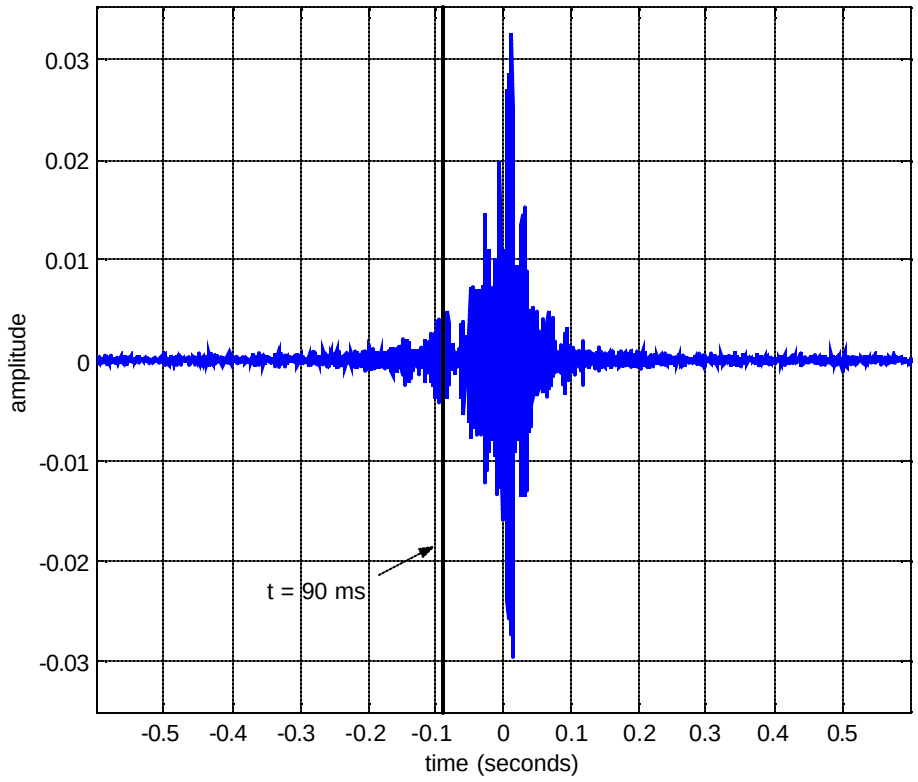

Figure 4-16. Time history of the optimum filter coefficients for DAVA#3.

The time-domain analysis of filter coefficients showed the optimum filter coefficients for DAVA exhibit a dominant character around 60 Hz. This can also be seen in Figure 4.9, where the DAVAs cannot attenuate the peak at 60 Hz, which means that the control effort at this frequency is high and dominant. Therefore, for better analyses of the filter coefficients on the targeted frequency range, the band-pass filter used for Figure 4.16 was set to 60-400 Hz range in order to eliminate this dominant frequency.

4.8 Analysis of Maximum Controllable External Level

Computing the maximum controllable external sound pressure level using the current system is significant in the sense that it gives information about the capacity of the control system. This determines the weight of the control system needed to achieve control in a realistic noise environment. The capacity of a control system with 4 loudspeakers is computed by using the assumption of linearity as follows. With the primary source producing a fixed output level,

the external sound level is measured while the control is on. Then the control filter coefficients are locked in order to keep the loudspeakers giving the same output while the primary source is shut off and internal sound level is measured. The loudspeaker outputs are brought to their maximum and the internal level is measured again. The difference between the two internal levels measured is equal to the amount by which the measured external level can be increased while maintaining control.

Figure 4.17 shows the maximum controllable external sound level at the external microphone location (between the external disturbance and the cylinder) for a range of frequencies. The amount of control in this case would be the same as shown in Figure 4.11 for the case where only 4 loudspeakers were used. The external level over 60-200 Hz bandwidth at normal testing conditions is measured to be 94.4 dB, and the maximum controllable external level by using 4 loudspeakers is computed to be 133.1 dB over the same frequency range.

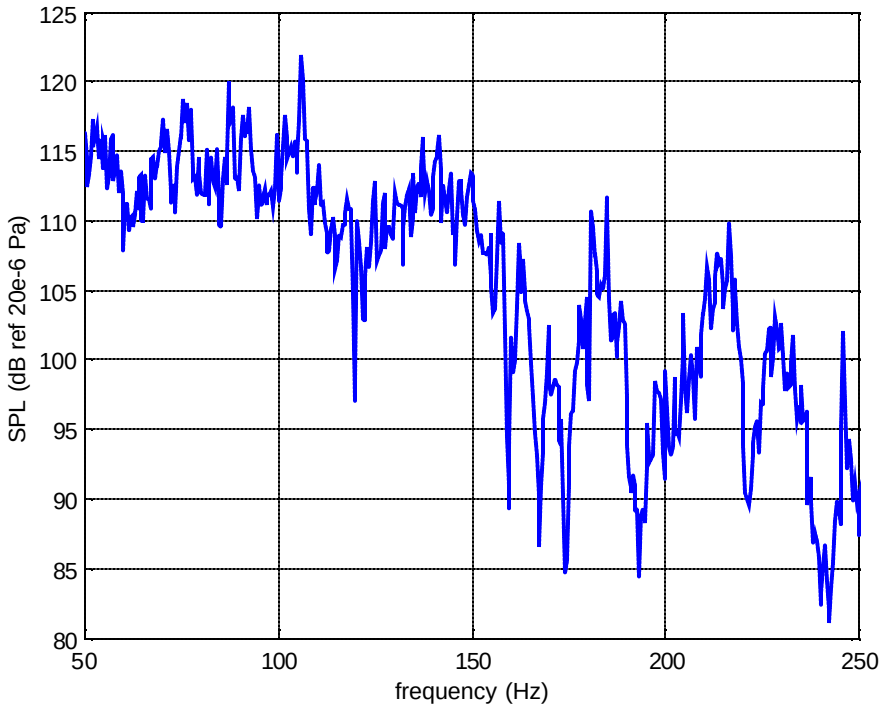

Figure 4-17. Maximum External SPL that can be controlled by 4 loudspeakers. This is the maximum external level for which the amount of control would still be equal to that given in Figure 4-11.

Chapter 5: Conclusions and Future Work

The goal of this chapter is to review and summarize the results of this thesis and to present some suggestions for future work. First, the conclusions about the design of lightweight acoustic devices will be given. Then, the results from the active control tests on the payload fairing using loudspeakers and DAVAs will be discussed. The last section suggests possible further improvements on both designing lightweight acoustic actuators and active control of sound in payload compartments.

5.1 Acoustic Devices

The weight reduction solutions for acoustic devices such as Helmholtz resonators and loudspeakers were investigated throughout this thesis and they share similar constraints.

5.1.1 Helmholtz resonators

In Chapter 2 Helmholtz resonators were investigated. Helmholtz resonators are almost always assumed to be rigid and the wall elasticity is not taken into account for any analysis. However, designing lightweight Helmholtz resonators requires the use of lighter and thinner materials, which results in a decrease in the stiffness of the walls, and therefore the forces associated with the air in the resonators can not be considered as negligible. For this purpose, equations including the wall stiffness terms were derived in order to be able to evaluate the performance of the resonators when wall deformation is present. The theory used a cylindrical resonator with perfectly rigid end caps and it was shown that deformation on the cylindrical sides are very small and the theoretical model showed that the resonators with PETG and acrylic walls had only 1% reduction in their performance compared to the a rigid walled resonator even for wall thicknesses as small as 0.5 mm. For a more stiff material such as aluminum the reduction in the performance is much less than 0.5% for this wall thickness value. In order to validate the theory and investigate the effects of the different parameters of the system such as wall material and end cap shapes, a series of finite element analyses (FEA) were performed using the ANSYS software. These analyses showed that the majority of the wall deformation of a cylindrical

Helmholtz resonator occurs at the end caps. A lightweight solution was to use hemispherical end caps which performed similarly to the rigid resonator whereas using thick flat and flat end caps resulted in performance losses of 6% and 20%, respectively.

Using aluminum for the walls of a Helmholtz resonator can result in high device mass; therefore two different materials having densities less than half of aluminum were used in the FEA: PETG and acrylic. For a wall thickness of 0.5 mm, both of these materials showed performance loss of less than 2% for hemispherical end caps. By using these materials, a 60cm-long 15-cm diameter resonator has a total weight of only 250 grams with a wall-thickness of 0.5mm. A 120cm-long 12.5cm-diamter PETG resonator with a wall thickness of 0.6mm and with a stiffened end cap was tested and the performance of this resonator was shown to be very close to the cardboard resonator which was assumed to be rigid. The resonator weighed 470 grams and this is larger than the model because of its larger dimensions and stiffeners used for the end caps. These tests validated the finite element results.

The finalized designs of Helmholtz resonators were used in passive control tests on a full-scale payload fairing at the Boeing facilities. 212 Helmholtz resonators were used together with the DVAs and the overall attenuation was measured to be 3.2 dB over 30-90Hz band and two dominant peaks in this band were attenuated by 5 dB and 10 dB. If the hemispherical end caps were used, the resonator would constitute only 3.9% of the total mass in the fairing.

5.1.2 Loudspeakers

Loudspeakers were selected for active noise control, because they are the most efficient active acoustic actuators, however they can be very heavy and bulky. The goal of Chapter 3 was to design lightweight loudspeakers so that they could be used in active noise control applications for payload fairings where weight savings are of great importance. A design approach based on choosing a commercially available loudspeaker as the reference and applying weight reduction solutions without loss of performance was applied. The reference was a 12” Pioneer loudspeaker which weighed 3065 grams. A rigid box for the loudspeaker was made from ¾” plywood and weighed 7.4 kg, which resulted in a total loudspeaker with enclosure weight of 10.4 kg. Loudspeaker characterization was made using mechanical, electrical and acoustical equations. Transfer function between the input voltage to the loudspeaker and the sound pressure at 1m away from the loudspeaker was computed as the output of the characterization. The targeted

frequency band for the active noise control in payload fairings was 60-200 Hz and the performance of the loudspeaker over this frequency range was taken into account throughout the design process.

The largest contribution of weight to the loudspeaker comes from the box and the magnet assembly. Keeping this in mind, the magnet assembly was re-designed to give almost equal performance with a much smaller mass. For this purpose very powerful rare-earth (Nd-Fe-B) magnets were used which offer stronger magnetic fields with the same weight as conventional ferrite magnets. Using a disc magnet instead of ring magnet, as in the reference loudspeaker, and building the rest of the assembly around the magnet resulted in a very small volume and therefore a small mass of the magnet assembly. The dynamics of the reference loudspeaker was maintained by using the same diaphragm, spider, surround, and an equal enclosure volume. Different magnet assembly sizes resulted in different performance levels and different loudspeaker weights. Therefore the magnet dimensions of the new design were optimized for the total sound pressure output over 60-200 Hz per unit mass of the loudspeaker (together with its box). The selected magnet to be used in the new design was slightly off of the optimum dimensions due to the fact that commercially available magnets come with standard sizes and machining rare-earth magnets is not favorable.

Other significant contributor to the mass was the box. Loudspeaker boxes should be rigid to prevent loss in loudspeaker performance. For this purpose glass-nomex honeycomb panels were used to build a 1 ft^3 loudspeaker box. To maintain rigidity triangular pieces were connected between the sides of the box. Table 5.1 summarizes the component weights of both the reference and the new loudspeakers together with their performance values.

Table 5-1. The summary of the weight contributions and performance values for both the reference (12" Pioneer) and the new lightweight loudspeakers.

		Reference 12" Pioneer Loudspeaker		New Lightweight Loudspeaker
		With ½" Box	*With ¾" Box*	*Lightweight Box*
Component Weight (grams)	*Magnet Assembly*	2,380		755
	Frame	685		
	Box	2,753	7,400	850
	Total	5,818	10,465	2,290
Performance rel. to the Reference	*Total Max SPL 60-200Hz @ 1m (dB)*	-3.3 dB	0 dB	+1.7 dB
	Pa/kg Cost Function	1.24	1	5.61

The new design of the loudspeaker and the box were tested together with the reference loudspeaker and the rigid box for comparison. The test setup in an anechoic chamber simulated free-field radiation and it consisted of a hemispherical array of microphones and two sets of measurements provided the sound pressure levels over a complete sphere. A single transfer function value for the measurements was calculated by spatially averaging the transfer functions from each microphone. Then the square of this single transfer function was summed over the desired frequency range to give a single number that represents the performance of the loudspeaker. Firstly, the new lightweight box was compared to the rigid box and the new box showed a 0.24 dB (2.8%) decrease over 60-200Hz bandwidth compared to the rigid box, which was a very good result considering the amount of weight reduction achieved. The new loudspeaker was tested and results showed that the new loudspeaker gave 2.8dB (38%) more output in the bandwidth than the reference loudspeaker. However, the nonlinear behavior of the loudspeakers could be seen when the input voltage was maximized and the transfer functions of the reference and new loudspeaker decreased by 1.6dB and 2.7dB, respectively. The total sound pressure output at 1m of the loudspeaker working in maximum voltage was measured to be 1.7dB more than the reference loudspeaker.

A cost function was defined as the total maximum sound pressure output (@ 1m over 60-200Hz) per unit mass of the loudspeaker gives a rough estimate of the loudspeaker mass required

to achieve certain pressure levels. When using this cost function the effects of using multiple loudspeakers and effects of different loudspeaker positioning should be taken into account. As summarized in Table 3-2, the value for this cost function relative to the reference loudspeaker was computed to be 5.61 for the lightweight loudspeaker. However, with an addition of a lighter loudspeaker frame, this value can be increased further to 6.60.

5.2 Active Control of Sound in Payload Compartments

In Chapter 4 of this thesis, active control tests on a scale payload fairing at Virginia Tech were performed using 4 loudspeakers and 4 DAVAs. The goals of these tests are to evaluate the performances of each of these devices in such an application and determine the actuator authority per mass to control a certain level of external noise. The test setup was composed of a loudspeaker providing external noise, a reference microphone placed between the noise source and the cylinder, and 12 error microphones placed inside the cylinder. The feed-forward control architecture used featured a multiple-input multiple-output filtered X-LMS algorithm and 8 channels were used for control output and 12 channels were used for control input together with the reference input.

Various aspects of the active control on the payload fairing were analyzed. For instance, an analysis determining the maximum control with the given setup was done by assuming perfect controller and perfect coherence and computing the optimum control coefficients. This analysis set an upper limit to the amount of control that can be achieved with this test configuration. Then the loudspeakers and DAVAs used both separately and together to control the noise inside the fairing. Two types of reference signals were used: external microphone signal and input voltage to the primary source. The difference between the two types of reference demonstrated the significance of the reference signal quality in active noise control treatments. A delay term incorporated in the controller, which enables the controller to predict the noise signals, demonstrated the amount of causality in the system. Table 5-2 summarizes the results of the active control test for different configurations.

Table 5-2. The results summary for the active noise control on the test cylinder.

Actuators	Controller Reference	Delay	Attenuation (60-200Hz)
4 DAVAs	External Microphone	-	1.5dB
4 Loudspeakers	External Microphone	-	2.2dB
Hybrid	External Microphone	-	3.2dB
Hybrid	Primary Source Input Voltage	-	7.4dB
Hybrid	Primary Source Input Voltage	90ms	9.1dB
Hybrid	*Maximum achievable control*		*13.6dB*

The maximum amount of external noise that can be controlled by the loudspeakers was also depicted by using a practical procedure in absence of very high levels of external noise, which could not be achieved under this test conditions. Table 5-3 summarizes the maximum controllable external levels for the two loudspeaker types. The cost function was calculated by dividing the maximum controllable external level (summed over 60-200 Hz and expressed in Pa) by the total mass of the loudspeakers (kg). The maximum controllable external level is assumed to vary linearly with the number of loudspeakers used. This might not present an accurate estimate in practice; however, it is very useful in comparing the two sets of loudspeakers. The previous results[2] from the outside tests conducted on the cylinder using 8 DAVAs are also presented. The comparison shows that the DAVAs are able to achieve similar control with less mass. However, loudspeaker mass can further be reduced as will be discussed in the next section.

Table 5-3. The results summary for the total mass and maximum controllable external level for 4 loudspeakers.

	4 12" Pioneer Loudspeakers with ½" Box	4 Lightweight Loudspeakers with Lightweight Boxes	8 DAVAs previously tested on the Cylinder [2]
Max Controllable External Level (60-200Hz)	133.1 dB	138.1 dB	Appr. 138 dB
Total Actuator Mass	23.3 kg	9.2 kg	2.9 kg
Pa/kg Cost Function rel. to the Reference	1	4.51	14.30

5.3 Future Work

In this section, possible future work on the design of lightweight acoustic devices and on the improvement of the performance of an active noise control treatment for payload fairings will be presented.

5.3.1 Acoustic Devices

Lightweight Helmholtz resonator designs discussed in Chapter 2 performed well in the passive control tests. However, the resonators can be built to be even lighter without any loss in the performance. For instance, materials with higher stiffness-to-mass ratios can be suitable for this purpose. Hemispherical end caps, which were shown theoretically to be very effective, could not be built because of the difficulties in manufacturing such a shape under the time constraints imposed by Boeing. Manufacturability also limits how thin the resonator walls can be made. In addition, although performing well acoustically, very thin walled resonators can be permanently deformed due to handling and other external effects in practice. Therefore, use of lightweight composite materials with high stiffness-to-mass ratios might be favorable in preventing the possible bending deformations due to these effects. Material selection together with solutions to manufacturability issues constitutes the possible next step to this subject.

In building a lightweight loudspeaker most of the design parameters were analyzed only in the theoretical model, since changing too many parameters and building a loudspeaker for each of these cases is practically difficult and costly. Although the new loudspeaker performed well and great weight reductions were achieved, it was still off of the optimum design. The optimum sized magnet can be built, and different magnet assembly configurations can be analyzed since the magnet assembly is still one of the heaviest components of the loudspeaker. Another approach would be using two radially magnetized rare-earth magnets and placing one of them inside and the other around the voice coil and optimize the design. This configuration eliminates the use of a yoke which would further decrease the magnet assembly weight.

The frame of the loudspeaker can be built from high stiffness-to-mass ratio materials such as carbon fibers with a simplified structure to reduce the weight. A lighter diaphragm can also be used to increase the output of the loudspeaker. For this thesis, the design procedure was based on using a reference loudspeaker which made the manufacturing process very easy.

However, a more customized loudspeaker can also built from scratch having better manufacturing opportunities. In addition, the enclosure can be built in a cylindrical shape rather than a rectangular box, which would increase the stiffness of the structure to give a better performance for a lighter structure.

5.3.2 Active Control of Sound in Payload Compartments

The amount of actuator mass required to control a certain external noise level for payload fairings can further be decreased in two ways. The performance of the control system can be improved to increase the amount of control for a given set of actuators. This can be done by using multiple references to receive better information about the external noise. Also, closer placement of the reference microphones to the primary source would reduce the length of the control path which would increase the predictability of the primary noise. This would improve the control performance since causality is an important issue for this application.

The performance of the control treatment can also be improved by building lighter and more efficient actuators. Loudspeakers can be built even lighter without performance loss which would reduce the total actuator mass required to achieve certain level of attenuation inside the fairing. The positions and number of actuators can also be optimized for this purpose, because the amount of coupling between acoustic and structural modes of the fairing is highly dependent on the positions of the actuators. The possibility of achieving similar amounts of attenuation with the proper actuator positioning using less number of actuators should also be investigated.

Appendix: 2-DOF Acoustic Actuator Modeling

In an attempt to create a two degrees of freedom acoustic actuator, a design combining a loudspeaker with a Helmholtz resonator was analytically modeled. The goal of this analysis was to investigate the performance of such an acoustic device and to determine whether an effect similar to that of a distributed active vibration absorber (DAVA) (which was shown to work effectively[2]) can be achieved.

A.1 Modeling

Since the stiffness values of the enclosures are derived from the differences in pressure due to the motion of the diaphragm or air in the neck, these values are written in a format where the three subscripts indicate the volume number, the mass on which the stiffness force is applied, and the mass whose displacement causes the stiffness force, respectively. Following is the sample stiffness calculation and Figure A-1 illustrates a box having two pistons at both ends with areas S_1 and S_2, and displacements y_1 and y_2.

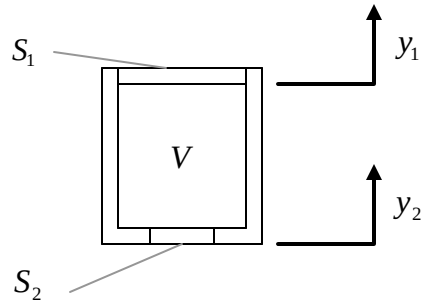

Figure A-1. The diagram for sample stiffness calculations.

The pressure p created by the displacements of the pistons can be calculated by

$$p = \frac{rc^2}{V}\left(S_2 y_2 - S_1 y_1\right) \tag{A.1}$$

where V is the box volume, r is the density of air, and c is the speed of sound in air. For example, the force exerted on the area 2 by this pressure is given by:

$$\begin{aligned} F_2 &= pS_2 \\ &= \frac{rc^2}{V}(S_2 y_2 - S_1 y_1)S_2 \\ &= \frac{rc^2}{V} S_2{}^2 y_2 - \frac{rc^2}{V} S_1 S_2 y_1 \\ &= k_{122} y_2 - k_{121} y_1 \end{aligned} \tag{A.2}$$

Therefore, k_{121}, for instance, represents the stiffness associated with the volume 1, affecting the mass 2 due to the displacement of the mass 1.

Two different configurations to combine loudspeakers with Helmholtz resonators were modeled. In the first model the loudspeaker was placed in a Helmholtz resonator, whereas in the second model a neck is placed on the bottom of the loudspeaker box. Figure A-2 illustrates both configurations together with their mechanical models on which the modeling equations were based.

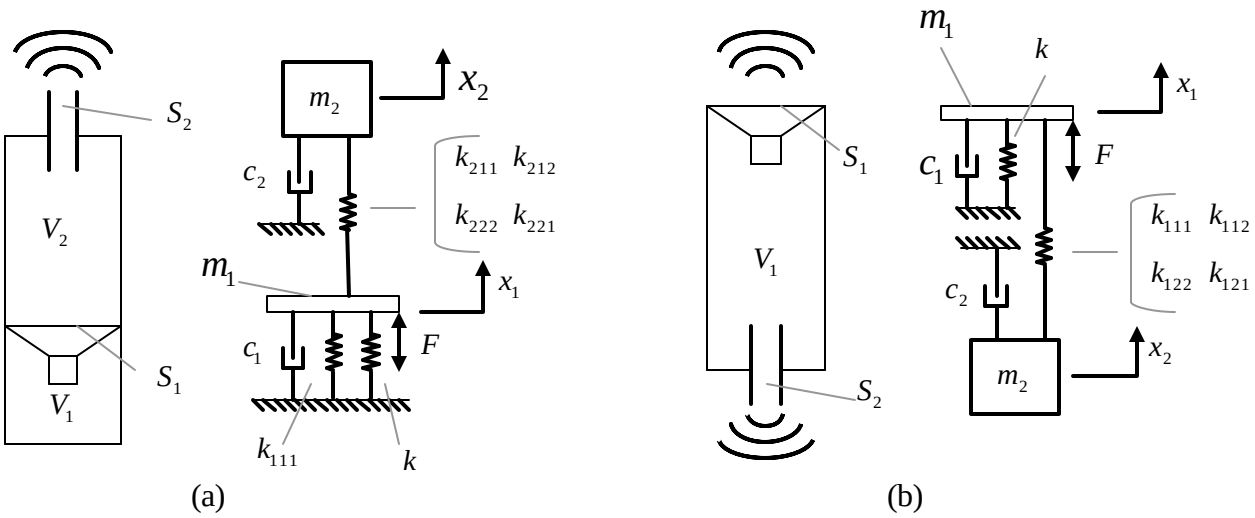

Figure A-2. Mechanical models of two different configurations: (a) configuration#1 (b) configuration#2.

As the output of the model equations, the transfer function between the input voltage to the loudspeaker and the total volume velocity out of the actuator was calculated. The transfer function for the loudspeaker was derived in Section 3.1. For the first configuration, the only volume velocity of the actuator is from the resonator neck. The following is the consequent transfer function for this case:

$$\frac{V_v}{V} = \frac{jwS_2}{T_1 \frac{R_E}{Bl} + jwBlQ_1} \tag{A.3}$$

where

$$\begin{aligned} Q_1 &= \left(\frac{-w^2 m_2 + jwc_2 + k_{222}}{k_{211}} \right) \\ T_1 &= \left(-w^2 m_1 + jwc_1 + k_{111} + k_{211} + k\right) Q_1 - k_{212} \end{aligned} \tag{A.4}$$

For the second configuration, the total volume velocity of the actuator is from both the resonator neck and the loudspeaker diaphragm. Therefore the difference between the two gives the total volume velocity out of the actuator. Individual transfer functions are calculated to be:

$$\begin{aligned} \frac{(V_v)_1}{V} &= \left(\frac{jwS_1 Q_2}{T_2 \frac{R_E}{Bl} + jwBlQ_2} \right) \\ \frac{(V_v)_2}{V} &= \left(\frac{jwS_2}{T_2 \frac{R_E}{Bl} + jwBlQ_2} \right) \end{aligned} \tag{A.5}$$

where

$$Q_2 = \left(\frac{-w^2 m_2 + jwc_2 + k_{122}}{k_{121}} \right)$$
$$T_2 = \left(-w^2 m_1 + jwc_1 + k_{111} + k\right) Q_2 - k_{121} \tag{A.6}$$

The following is the consequent transfer function for this configuration:

$$\frac{V_v}{V} = \frac{jw\left(Q_1 S_1 - S_2\right)}{T_2 \frac{R_E}{Bl} + jwBlQ_2} \tag{A.7}$$

A.2 Results

In order to be able to determine the effectiveness of these actuators, their performances are compared to the loudspeaker over the 60-200Hz frequency band using the sum of the squares of the transfer function at every frequency as the performance indicator. For the resonator and neck sizes used in Sections 2.3 and 2.4, the new actuator with the first configuration gives a lower output compared to the loudspeaker itself as can be seen in Figure A-3. This is because the neck radius and resonator volume are not large enough to provide high volume velocities. The values for the volume of the enclosure, volume of the resonator, neck length and neck radius were taken to be 0.019m^3, 0.01m^3, 5cm and 3cm, respectively. The total outputs of the two configurations relative to the loudspeaker are -9.32dB and 1.38dB, respectively. The response for the first configuration is not optimum since it is out of the frequency range, however the response can not be increased unless the values for the resonator volume and neck area are increased. The second configuration gives a better output, however it is effective around a single frequency, which is not desired effect as for DAVAs.

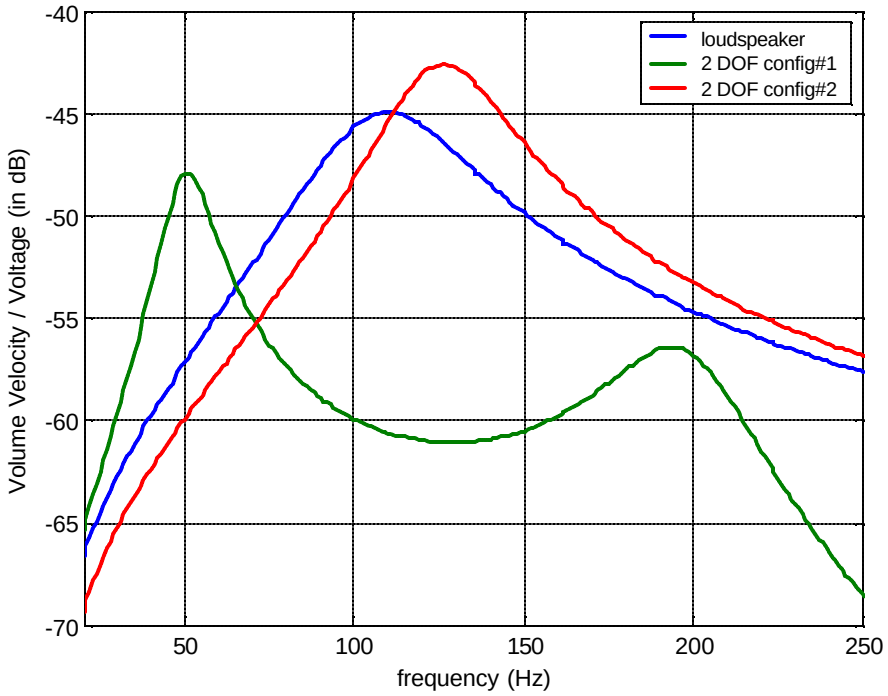

Figure A-3. Comparison of the performances of the loudspeaker and two configurations of the 2 DOF actuators.

The new actuators with the first configuration started giving more output than the loudspeaker as the neck area and resonator volume are increased. Figure A-4 illustrates the transfer functions for all three cases where, for the first configuration, the volume of the enclosure, volume of the resonator, neck length and neck radius were taken to be $0.019m^3$, $0.031m^3$, 5cm and 11.3cm, respectively. For the second configuration, volume of the enclosure (loudspeaker and resonator sharing the same volume), neck length and neck radius were taken to be $0.035m^3$, 10cm and 10cm, respectively.

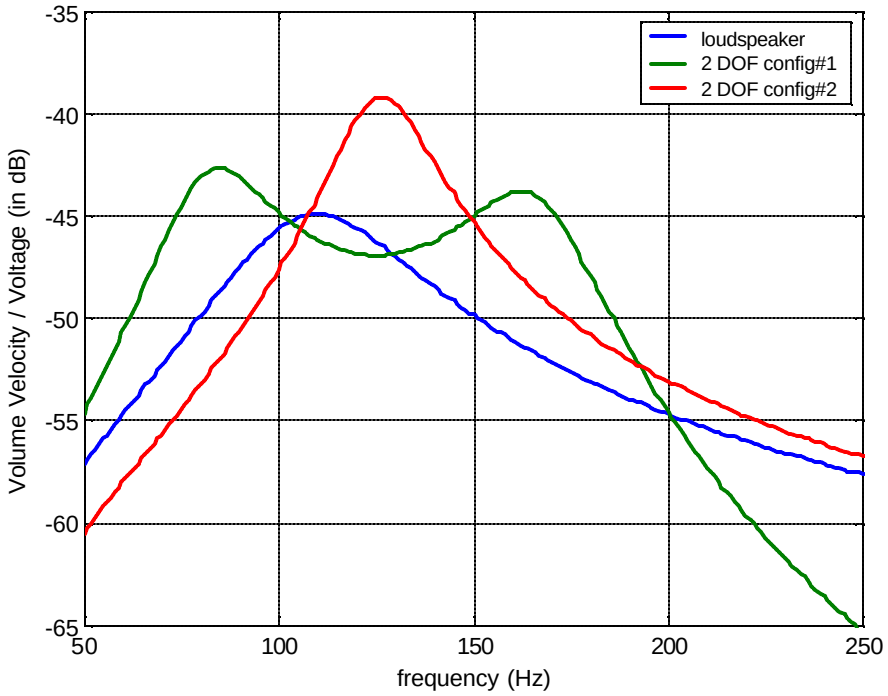

Figure A-4. Comparison of the performances of the loudspeaker and two configurations of the 2 DOF actuators using larger volume and neck area.

The first and the second configurations give 2.96dB and 3.31dB more output than the loudspeaker over the 60-200Hz frequency range. The first configuration offers a response with two peaks which is similar to that of a DAVA. On the other hand, the second configuration also provides a higher response, however the response is concentrated around a single frequency.

It can be concluded that for the new devices to be more effective than the loudspeaker the resonator volume and neck area must be large enough. For instance, for the cases plotted in Figure A-4, the volume of the first configuration was about three times than the volume of the resonators used in the Boeing tests. In addition, the neck areas are more than 15 times larger. Although the outputs of the new devices are higher than the loudspeaker over the frequency of interest, the analytical equations used for the models might not be accurate for such large values of resonator volume and neck area and therefore the devices of this size should be built and tested to check whether the model is valid.

References

[1] M. Johnson, C. R. Fuller, P. Marcotte, H. Osman, "Optimization of Distributed Vibration Absorbers for Sound Transmission into a Composite Cylinder", AIAA-2001-2232, 7th AIAA/CEAS Aeroacoustics Conference, Maastricht, The Netherlands, May 2001.

[2] A. F. Harris, "Multi-Degree of Freedom Passive and Active Vibration Absorbers for the Control of Structural Vibration", Master's Thesis, Virginia Polytechnic Institute & State University, 2003.

[3] S. Esteve, M. Johnson, "Reduction of Sound Transmitted into a Composite Cylinder using Distributed Vibration Absorbers and Helmholtz Resonators", Journal of the Acoustical Society of America, 112(6), December 2002.

[4] H. Osman, M. Johnson, C. R. Fuller, S. Esteve, P. Marcotte, "Application of Damped Helmholtz Resonators and Distributed Vibration Absorbers for the Control of Noise Transmission into a Cylinder", Paper #509, Proceedings of the ninth International Congress on Sound and Vibration, Orlando Florida, July 2002.

[5] Frahm, Hermann, "Device for Damping Vibrating Bodies," German Patent Serial Number 525,455, 1909, U.S. Patent Serial Number 989,958, (1911).

[6] M. R. Jolly, J. Q. Sun, "Passive Tuned Vibration Absorbers for Sound Radiation Reduction from Vibrating Panels", Journal of Sound and Vibration, 191(4), pp.577-583 (1996).

[7] K. Nagaya, L. Li, "Control of Sound Radiated from a Plate using Dynamic Absorbers under the Optimization by Neural Network", Journal of Sound and Vibration, 208(2), pp.289-298 (1997).

[8] F. Charette, C. R. Fuller, J. P. Carneal, "Adaptive Vibration Absorbers for Control of Sound Radiation from Panels" Proceedings of the 3rd AIAA/CEA Aeroacoustics Conference, Atlanta, GA, 1997.

[9] Y. M. Huang and C. R. Fuller, "The Effects of Dynamic Absorbers on the Forced Vibration of a Cylindrical Shell and its Coupled Interior Sound Field", Journal of Sound and Vibration 200, 401-418 (1997).

[10] Y. M. Huang and C. R. Fuller, "Vibration and Noise Control of the Fuselage via Dynamic Absorbers", J. Vibr. Acoust. 120, 496-502 (1998).

[11] H. Osman, M. Johnson, C. R. Fuller, P. Marcotte, "Interior Noise Reduction of Composite Cylinders using Distributed Vibration Absorbers", AIAA-2001-2230, 7th AIAA/CEAS Aeroacoustics Conference, Maastricht, The Netherlands, May 2001.

[12] M. Alster, "Improved Calculation of Resonant Frequencies of Helmholtz Resonators", Journal of Sound and Vibration, Volume 24, Issue 1, 8 September 1972, Pages 63-85.

[13] M. S. Howe, "On the Helmholtz Resonator", Journal of Sound and Vibration, Volume 45, Issue 3, 8 April 1976, Pages 427-440.

[14] R. L. Panton, J. M. Miller, "Resonant Frequencies of Cylindrical Helmholtz Resonators", Journal of the Acoustical Society of America, 57, 1533 (1975).

[15] F. J. Fahy, C. Schofield, "Note on the Interaction Between a Helmholtz Resonator and an Acoustic Mode of an Enclosure", Journal of Sound and Vibration 72(3), pp.365-378, 1980.

[16] A. Cummings, "The Effect of a Resonator Array on the Sound Field in a Cavity", Journal of Sound and Vibration 154(1), pp.25-44, 1992.

[17] A. Doria, "Control of Acoustic Vibrations of an Enclosure by means of Multiple Resonators" Journal of Sound and Vibration 181, 673-685 (1995).

[18] D. Photiadis, "The Effect of Wall Elasticity on the Properties of a Helmholtz Resonator", Journal of the Acoustical Society of America, 90 (2), pp. 1188-1190, 1991.

[19] A. N. Norris, G. Wickham, "Elastic Helmholtz Resonators", Journal of the Acoustical Society of America, 93 (2), pp. 617-630, 1993.

[20] M. Johnson, S. Esteve, "Comparison of Local and Global Adaptive Strategies for the Control Broadband Noise in an Enclosure using Adaptive Helmholtz Resonators", Active 2002, Institute of Sound and Vibration Research, University of Southampton, UK, July 2002.

[21] S. Esteve, M. Johnson, "Control of Noise Transmission into a Cylinder using Adaptive Helmholtz Resonators and Passive Vibration Absorbers", AIAA-2003-1815, 44th Structures, Structural Dynamics, and Materials Conference, April 2003, Norfolk, Virginia.

[22] P. E. Cambou, "A Distributed Active Vibration Absorber (DAVA) for Active-Passive Vibration and Sound Radiation Control", Master's Thesis, Virginia Polytechnic Institute & State University, 1998.

[23] P. Marcotte, C. R. Fuller, P. Cambou, "Control of Noise Radiated by a Plate using a Distributed Active Vibration Absorber (DAVA)", Proc, Active 99, Vol 1, pp.447-456, 1999.

[24] S. O'Regan, B. Burkewitz, C. R. Fuller, S. Lane, M. Johnson, "Payload Noise Suppression using Distributed Active Vibration Absorbers", Proceedings of the SPIE San Diego Conference, March 2002.

[25] V. Dickason, *The Loudspeaker Design Cookbook*, Audio Amateur Press Publishers, Peterborough, New Hampshire, 1991.

[26] S. J. Elliott, "Active Control of Structure-borne Noise", Journal of Sound and Vibration, 177(5), Pages 651-673, 1994.

[27] W. Neise, L. Enghardt, "Technology Approach to Aero Engine Noise Reduction", Aerospace Science and Technology 7, 352-363, 2003.

[28] S. A. Lane, R. L. Clark, "Improving Loudspeaker Performance for Active Noise Control Applications", Journal of Audio Engineering Society,Vol.46, No.6, pp.508-519, 1998.

[29] B. K. Henderson, S. A. Lane, J. Gussy, "Development of an Acoustic Actuator for Launch Vehicle Noise Reduction", Journal of the Acoustical Society of America, 111 (1), pt 1, Jan. 2002.

[30] R. Heydt, R. Kornbluh, R. Pelrine, V. Mason, "Design and Performance of an Electrostrictive-Polymer-Film Acoustic Actuator", Journal of Sound and Vibration, 215(2), 297-311, 1998.

[31] R. Heydt, R. Pelrine, J. Joseph, J. Eckerle, R. Kornbluh, "Acoustical Performance of an Electrostrictive Polymer Film Loudspeaker", Journal of the Acoustical Society of America, 107 (2), Feb. 2000.

[32] V. Jayachandran, N. E. Meyer, M. A. Westervelt, J. Q. Sun, "Piezoelectrically Driven Speakers for Active Aircraft Interior Noise Suppression", Applied Acoustics 56, 263-277, 1999.

[33] P. A. Nelson, S. J. Elliott, *Active Control of Sound*, Academic Press, 1992.

[34] C. R. Fuller, S. J. Elliott, P. A. Nelson, *Active Control of Vibration*, Academic Press Limited, London, Great Britain, 1996.

[35] Y. Tu, C. R. Fuller, "Multiple Reference Feedforward Active Noise Control Part 1: Analysis and Simulation of Behavior", Journal of Sound and Vibration, 233(5), pp.745-759, 2000.

[36] Y. Tu, C. R. Fuller, "Multiple Reference Feedforward Active Noise Control Part 2: Reference Preprocessing and Experimental Results", Journal of Sound and Vibration, 233(5), pp.761-774, 2000.

[37] C. R. Fuller, A. H. von Flotow, "Active Control of Sound and Vibration", IEEE Control Systems Magazine, pp. 9-19, December, 1995.

[38] P. Lueg, "Process of Silencing Sound Oscillations", 1936, US Patent No. 2,043,416.

[39] H. L. Olson, E. G. May, "Electronic Sound Absorber", Journal of the Acoustical Society of America, Vol.25, No.6, 1953, pp.1130-1136.

[40] S. A. Lane, R. L. Clark, S. C. Southwaed, "Active Control of Low Frequency Modes in an Aircraft Fuselage using Spatially Weighted Arrays", Transaction of the ASME Journal of Vibration and Acoustics Volume 122, 2000, pp 227-234.

[41] C. Niezrecki, "Structural & Acoustic Response of Cylinders with Applications to Rocket Payload Fairings", PhD Thesis Virginia Polytechnic Institute & State University, 1999.

[42] D. J. Leo, E. H. Anderson, "Vibroacoustic Modeling of a Launch Vehicle Payload Fairing for Active Acoustic Control", Proceeding of the 99th Structures, Structural Dynamics, and Materials conference, 1998, pp. 3212-3222.

[43] M. E. Johnson, S. J. Elliott, "Experiments on the Active Control of Sound Transmission into a Stiff Cylinder using Piezoelectric Actuator", Proc. Inst. Acoust. 16(1), pp.201-210 (1994).

[44] M. E. Johnson, O. Sacarcelik, "Reference Signal Requirements for the Feedforward Control of Sound Transmission into a Payload Fairing", Proceedings of Noise-Con 2003, Cleveland, Ohio.

[45] L. E. Kinsler, A. R. Frey, A. B. Coppens, J. V. Sanders, *Fundamentals of Acoustics*, 4th Edition, John Wiley & Sons, 2000.

Vita

Ozer Sacarcelik was born in 1980, in Turkey. He attended Malatya Science High School and entered Bogazici (Bosphorus) University in Istanbul in 1997. He received a B.S. degree in mechanical engineering in July 2002 and in August he moved to the U.S. so start his graduate study at Virginia Polytechnic Institute and State University. He joined the Vibrations and Acoustics group in January 2003 as a graduate research assistant and completed this thesis to receive an M.S. degree in mechanical engineering in May 2004.